Jül-4367

Jülich Center for Hadron Physics (JCHP)
Institut für Kernphysik (IKP)
COSY

2 MeV Electron Cooler at COSY

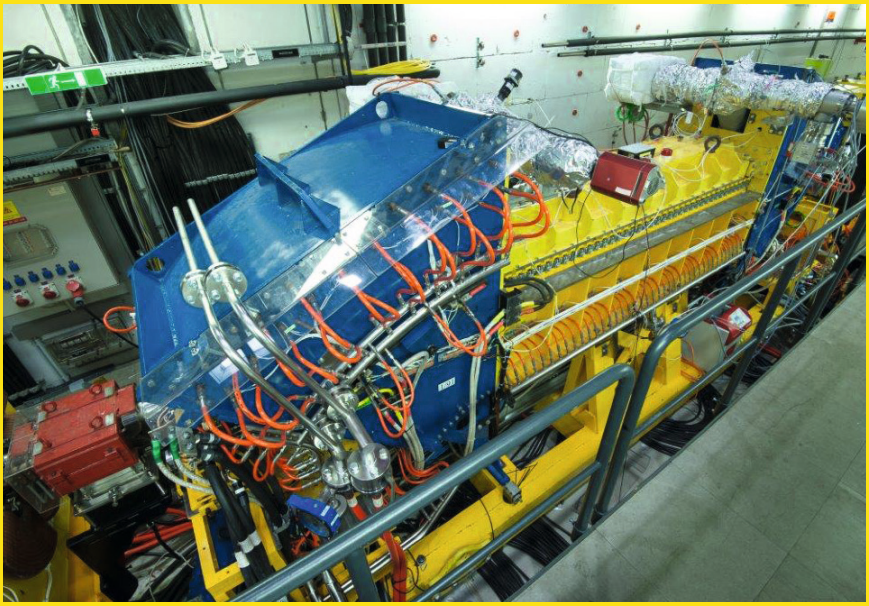

ANNUAL REPORT 2013

Mitglied der Helmholtz-Gemeinschaft

JÜLICH
FORSCHUNGSZENTRUM

Annual Report 2013

Jülich Center for Hadron Physics / Institut für Kernphysik / COSY

Cover picture:

The 2 MeV electron cooling system installed in the cooler synchrotron COSY; it was proposed to further boost the luminosity even in presence of strong heating effects of high-density internal targets. The installation and commissioning of the cooler took place in the summer shutdown 2013. The design and construction of the cooler was accomplished in cooperation with the Budker Institute of Nuclear Physics in Novosibirsk, Russia. The 2 MeV cooler is also well suited in the start up phase of the High Energy Storage Ring (HESR) at FAIR in Darmstadt. It can be used for beam cooling at injection energy and is intended to test new features of the high energy electron cooler for HESR. Two new prototypes of the modular high voltage system were developed, one consisting of gas turbines the other based on inductance-coupled cascade generators. The technical layout of the 2 MeV electron cooler is described and the status of component manufacturing with the latter one implemented is reported in more detail in Sect. 4.

Preface

During the past year the Institute for Nuclear Physics (IKP) has faced a couple strategic watersheds. Foremost of these is the upcoming retirement of Rudolf Maier, the head of the accelerator institute (IKP-4), in early 2014. It is obvious that the accelerator group needs strong scientific leadership given the tasks and commitments of IKP-4 — in particular in the context of building HESR at FAIR and of conceiving a possible future storage-ring project. Fortunately, the process of interviewing and subsequently hiring a successor to lead IKP-4 in the future is proceeding on track. Moreover, we have decided to phase out the hadron physics program at COSY. On the one hand this is motivated by the upcoming physics opportunities at HESR/PANDA, and on the other side by serious budgetary restrictions imposed on us. Consequently, we have readjusted our priorities as presented in the application for Programme-oriented Funding (PoF-3). Here about 70% of our resources (HESR; PANDA and PAX) are connected with FAIR, which according to a decision by the Helmholtz senate will not be evaluated. The remaining 30% are largely foreseen for the JEDI-project, which aims at a search for charged-particle electric-dipole moments in storage rings with unprecedented sensitivity. A smaller part will be used for research and development of accelerator components and advanced detector technologies. The corresponding PoF-applications for Matter and the Universe (MU) and Matter and Technology (MT), have been submitted and will be evaluated in the first quarter of 2014. In order to strengthen the cooperation between IKP and the physics department of the RWTH Aachen University in the field of basic research, a new section of the Jülich-Aachen Research Alliance (JARA) was founded last year and inaugurated in January 2013. Named JARA-FAME (Forces and Matter Experiments), its aim is to investigate the fate of antimatter (i) by searching for it with the Alpha Magnetic Spectrometer (AMS) on the International Space Station (ISS) and (ii) by investigating possible reasons for its disappearance, e.g., via the search for EDMs within JEDI.

The technological highlight of 2013 was the installation and commissioning of the high-energy electron cooler in the COSY ring (see cover page). After delivery in December 2012 by the Budker Institute (Novosibirsk, Russia), it has been set up together with our Russian colleagues. In the meantime it has been tested at lower values of high voltage to prove that it works. As the next step we will study the device in detail with COSY beams and carefully increase the electron beam energy up to the maximum value of 2 MV during the upcoming year.

Physics highlights of the past year comprise:

Spin correlation measurements Transverse spin correlations for the double polarized $np \to d\pi^0$ and $np \to \{pp\}_s\pi^-$ reactions were measured at COSY-ANKE using a polarized deuteron beam incident on polarized hydrogen from an atomic beam source, which was fed into a target storage cell.

Double-pionic fusion The isospin decomposition of the basic double-pionic fusion reactions $pn \to d\pi^0\pi^0, pn \to d\pi^+\pi^-$ and $pp \to d\pi^+\pi^0$ was measured at WASA-at-COSY in the region of the ABC effect, shedding further light on the presumed resonance-like structure in the isoscalar final state.

Dark photon search The world's largest sample of $\pi^0 \to \gamma e^+e^-$ decays from WASA-at-COSY was used to provide constraints on the possible existence of a light dark photon in the mass range below 100 MeV, extending the existing upper limits and excluding a significant fraction of the parameter space needed as a potential explanation for the $(g-2)_\mu$ result.

Spin Coherence Time The srEDM and JEDI collaborations at COSY have achieved a major milestone towards a storage ring EDM measurement by increasing the spin coherence time (SCT) of a polarized deuteron beam circulating in COSY to about 400 s with the help of adjustments of sextupole magnets in the ring.

Spin Tune measurement In cooperation with the COSY accelerator crew, the JEDI and srEDM collaborations have been able to map the spin tune of a deuteron beam in COSY with unprecedented precision (10^{-8} per 6 s time interval) by exploiting a time-stamp technique.

Restrictions for carbon-based life The fusion of three helium nuclei to carbon in stars is catalyzed by the so-called Hoyle state in ^{12}C. Nuclear lattice simulations have been performed to study the dependence of that state on the quark masses and on the fine structure constants leading to variations of about 2% being compatible with carbon-based life.

Hunting for hadronic molecules In order to test the hypothesis of the molecular nature of both the $Y(4260)$ and $Z_c(3900)$, our theory group proposed that the $X(3872)$ must give a strong signal in the radiative decays of the $Y(4260)$. Subsequently, the $X(3872)$ was discovered in the transition $Y(4260) \to J/\psi\pi\pi$ providing strong support to the molecular picture.

Noteworthy further items are:

Professorships A. Lehrach (IKP-4) and M. Büscher (IKP-2, now PGI-6) have received and accepted Professorships (W2) at the RWTH Aachen University and Heinrich Heine University Düsseldorf, respectively.

IKP conferences and meetings:

JARA-FAME Inauguration In a ceremonial act earlier this year the new FAME-section of JARA was inaugurated with a Jülich-Lecture on the Alpha Magnetic Spectrometer by Nobel Laureate S. Ting (MIT).

Autumn Lectures in Tbilisi (Georgia) In the context of the cooperation agreement between Georgian Universities and Forschungszentrum Jülich (Georgian-German Science Bridge), a two-week lecture series has been held at the Georgian Technical University (GTU) with participation of IKP (H. Ströher, D. Gotta and A. Kacharava).

WE-Heraeus-Seminar at Bad Honnef Within the HGF portfolio process a platform for the development of advanced detector systems has been established. Based on this, IKP (J. Ritman and T. Stockmanns) co-organized an international workshop (532. WE-Heraeus Seminar) on Development of High-Resolution Pixel Detectors and their Use in Science and Society.

I would like to express my sincere gratitude to all our colleagues and co-workers, since without their help and commitment, we would not have been able to achieve our milestones. We also acknowledge the continuous support by the Board of Management of Forschungszentrum Jülich.

Jülich, December 2013 Hans Ströher

Contents

1 Physics at COSY 1

2 COSY Operation and Developments 8

3 Theoretical Investigations 11

4 Progress of the HESR 17

5 Day-1 Experiment at HESR 20

6 The PANDA Experiment 23

7 Towards electric dipole moment measurements (JEDI) 29

8 Further Experimental Activities 31

Appendix

A Councils 34

B Publications 35

C Talks and Colloquia 41

D Diploma and Ph.D. Theses 52

E Awards & Offers for Professorships 54

F Funded Projects 55

G JCHP-FFE Projects 56

H Conferences (co-)organized by the IKP 58

I Teaching Positions 61

J Personnel 62

K Further Contributions 65

1 Physics at COSY

1.1 Overview

The cooler synchrotron and storage ring COSY delivers unpolarized and polarized beams of protons and deuterons with momenta up to 3.7 GeV/c for three internal experiments — ANKE, PAX and WASA — and one experiment — TOF — at an external target position. All detection systems are operated by large international collaborations.

- **ANKE** (Apparatus for Studies of Nucleon and Kaon Ejectiles) is a large acceptance forward magnetic spectrometer at an internal target station in the COSY ring. The central dipole is movable to adjust the momenta of the detected particles independent of the beam momentum. Using deuterium cluster targets, reactions on the neutron are tagged by detecting the low-energy recoil proton in silicon strip detectors in vacuum next to the target. In addition, a polarized internal target with a storage cell can be used. An openable storage cell is under development.
- **PAX** (Polarized Antiproton EXperiment) is the test set-up to investigate spin filtering as a method to produce polarized beams. It uses an atomic beam source, an openable storage cell and a Breit-Rabi polarimeter in a low-β section of COSY. After delivery of a Siberian Snake, longitudinal spin filtering will be investigated.
- **TOF** (Time Of Flight) is a non-magnetic spectrometer combining excellent tracking capabilities with large acceptance and full azimuthal symmetry allowing to measure complete Dalitz plots. TOF is optimized for final states with strangeness. With the new straw tube tracking system (STT), TOF has a significantly improved mass resolution and reconstruction efficiency. TOF has finalized its scientific program at the end of 2013.
- **WASA** (Wide Angle Shower Apparatus), an internal 4π spectrometer for neutral and charged particles, is operated at the internal COSY beam. WASA comprises an electro-magnetic calorimeter, a very thin superconducting solenoid, inner and forward trigger and tracking detectors, and a frozen-pellet target for hydrogen and deuterium.

The unique COSY capabilities are also used by the Storage-Ring EDM (srEDM) and JEDI (Jülich Electric Dipole Moment Invstigations) collaborations to investigate spin-manipulations as preparation to build (a) dedicated storage ring(s) to search for electric dipole moments of light ions (p, d, ^{3}He). The EDDA detector is used as polarimeter.

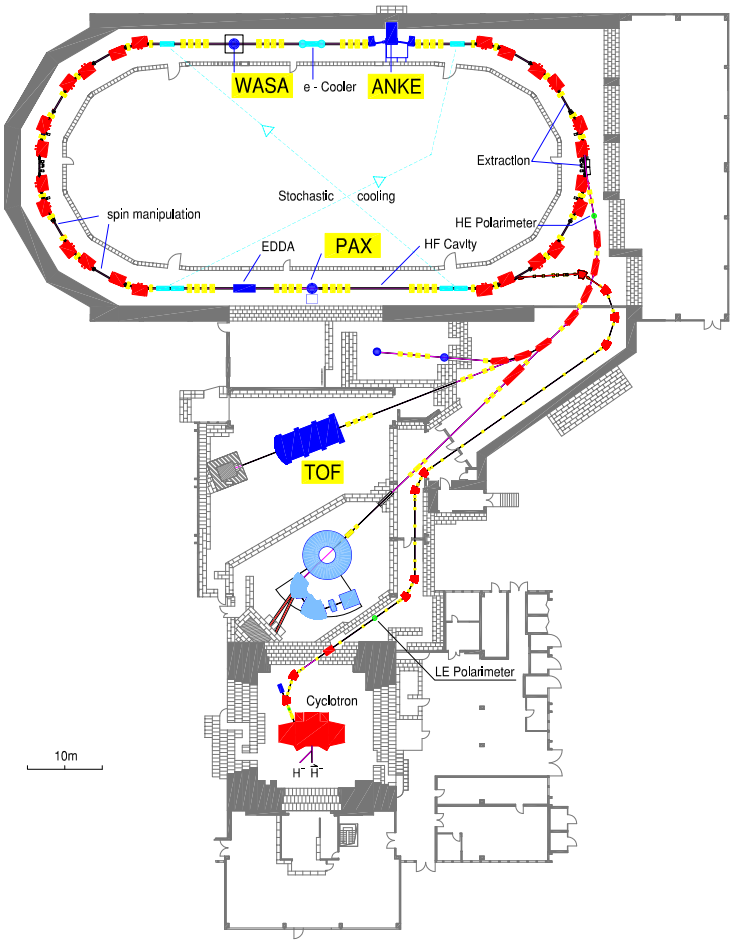

1.2 Major Physics Results at COSY

1.2.1 *np* Analyzing Power in Search of the ABC Resonance Structure

The ABC effect denotes an extraordinary low-mass enhancement in the $\pi\pi$ invariant mass spectrum and is observed to happen, if the initial nucleons or light nuclei fuse to a bound final nuclear system and if the produced pion pair is isoscalar. It has been named after the initials of Abashian, Booth and Crowe, who first observed it in the inclusive measurement of the $pd \rightarrow {}^3\mathrm{HeX}$ reaction more than fifty years ago, but until now, no real understanding of this phenomenon has been achieved.

In exclusive high-statistics measurements of the isoscalar $pn \rightarrow d\pi^0\pi^0$ reaction and of the isospin mixed $pn \rightarrow d\pi^+\pi^-$ reaction we could demonstrate that this ABC effect is correlated with a pronounced resonance structure in the total cross section at $\sqrt{s}$ = 2.37 GeV with a width of only 70 MeV and quantum numbers $I(J^P) = 0(3^+)$. This structure is located about 90 MeV below $\sqrt{s} = 2m_\Delta$, the peak position of the conventional t-channel $\Delta\Delta$ process, and its width is about three times narrower than this process.

If this structure originates from a s-channel resonance in the entrance channel, then also an pn elastic scattering should be affected. From the meanwhile experimentally known decay widths into $d\pi^0\pi^0$, $d\pi^+\pi^-$ and $pp\pi^0\pi^-$ channels we may estimate the expected decay width into the pn channel. As a result we obtain $\Gamma_{pn} \approx 7$ MeV, i.e. 10% of the total width. If we add the corresponding resonance amplitude in the ${}^3D_3$ and ${}^3G_3$ partial wave, respectively, to the SAID partial wave solution for pn scattering, then we get small, but sizeable effects for the pn observables. Though the changes amount to only about 3% in the total cross section, they are in agreement with the previous measurements in the ABC region of T_n = (1.0 - 1.3) GeV. Whereas these small resonance effects cause only tiny changes in the differential cross section, the changes become substantial in the analyzing power, which consists of interference terms of partial waves rather than their squares and hence is particularly sensitive to a small admixture of a resonance.

We have investigated this reaction experimentally by having a polarized deuteron beam at T_p = 2.27 GeV incident on the pellet target of the WASA detector facility at COSY. From this data sample we have analyzed the analyzing power for np scattering using quasifree kinematics. Utilizing the Fermi motion of the nucleons bound within the beam deuteron the analyzed data span the energy region 2.32 GeV $\leq \sqrt{s} \leq$ 2.46 GeV (1.0 GeV $\leq T_n \leq$ 1.4 GeV) and thus cover just the region of the ABC effect and its associated resonance structure. Preliminary results are shown in Fig. 1. At the top the angular distribution of the np analyzing power is shown without consideration of the spectator momentum, *i.e.* being thus the weighted average over the measured interval. The data are in full agreement with the resonance residing in the ${}^3G_3$ partial wave. At the bottom the energy dependence of the analyzing power is shown for angles near 90°, where the resonance effect in A_y is at its maximum. We again observe good agreement with the predictions for the resonance effect.

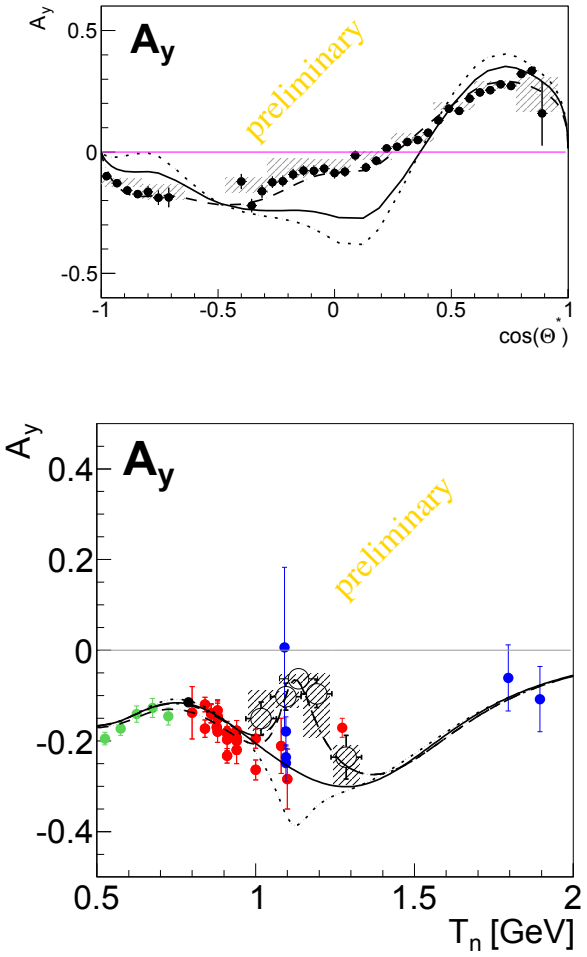

Fig. 1: Analyzing power for quasifree np scattering. Top: Angular distribution of the analyzing power without consideration of the spectator momentum, *i.e.* without classifying the collected pn scattering events according to their effective total center-of-mass energy $\sqrt{s}$. This data set corresponds to the weighted average over the interval 2.32 GeV $\leq \sqrt{s} \leq$ 2.46 GeV. The preliminary results from this work are shown by solid circles. Current estimates of systematic uncertainties are indicated by the hatched area. The solid line represents the SAID SP07 phase-shift solution, whereas the dotted (dashed) curve gives the result, when the ABC resonance amplitude is added in the ${}^3D_3$ (${}^3G_3$) partial wave. Bottom: Energy dependence of the np analyzing power at $\Theta_n^{cm} = 83°$. The open symbols denote the preliminary results of this work. The meaning of the curves and the hatched area are the same as above.

1.2.2 Study of the $\vec{n}\vec{p} \to \{pp\}_s\pi^-$ reaction in the near-threshold region at ANKE

One of the major challenges in today's physics is to relate the properties of few nucleon systems and nuclei to the theory of strong interactions, QCD. It is chiral symmetry that provides the preconditions for the construction of an effective field theory, called chiral perturbation theory. A modification to the standard χPT approach is necessary when it is applied to pion production in nucleon-nucleon collisions. The large scale, introduced by the initial momentum, has to be considered explicitly.

One important step forward in our understanding of pion reactions at low energies (C. Hanhart, Phys. Rept. **397**, 155 (2004)) will be to establish that the same short-range $NN \to NN\pi$ vertex contributes to both p-wave pion production, where both initial and final NN pairs are in relative S waves, and to low energy three-nucleon scattering, as well as to a number of other low energy phenomena. The strength of this production operator cannot be fixed from processes in the one-nucleon sector, such as in pion-nucleon scattering.

The COSY-ANKE collaboration has embarked on an ambitious program of performing a complete set of measurements of the $NN \to \{pp\}_s\pi$ reactions at low energy so that a full amplitude analysis can be carried out. By selecting events with excitation energy in the proton-proton system $E_{pp} < 3$ MeV, the resulting diproton $\{pp\}_s$ is overwhelmingly in the $^1S_0$ state. Measurements at $T_p = 353$ MeV of the cross sections $d\sigma/d\Omega$ and proton analyzing powers A_y^p in the $\vec{p}p \to \{pp\}_s\pi^0$ reaction (D. Tsirkov *et al.*, Phys. Lett. B **712**, 370 (2012)) and the quasi-free $\vec{p}n \to \{pp\}_s\pi^-$ reaction, where a polarized proton beam was incident on a deuterium target (S. Dymov *et al.*, Phys. Lett. B **712**, 375 (2012)), have already reported as parts of this program.

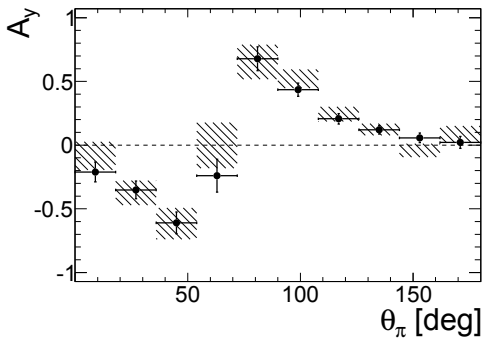

Fig. 2: The proton analyzing power A_y^p (points) and neutron analyzing power A_y^n (shaded bands) for the $pn \to \{pp\}_s\pi^-$ reaction at 353 MeV, obtained simultaneously in the double-polarized experiment at ANKE.

This information complemented recently through measurements with a polarized deuteron beam colliding with a polarized hydrogen target (S. Dymov *et al.*, Phys. Rev. C **88**, 014001 (2013)). This has led to a determination of the proton-neutron transverse spin correlations $A_{x,x}$ and $A_{y,y}$ in the quasi-free $\vec{n}\vec{p} \to \{pp\}_s\pi^-$ reaction and also an independent measurement of the proton and neutron analyzing powers for $np \to \{pp\}_s\pi^-$. When this information was used in conjunction with a refined analysis of the earlier data, a more robust amplitude decomposition could be developed for both the $I = 1$ and $I = 0$ channels.

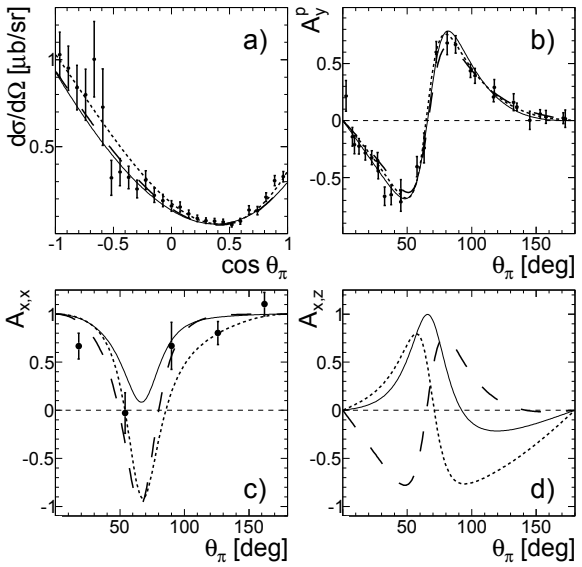

Fig. 3: Predictions of the partial wave analysis (PWA) for the $pn \to \{pp\}_s\pi^-$ reaction at 353 MeV. Also shown are the ANKE data with statistical errors. The full, long-dashed, and short-dashed lines correspond to the three PWA solutions. a) Differential cross-section, b) A_y^p, c) $A_{x,x}$, d) $A_{x,z}$, for which there are yet no experimental data.

The outcome of the partial wave analysis (PWA) of the combined $pp \to \{pp\}_s\pi^0$ and $np \to \{pp\}_s\pi^-$ data sets is shown in Fig. 3. Even after making phase assumptions on the isospin-1 production amplitudes, the PWA results in 3 distinct solutions that can all describe reasonably well the measured values of the $np \to \{pp\}_s\pi^-$ reaction. Furthermore, the $pp \to \{pp\}_s\pi^0$ observables are well reproduced. However, the predictions for $A_{x,z}$ in Fig. 3d are radically different. Hence even a low statistics measurement of this parameter would be sufficient to resolve some of the residual ambiguities. This would require the rotation of the proton polarization into the longitudinal direction, which could be achieved for a proton beam through the use of a Siberian snake. It is hoped that such an experiment will be carried out at ANKE once the Snake is delivered and commissioned using the polarized deuterium target successfully commissioned in 2012.

1.2.3 Testing the strong final state interaction in the η^3He system

The reaction $dp(pd) \to {}^3\mathrm{He}\,\eta$ is known for its anomalous behaviour of the total cross section near threshold, which rapidly rises within the first 1 MeV of excess en-

ergy Q to its plateau. In an attempt to describe the energy dependence a strong final state interaction (FSI) between the η and the ^{3}He was suggested, which could even point towards a quasi-bound η-nuclear state. Support for this ansatz was found by also studying the angular asymmetry of the differential cross section in dependence of Q. The observed data indicate a rapid variation of the phase of the amplitudes which might also be an indication for the presence of a quasi-bound state. In order to further investigate this system, data with a polarised deuteron beam have been acquired, enabling the study of the deuteron tensor analysing power t_{20}.

Very close to the production threshold, the η^3He system can be produced in a relative s-wave via two different initial states with total spin $S = \frac{3}{2}$ or $S = \frac{1}{2}$. Differences between these states will influence the energy dependence of t_{20} of the $\vec{d}p \to {}^3\mathrm{He}\,\eta$ reaction. In case of a pure s-wave FSI, t_{20} is required to be a constant as a function of energy.

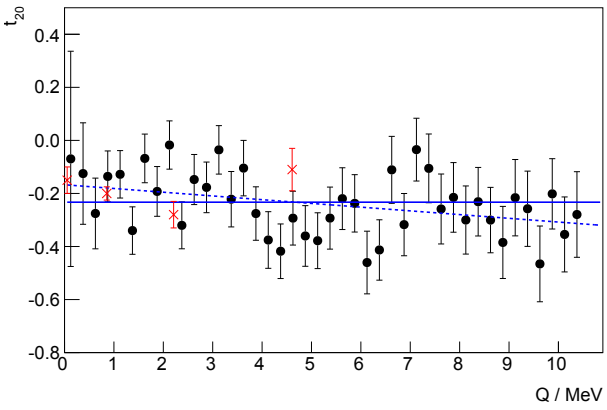

Fig. 4: The tensor analysing power t_{20} (black circles) of the $\vec{d}p \to {}^3\mathrm{He}\,\eta$ reaction. A constant (solid line) and a linear (dashed line) fit has been applied to these data. Data from Saclay (red crosses) are shown for comparison.

While the values of t_{20} were obtained by using a continuously ramped deuteron beam, the data, summed over the full ^{3}He angular range, are binned to a width of $\Delta Q = 0.25\,\mathrm{MeV}$ in order to match the statistics. The preliminary values are shown in Fig. 4. The results are consistent with values previously obtained at Saclay and can be described with a constant value of t_{20}, although a linear fit leads to a slightly better description of the data.

The unpolarised data on the differential cross section have shown a significant but linear dependence on $\cos\theta$ for $Q > 4\,\mathrm{MeV}$. In order to investigate the angular dependence of t_{20}, all events in both the forward and backward hemisphere have been summed and grouped together in Fig. 5 in $\Delta Q = 0.5\,\mathrm{MeV}$ bins. The forward hemisphere points have been plotted to the right and the backward to the left. Once again, the data have been fitted with a constant as well as with a linear function. However, the

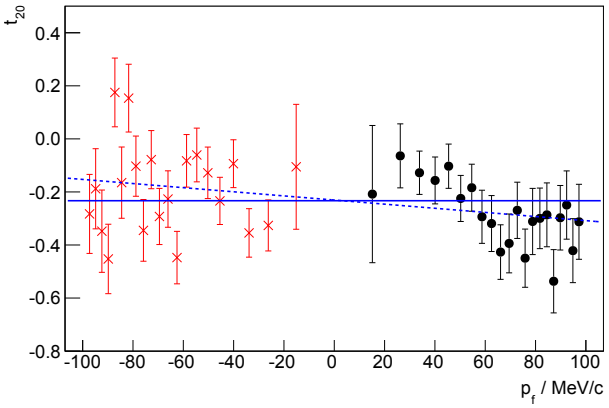

Fig. 5: The variation of t_{20} as a function of the ^{3}He c.m. momentum. The data in the forward (black circles) and backward hemisphere (red crosses) are plotted separately.

slope was found to be very small, especially when compared with the variation of the asymmetry in the unpolarised differential cross section. This kind of behaviour leads to the assumption that the spin dependence of the production amplitude can be written in terms of two independent scalar amplitudes A and B:

$$f = \bar{u}_{^3\mathrm{He}}\,\hat{p}_p \cdot (A\,\vec{\varepsilon}_d + iB\,\vec{\varepsilon}_d \times \vec{\sigma})\,u_p, \qquad (1)$$

with $u_{^3\mathrm{He}}$ and u_p being Pauli spinors, $\vec{\varepsilon}_d$ the polarisation vector of the deuteron, and $\hat{p}_p$ the direction of the incident proton beam in the c.m. frame. Any of the more complicated spin terms that might occur in the observed energy range would most likely cause a much stronger energy dependence of t_{20}. In terms of A and B, the differential cross section and the deuteron tensor analysing power may be expressed as:

$$\frac{d\sigma}{d\Omega} = \frac{p_\eta}{3p_p}\left(|A|^2 + 2|B|^2\right) \text{ and } t_{20} = \sqrt{2}\,\frac{|B|^2 - |A|^2}{2|B|^2 + |A|^2}. \qquad (2)$$

While a FSI would be common to both amplitudes A and B, it would cancel out in t_{20}, as can be shown from equation 2, leaving only a difference between the entrance channels to affect the energy dependence of the tensor analysing power. Since the square of the production amplitude has been shown to vary by more than a factor of five over the observed energy range, any spin-dependent effects allowed by the slope in Fig. 4 are dwarfed in comparison.

In conclusion, the absence of a significant energy dependence of t_{20} supports the strong FSI interpretation. Interestingly, the asymmetries of the differential cross section in $\cos\theta$ do not show up in the angular dependence of t_{20} in Fig. 5. This is considered very unlikely if p-wave contributions come into play via more complicated spin amplitudes. Instead, the lack of a forward/backward asymmetry in t_{20} might require the introduction of p-wave terms in A and B.

1.2.4 The measurement of the analysing power of small-angle proton-proton elastic scattering at ANKE

A thorough understanding of the nucleon-nucleon interaction remains one of the principal goals of nuclear and hadronic physics. Apart from their intrinsic importance for the study of nuclear forces, elastic *NN* scattering data are also necessary ingredients in the modeling of meson production and other nuclear reactions at intermediate energies. It therefore goes without saying that all facilities should try to fill in any residual gaps in our knowledge in this field. This was the underlying philosophy of very successful COSY–EDDA collaboration that carried out extensive measurements on a variety of spin-dependent observables in proton-proton elastic scattering for energies between 450 MeV and 2.5 GeV.

However, the basic design of the EDDA detector meant that only centre-of-mass angles $\theta_{cm} \gtrsim 30^\circ$ were covered and there is in fact a significant hole in the pp data base near the *forward* direction above about 1.0 GeV. As a consequence, there are severe problems with the small angle predictions of the SAID partial wave analysis above 2 GeV. The small angle region has now been studied at six energies from 800 MeV to 2.4 GeV at COSY-ANKE.

Very little is known experimentally on either the $pp \to pp$ elastic differential cross section or the proton analysing power in the angular region $5^\circ < \theta_{cm} < 30^\circ$ for energies above about 2 GeV. Those cross section data that do exist seem to fall systematically below the predictions of the SAID program! In these kinematic regions the fast proton emerging at small angles from the hydrogen cluster target can be well measured in the Forward Detector of the ANKE magnetic spectrometer. The slow recoil proton emerging at large angles can be measured in parallel in one of the Silicon Tracking Telescopes (STT). Both these devices have very high acceptance for much of this range of angles and energy and, in their overlap region, can provide invaluable cross-checks on systematic effects in the two detection systems that significantly improves the accuracy and reliability of the measurements.

One of the main tools in the measurements of the differential cross-section is the independent and accurate determination of the absolute luminosity. The technique relies on measuring the energy losses due to the electromagnetic interactions of the beam as it repeatedly passes through the target by studying the shift of the revolution frequency using the Schottky spectrum [see the IKP annual report 2011].

The new experiment at COSY–ANKE was performed in April 2013 using a polarised proton beam at six different beam energies, $T_p \approx 0.8, 1.6, 1.8, 2.0, 2.2, 2.4$ GeV that interacted with a hydrogen cluster-jet target. Elastic pp scattering events were identified by detecting one or both of the final protons in the FD and/or STT system of ANKE.

The beam polarisations were measured in parallel with the ANKE experiment by using the EDDA detection system as a polarimeter. The COSY beam was prepared as an alternating sequence of cycles with different signs of the polarisation, positive ('up') and negative ('down').

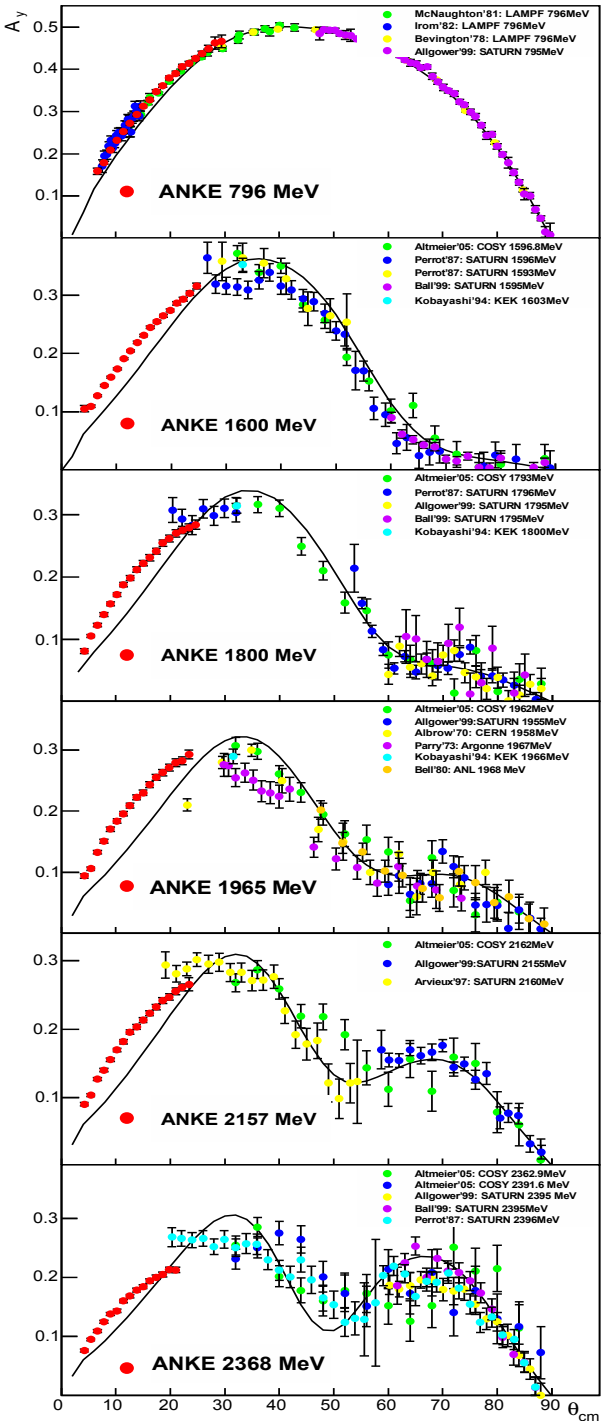

Fig. 6: The preliminary values of the analysing powers for elastic pp scattering measured with the ANKE STT at several energies (red circles) are compared to published data. Also shown are curves corresponding to the SAID 2007 partial wave solution.

After the acceleration of the injected beam from the polarised ion source, the corresponding flattop signals for the data taking at ANKE were prepared for each of the beam energies. The typical data-taking time was set at

around three minutes. In order to perform the faster polarisation determination, in the last 20 seconds at the end of each cycle, a carbon target was moved into the COSY beam and quasi-elastic scattering data were taken with the EDDA polarimeter. The average values of the beam polarisations for all the energies of the experiment are listed in Table 1. The systematic uncertainty in the absolute polarisations was estimated to be less than 5%.

Beam energy [MeV]	Average polarisation	Statistical error
796	0.5322	0.0020
1600	0.4897	0.0001
1800	0.4844	0.0025
1965	0.4395	0.0020
2157	0.4827	0.0030
2368	0.4090	0.0042

Table 1: Values of the beam polarisations measured with the EDDA polarimeter.

Elastic proton-proton scattering events were identified using the missing-mass technique. For data taken with either the STT or the ANKE Forward Detector there is a clear proton peak with minimal background, which is well separated from pion-production reactions. The data from the STT system (alone) and in coincidence with ANKE have been fully analysed. Preliminary results on the proton analysing power A_y from these measurements are presented in Fig. 6 (up to now are shown only the data from the STT system). These are compared to the available world data base and the SAID predictions. Excellent agreement is found between our results and the published data at 796 MeV, where there is little ambiguity in the experimental results or the partial wave analysis.
These first results show that ANKE is capable of providing robust pp elastic scattering data in the energy region of $T_p = 0.8 - 2.4$ GeV at small centre-of-mass angles. Further analysis is in progress and final A_y results with total errors of better than 5% are expected.

1.2.5 PAX: Recent results and future plans

The PAX Collaboration continues the program devoted to the study of viable methods to produce the first intense beam of polarized antiprotons for the future FAIR facility [see PAX Collaboration Technical Proposal at http://collaborations.fz-juelich.de/ikp/pax/documents/proposals.shtml].
In the past years, two milestones for the field have been accomplished through the experimentation with protons at the COSY ring:

- In 2008 a dedicated experiment has ruled out the use of spin-flip as a viable way to polarize in situ a stored beam [D. Oellers et al. Phys. Lett. B 674 , 269 (2009)].
- In 2011 a spin-filtering experiment with a transverse polarized hydrogen target has been successfully performed [W. Augustyniak et al. Phys. Lett. B 718 , 64 (2012)]. The measurement has definitely proven that spin-filtering can be used to polarize a stored beam in situ and confirmed that the theoretical understanding of the spin-filtering mechanism is in excellent agreement with the experimental results.

As natural extension of this activity, the Collaboration is now preparing the first ever spin-filtering test with longitudinal polarization. The motivation for this new measurement is given by the evidence that only the combination of longitudinal and transverse spin-filtering experiments allows the determination of the complete spin-dependent hadronic cross section (shown in Eq. 3). The measurement of the total cross section is the ultimative goal of the final experimentation with antiprotons.

$$\sigma_{tot} = \sigma_0 + \sigma_1(\vec{P}\cdot\vec{Q}) + \sigma_2(\vec{P}\cdot\hat{k})(\vec{Q}\cdot\hat{k}) \qquad (3)$$

In Eq. 3 $\vec{P}$ is the beam polarization, $\vec{Q}$ is the target polarization, $\hat{k}$ is the beam momentum direction, σ_0 denotes the spin-independent part, σ_1 and σ_2 the transverse and longitudinal spin-dependent parts of the total cross section respectively.
The two spin-dependent components of the cross section can be experimentally accessed from the time constants τ_1 and τ_2 of the polarization buildup obtained with transverse and longitudinal polarization respectively:

$$\tau_1^{\perp} = \frac{1}{\tilde{\sigma_1} \mathrm{Qd_t f}}, \qquad \tau_1^{\parallel} = \frac{1}{(\tilde{\sigma_1} + \tilde{\sigma_2})\mathrm{Qd_t f}} \qquad (4)$$

where $\tilde{\sigma_1}$ and $\tilde{\sigma_2}$ are the σ_1 and σ_2 cross sections integrated over the machine acceptance, $\mathrm{d_t}$ is the target density, and f the spin revolution frequency.
In order to determine σ_2 the polarization direction has to be longitudinal at the position of the Polarized Internal Target. The obtainment of a stable longitudinal direction for the beam polarization at the PAX interaction point requires the installation of a a dedicated solenoid (a so called Siberian Snake) on the opposite side of the ring, namely at the ANKE place. The snake (ordered from *Cryogenic* London,UK) is awaited at FZJ in winter 2013-14. The plan is to install it at the PAX interaction point in the commissioning phase. It will be successively moved to the ANKE interaction point to free the PAX region for the installation of the experimental setup necessary for the longitudinal spin-filtering test.
The main part of the new setup is represented by a large acceptance detector. The detector, designed in collaboration with the Ferrara-INFN, consists of 4 silicon telescopes symmetrically disposed around the storage cell in a diamond shape configuration (see Fig. 7). Each telescope will consist of three double sided silicon strip layers, the first two having a thickness of 300 μm, and the third of 1500 μm. The configuration will allow both track reconstruction and energy determination for protons up to 30 MeV (40 MeV for deuterons). A new dedicated readout and control system is under development on the basis

of the experience gained with the ANKE recoil detector. The detector construction will start in 2014.

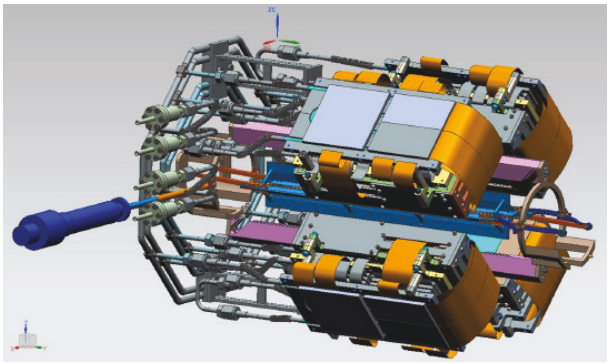

Fig. 7: The PAX large acceptance silicon detector.

The detector will measure the induced polarization in the beam by using the double spin asymmetry A_{zz} obtained by reversing the target or the beam polarizations. In the energy region of interest (50MeV - 140MeV) the spin-correlation coefficient C_{zz} is known to be large.
The same detector setup, complemented with a polarized deuterium target, will allow the Collaboration to address two additional physics goals: namely, a double polarized deuteron-breakup experiment and a test of Time Reversal Invariance. The necessary modifications to the polarized atomic source and to the Breit-Rabi polarimeter have started in 2013 and will be finalized in 2014. The implemented changes will allow to operate the target and its polarimeter both with Hydrogen and Deuterium gases without the necessity of vacuum breaks.
The present work is supported by the EU grants of the Projects I3HP2 and I3HP3 (Grant Agreements 227431 and 283286) and of the ERC Advanced Grant POLPBAR (Grant Agreement 246980).

1.2.6 Study of the ΣN Cusp in the Reaction $pN \to pK\Lambda$

The COSY-TOF detector provides high resolution data of the associated strangeness production pN $\to$ pKΛ which are exclusive and kinematically complete. Therefore, final state interactions, the influence of resonances, and possible coupled channel effects can be studied. At beam momenta around 3 GeV/c a strong cusp effect has been seen in the pΛ invariant mass spectrum at the threshold of the pΣ channel. [The COSY-TOF Collaboration, Eur.Phys.J.A.(2013)**49**:41]
In order to understand the mechanism of this cusp effect, further measurements and analyses have been performed. A detailed comparison of angular and energy distributions with model calculations may allow to extract information about the strength of the proton - Sigma interaction.
This cusp is confirmed by the analysis of a pK$^+\Lambda$ data set with 130.000 events at 2.95 GeV/c (Fig. 8 center) and with a data set of the pK$^0\Lambda$ channel with 20.000 events at

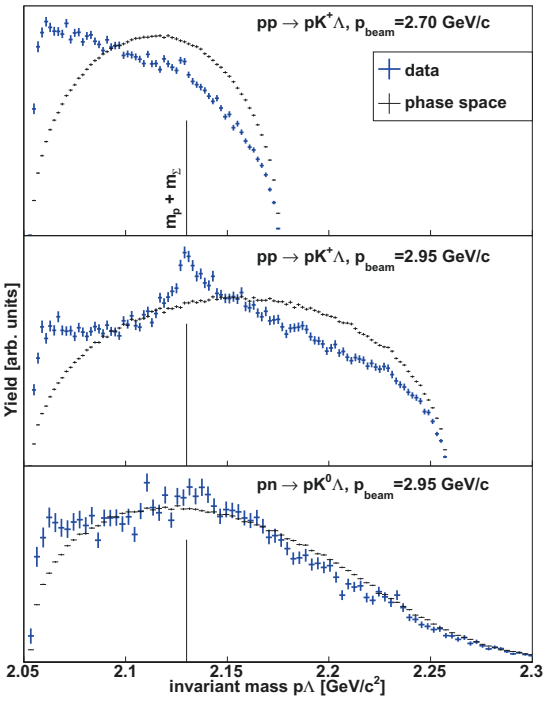

Fig. 8: pΛ invariant mass spectra. Blue data points: acceptance corrected data (preliminary), black curve: phase space, in case of the pK^0 Λ folded with the Fermi momentum of the target nucleon. The threshold of the pΣ channel is indicated by the vertical line. The excess yield at low invariant masses shown by all data curves is due to the pΛ final state interaction.

the same beam momentum (Fig. 8 lower part) a similar effect is seen. The data have been taken with a deuteron target, where the Fermi momentum of the neutron has been taken into account.
In contrast to these results a measurement at a beam momentum of 2.7 GeV/c with more than 150.000 events reveals a much weaker cusp effect (Fig. 8 upper part).
This different behavior is not yet understood. Studies are ongoing to find out, whether interference with nucleon resonances or with the coupled channel KΛ $\leftrightarrow$ KΣ causes this difference.

2 COSY Operation and Developments

2.1 Beam Time at COSY

For 2013 in total 6552 hours of operation were scheduled. 3376 hours (38.5%) were scheduled for user beam time, 2016 hours (23%) were scheduled for dedicated beam dynamic studies, equipment tests for HESR, FAIR and EDM related activities, 1160 hours (13.2%) were used for COSY machine development and experimental set-up, see Fig. 9. Maintenance/shutdown duration was 2208 hours (25.2%). The distribution of user weeks is listed in Table 2.

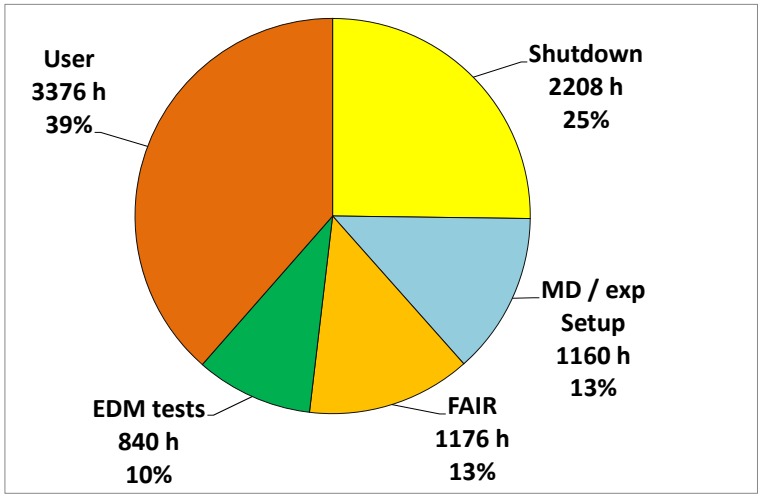

Fig. 9: COSY beam-time statistics in 2013.

Table 2: Overview COSY user beam time and EDM/FAIR weeks in 2013.

Date	Experiment	Duration	Reaction, experiment #
19.01.13.–27.01.13	WASA	1 week	Few nucleon interaction dyn. in dp collisions, 214
02.02.–10.02.	EDM	1 week	Studies of the Horizontal Spin Coherence Time, 176.6
11.02.–24.02.	EDM(JEDI)	2 weeks	EDM, COSY proposal 216
02.03.–17.03.	ANKE	2 weeks	Quasi-free $pn \to d\eta$ cross section, 211.1
23.03.–21.04.	ANKE	4 weeks	NN elastic scat. at small angles, 212
24.06.–30.06.	FAIR	1 week	Commissioning e-cooler, nights for CBM-group
08.07.–14.07.	EDM(JEDI)	1 week	EDM, COSY proposal 216
15.07.–21.07.	FAIR	1 week	FAIR, day-1 experiment
22.07.–18.08.	WASA	4 weeks	Test of the Standard Model in π^0 decays, 196.3
24.08.–08.09.	EDM	2 weeks	Extending in-plane spin coherence time, 176.7
09.09.–22.09.	EDM(JEDI)	2 weeks	EDM, COSY proposal 216
23.09.–29.09.	FAIR	1 week	FAIR, day-1 experiment
21.10.–03.11.	FAIR	2 weeks	FAIR, PANDA-STT at TOF
09.11.–24.11.	ANKE	2 weeks	Ax,z of quasifree $p_{(pol)}n_{(pol)} \to pp_s\pi^-$ reac., 213.1
30.11.–08.12.	ANKE	1 week	Spin-singlet/triplet Λp ampl. in $p_{(pol)}p_{(pol)} \to K^+\Lambda p$, 219
09.12.–15.12.	FAIR	1 week	FAIR, CBM, PANDA-MVD, Muon-chambers
16.12.–22.12.	FAIR	1 week	FAIR, beam dyn., PANDA-MVD
Total 2013		29 weeks	
user weeks		17 weeks	
EDM weeks		5 weeks	
FAIR weeks		7 weeks	

2.2 A RF-E-B-Dipole for Spin Manipulation at

Permanent EDMs (**E**lectric **D**ipole **M**oments) of fundamental particles violate both time invariance and parity and thus, according to the CPT theorem, imply CP violation. The standard model prediction for the EDM gives unobservably small magnitudes, therefore any measurement of non-vanishing EDMs would be a signature of "new physics".

EDM experiments with charged particles are only possible in storage rings. They incorporate measurements with horizontally polarized particles. To maximize the spin coherence time, systematic studies of unwanted spin rotations utilizing for instance a vertical RF–B field are required. To avoid simultaneous kicking of the beam in the transverse plane, the resulting *Lorentz* force needs to be compensated by the force of an orthogonal electric field, leading to a *Wien-Filter* configuration. This is realized at COSY in the form of a new RF-E-B-Dipole (see Figure 2). For deuterons at 970 MeV/c ($\beta = 0.459$) compensation occurs at an impedance of

$$Z = \frac{E_x}{H_y} = -\frac{E_y}{H_x} = Z_0\beta_z = 172.9\,\Omega.$$

The RF-B part consists of a 560 mm long coil made out of 6 mm copper tubes with 8 windings around a titanium coated, ceramic section of the beamchamber (see Figure 3).

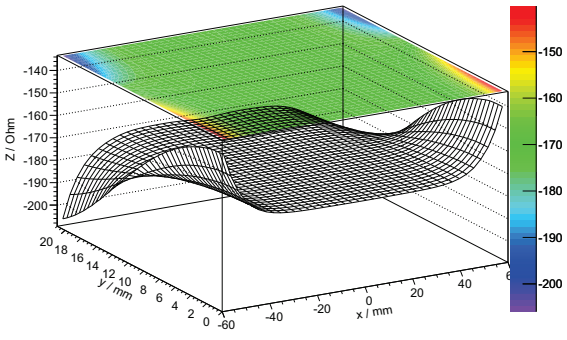

Figure 1: Simulation of the impedance distribution in the central field region.

The inductance is $L = 20\,\mu H$, this leads to a maximum magnetic flux in the horizontal plane of $\hat{B}_x = 0.40\,\mathrm{mT}$ at a current amplitude of $\hat{I} = 10\,\mathrm{A}$. The integrated field along the beam axis is $\int \hat{B}_x\,dl = 0.20\,\mathrm{T\,mm}$. Introduction of ferrites into this system will flatten the field distribution in the transverse plane, increase the inductance up to 70 µH and the maximum flux up to 0.59 mT at $\hat{I} = 10\,\mathrm{A}$. The integrated field along the beam axis will increase up to $\int \hat{B}_x\,dl = 0.33\,\mathrm{T\,mm}$.

Two stainless steel electrodes (AISI 316L) inside the vacuum chamber made out of 50 µm thin foil provide the electric field. Due to the large penetration depth of $\delta \approx 450\,\mu m$ in this material, the overall damping of the external magnetic field is negligible.The electrodes are spanned over glass rods held by a frame inside the flanges of the ceramic beam-chamber (see Figure 3). At an electrode distance of 54 mm, the required total potential difference between the electrodes is 4388 V.

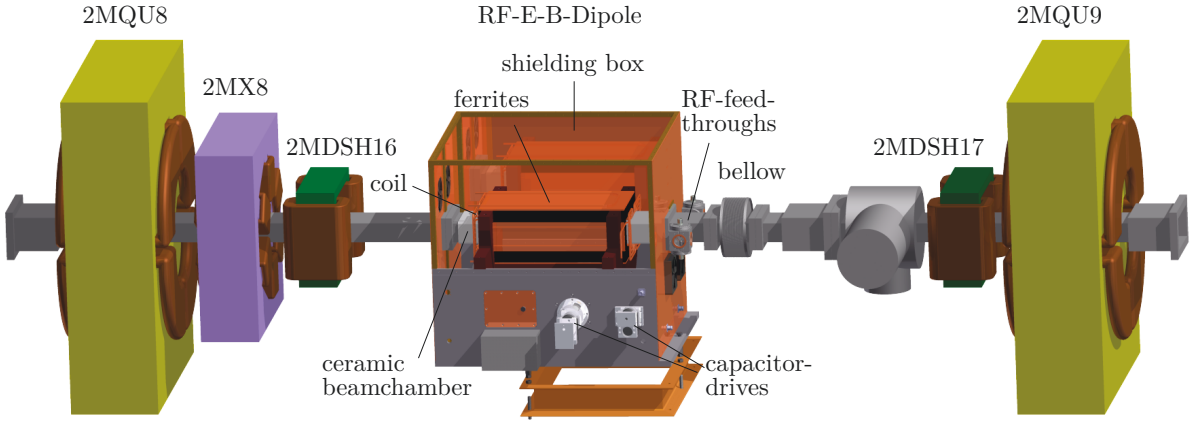

Figure 2: Location of the RF-E-B-Dipole inside a RF-shielding box in the arc of COSY.

The RF-Dipole is operated at the first few harmonics of the spin tune ($\gamma G + k$). Within the momentum range at COSY, this involves frequencies of 100 kHz to 2000 kHz. The RF-power is supplied by two separate frequency-generator and amplifier pairs. Adjustable capacitors (see Figure 2) together with the coil in case of the RF-B-Dipole and a 180°-phase-splitter between the electrodes in the case of the RF-E-Dipole form two parallel resonance-circuits. This provides the possibility of tuning the system to the required range of resonance frequencies while simultaneously matching the circuits' impedances to 50 Ω.

First successful tests of the RF-B-Dipole have already been undertaken during a beamtime of the JEDI collaboration (**J**ülich **E**lectric **D**ipole **I**nvestigations) in March of 2013. During the winter shutdown 2013, the vacuum chamber will be supplemented with the electrodes and the necessary feedthroughs. A dedicated week of beamtime in February 2014 is planned for final commissioning and calibration of the whole system

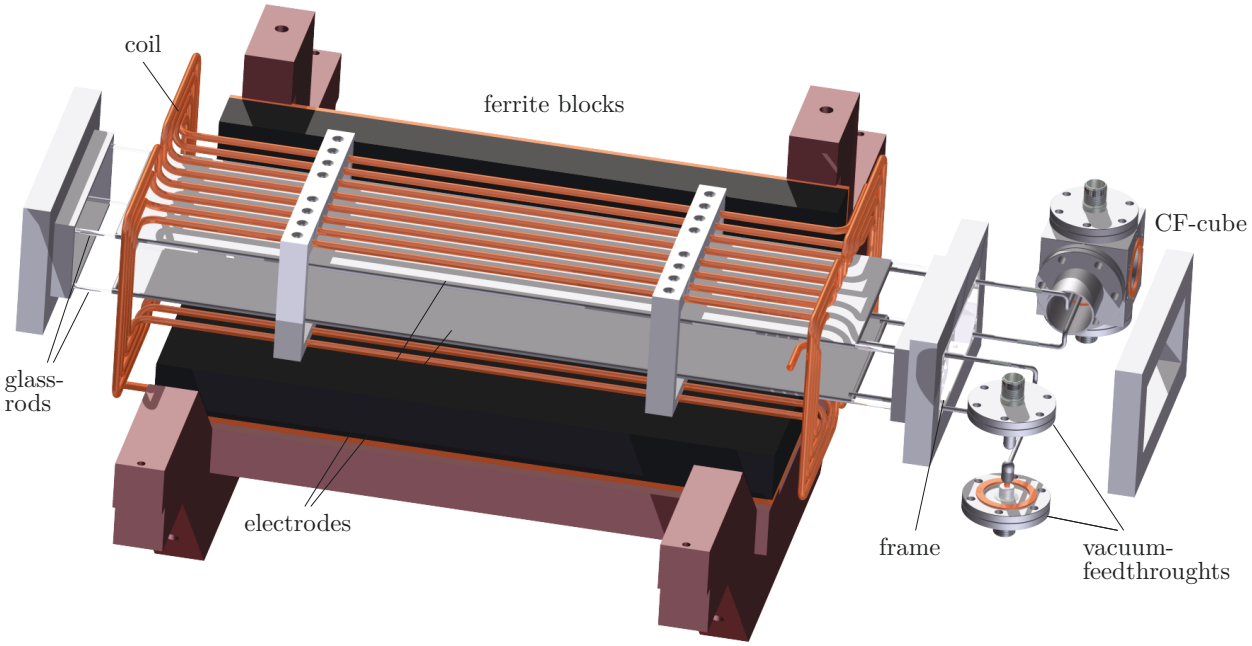

Figure 3: A view inside the RF-E-B-Dipole.

3 Theoretical Investigations

3.1 Introduction

The IKP theory group studies the strong interactions in their various settings — spanning topics in hadron structure and dynamics, the nuclear many-body problem and symmetry tests in Quantum Chromodynamics (QCD) and physics beyond the Standard Model. The main focus is on the formulation and application of effective field theories for precision hadron and nuclear physics based on the symmetries of QCD. A shift of focus with more emphasis on high performance computing is presently taking place, spear-headed by the work on nuclear lattice simulations. Since July 2012, the group is heavily involved in the activities of the collaborative research center "Symmetries and the emergence of structure in QCD" (CRC 110) together with researchers from Bonn University, TU München, IHEP (Beijing, China) and Peking University (China). Some of the high-lights of these activities are discussed in the following.

3.2 The fate of carbon-based life

Life as we know it depends on the availability of carbon and oxygen. These two essential elements are produced during helium burning in red giant stars. The initial reaction is the so-called triple-alpha process, where three helium nuclei fuse to generate ^{12}C. An essential ingredient in this reaction chain is the so-called Hoyle state in ^{12}C, which is located very close to the 3α threshold, providing the necessary resonance enhancement of carbon production. Given its role in the formation of life-essential elements, the Hoyle state has been called the "level of life". Thus it is often considered a prime example of the anthropic principle, which states that the observed values of the fundamental physical and cosmological parameters are restricted by the requirement that life can form to observe them, and that the current universe be old enough for that to happen. Nuclear lattice simulations allow to address the question whether this life-essential condition, i.e.the proximity of the Hoyle state to the 3α threshold, is robust or delicately fine-tuned by measuring its dependence on the fundamental constants of nature, specifically the light quark mass and the strength of the electromagnetic interaction. For that, we investigate the changes of all energies relevant to the tripe-alpha process as a function of the pion mass and the fine-structure constant $\alpha_{\rm em}$ by varying these around their physical values, so that all changes can be treated in perturbation theory. Further, as $M_\pi^2 \sim (m_u + m_d)$, the variation in M_π amounts to a variation of the light quark mass $m_q = (m_u + m_d)/2$. To leading order in the chiral expansion, all energies depend on variations of the pion mass through the one-pion exchange potential, the nucleon mass, the pion-nucleon coupling strength and the two lowest order four-nucleon interactions. Using data from lattice simulations, all energy variations can be expressed in terms of the quark mass dependence of the inverse singlet and triplet nucleon-nucleon scattering lengths, $\bar{A}_s \equiv \partial a_s^{-1}/\partial M_\pi\big|_{M_\pi^{\rm phys}}$, $\bar{A}_t \equiv \partial a_t^{-1}/\partial M_\pi\big|_{M_\pi^{\rm phys}}$. Based on such a representation, one finds strong correlations between the binding energy of the α particle (E_4) with the energy differences $E_8 - 2E_4$ and $E_{12^\star} - 3E_4$, with $E_8, E_{12^\star}$ the energy of the ^{8}Be ground state and the Hoyle state, respectively. This is reminiscent of α-clustering. Further, from stellar modellig it is known that the distance of the Hoyle state to the 3α threshold should not exceed ± 100 keV to generate a sufficient amount of carbon and oxygen. This translates into bounds on the variations of the light quark mass. In Fig. 10, we show "survivability bands" for carbon-oxygen based life due to 1% and 5% changes in the quark masses (in terms of the parameters $\bar{A}_s$ and $\bar{A}_t$). To be precise, for a 5% change in the light quark mass, $\bar{A}_{s,t}$ must take the values within the red (narrow) band to allow for sufficient production of carbon and oxygen. The most up-to-date knowledge of these parameters is depicted by the data point with horizontal and vertical error bars. This determination of $\bar{A}_{s,t}$ shows that carbon-based life survives at least a $\simeq 0.8\%$ shift in m_q. In addition to this "worst-case scenario", we find that the theoretical uncertainty in $\bar{A}_{s,t}$ is also compatible with a vanishing $\partial(E_{12^\star} - 3E_4)/\partial M_\pi$ (complete lack of fine-tuning). Given the central values of $\bar{A}_{s,t}$, we conclude that variations of the light quark masses of $2-3\%$ are unlikely to be catastrophic to the formation of life-essential carbon and oxygen in our universe. In a similar manner, we may calculate the corresponding changes induced by variations of the fine-structure constant $\alpha_{\rm em}$. For a fixed quark mass, we find that a variation of $\alpha_{\rm em}$ by as much as $\simeq 2.5\%$ would be compatible with the formation of carbon and oxygen in our universe. In order to make more definitive statements about carbon and oxygen production for larger changes in the fundamental parameters, a more precise determination of $\bar{A}_s$ and $\bar{A}_t$ will be needed from future lattice QCD simulations.

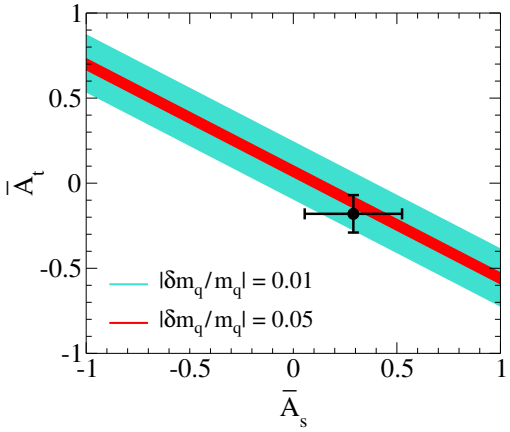

Fig. 10: "Survivability bands" for carbon-oxygen based life due to 1% and 5% changes in the light quark mass in terms of the parameters $\bar{A}_s$ and $\bar{A}_t$. The most up-to-date information on $\bar{A}_{s,t}$ is depicted by the data point with horizontal and vertical error bars.

3.3 Medium mass nuclei from nuclear lattice simulations

Nuclear lattice simulations have been established as a new quantum many-body method that allows for truely *ab initio* calculation of the properties of atomic nuclei. Here, we report on the extension of Nuclear Lattice Effective Field Theory (NLEFT) to the ground states of ^{16}O, ^{20}Ne, ^{24}Mg and ^{28}Si. NLEFT is a first-principles approach, in which chiral EFT for nucleons is combined with numerical Auxiliary-Field Quantum Monte Carlo lattice simulations. NLEFT differs from other *ab initio* methods in that it is an unconstrained Monte Carlo calculation, which does not rely on truncated basis expansions or many-body perturbation theory, nor on prior information about the structure of the nuclear wave function. As in chiral nuclear EFT, the calculations are organized in powers of a generic soft scale Q associated with factors of momenta and the pion mass. We denote $\mathcal{O}(Q^0)$ as leading order (LO), $\mathcal{O}(Q^2)$ as next-to-leading order (NLO), and $\mathcal{O}(Q^3)$ as next-to-next-to-leading order (NNLO) contributions.

In NLEFT, one computes the binding energies E_A of the nuclei under consideration by Euclidean time projection. We define $H_{\rm LO}$ as the LO lattice Hamiltonian, and $H_{\rm SU(4)}$ as the equivalent Hamiltonian with the pion-nucleon coupling $g_A = 0$ and contact interactions that respect Wigner's SU(4) symmetry. This symmetry s particulary useful as it leads to a strong suppression of the sign oscillations that plague any MC simulation of fermions at finte baryon density. In Fig. 11, we show the LO "transient energy" $E_A(t)$ as a function of the number of temporal lattice steps $N_t \equiv t/a_t$ (with a_t the temporal lattice spacing), for ^{16}O through ^{28}Si. As sign oscillations limit the maximum value of N_t, we obtain E_A by extrapolation to infinite Euclidean projection time t. The curves in Fig. 11 show a simultaneous fit to multiple trial states, with a common spectral density $\rho_A(E)$. The trial states differ in the choice of the coupling $C_{\rm SU(4)}$ in $H_{\rm SU(4)}$. The extrapolation for E_A is correlated with the isospin-symmetric correction, the sum of the electromagnetic and strong isospin-breaking corrections, and the contribution of the three-nucleon force, all of which are computed as a function of t up to NNLO in perturbation theory.

In summary, we have extended NLEFT to the regime of medium-mass nuclei, and obtained more accurate results for ^{4}He, ^{8}Be and ^{12}C than hitherto possible. While our NNLO results are good up to $A = 12$, an increasing over-binding (associated with the momentum-cutoff scale and neglected higher-order contributions) manifests itself for $A \geq 16$. While the long-term objectives of NLEFT are to decrease the lattice spacing and include higher orders in the EFT expansion, we also find that the missing physics can be approximated by an effective 4N interaction. Fixing its strength parameter from the ^{24}Mg binding energy, we find a good description of all nuclei along the α-chain. The pertinent binding energies (in MeV) are: $E(^4\text{He}) = -28.93(7)$ $[-28.30]$, $E(^8\text{Be}) = -56.3(2)$ $[-56.35]$, $E(^{12}\text{C}) = -90.3(2)$ $[-92.16]$, $E(^{16}\text{O}) = -131.3(5)$ $[-127.62]$, $E(^{20}\text{Ne}) = -165.9(9)$ $[-160.64]$, $E(^{24}\text{Mg}) = -198(2)$ $[-198.26]$, $E(^{28}\text{Si}) = -233(3)$ $[-236.54]$ with the experimental values given in the square brackets. Much work remains to be done, including detailed studies of the underlying structure of the alpha nuclei, as well as of nuclei not on the alpha ladder. The current exploratory results represent an important step towards more comprehensive NLEFT simulations of medium-mass nuclei in the future.

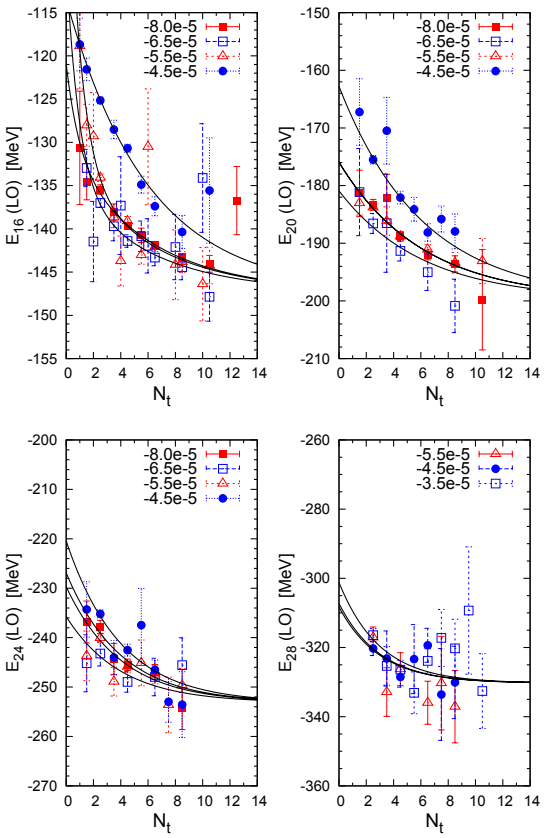

Fig. 11: NLEFT results for $E_A(t)$ for $A = 16$ to $A = 28$, with $C_{\rm SU(4)}$ given (in MeV^{-2}) for each trial state. The curves show a fit using a common spectral density $\rho_A(E)$.

3.4 Electric dipole moments of light nuclei

Under the assumption that the CPT theorem is valid, permanent electric dipole moments (EDMs) of elementary particles and nuclei, which arise under parity (P) *and* time-reflection (T) breaking, belong to the most promising signals of CP-violating physics beyond the Cabibbo-Kobayashi-Maskawa (CKM) phase of the Standard Model (SM). Possible mechanisms are the dimension-four θ vacuum angle term of Quantum Chromodynamics (QCD) and the effective dimension-six quark, quark-color, and gluon-color terms (including certain combinations of four-quark terms) resulting from extensions of the SM such as supersymmetry, many-Higgs

scenarios, left-right symmetric models etc.

However, a single successful measurement of an EDM signal of the neutron, say, would not suffice to isolate the specific CP-violating mechanism. Therefore, more than one EDM measurement involving other hadrons and (light) nuclei, *e.g.* the proton, deuteron, helium-3, are necessary in order to uncover the source(s) of the CP breaking.

From the theory point of view, the established relation between the QCD θ-term and the isospin-conserving CP-odd πNN coupling constant g_0^θ is not sufficient to predict the size of the electric dipole moment of a *single* nucleon (neutron or proton) with the help of effective field theory alone, since the calculable one-loop contributions are of the same order as undetermined counter terms. However, this feature is not present for the two-nucleon contributions of the deuteron and other light nuclei, since the former contribute already at tree-level order and can be derived up-to-and-including the next-to-next-to-leading order $\mathrm{N^2LO}$—unaffected by any counter terms. Any contribution with unknown coefficients can only show up at $\mathrm{N^3LO}$.

The dominant part of the deuteron's two-nucleon EDM from the QCD θ-term results from the isospin-violating, CP-odd πNN coupling constant, g_1^θ. The isospin-violation of this coupling can be estimated from the strong contribution to the pion mass-square splitting $(\delta M_\pi^2)^{\mathrm{str}}/(M_\pi^2\varepsilon)$, where ε is related to the light quark mass ratio. Although this ratio gives a small number, its contribution to g_1^θ gets enhanced by the relatively large pion-nucleon sigma term. Nominally, g_1^θ should be suppressed by two orders relative to its isospin-conserving counter part, g_0^θ. However, the latter is governed by the strong part of the neutron-proton mass splitting and therefore is found to be exceptionably small. Thus the isospin-violating coupling g_1^θ is effectively only suppressed by one power in the counting. This is important since the one-pion exchange with one g_0^θ vertex cannot contribute to the two-nucleon part of the deuteron EDM because of isospin selection. This was summarized in the folklore that the deuteron would be blind to the two-nucleon contributions generated by the θ-term. This folklore, however, should be abandoned. A measurement of a non-vanishing neutron, a non-vanishing proton and a non-vanishing deuteron EDM would suffice to determine the strength of the QCD θ-term, $\bar\theta$, from data. Namely, under the assumption that the electric dipole moments are driven by the CP violation that is induced by the QCD θ-term, the following relation between the total EDMs of the deuteron, the neutron and the proton and the calculated two-nucleon EDM part of the deuteron holds:

$$d_D = d_n + d_p - (5.4\pm3.9)\times 10^{-4}\,\bar\theta\, e\,\mathrm{fm}.$$

A cross-check of the so-extracted $\bar\theta$ value solely from data would be possible by a measurement of the EDM of ^{3}He. Another strategy to test or falsify the $\bar\theta$ value would involve lattice QCD calculations and just two successful EDM measurements, namely one single-nucleon EDM, *i.e.* the one of the neutron or proton, and the deuteron EDM. If even all three of them are measured, then one could use lattice QCD for a first test correlating the proton and neutron EDM results in terms of the parameter $\bar\theta$ and to use the formula from above for an additional, orthogonal test.

In case the θ-term would have failed these tests—either by a direct comparison of data or by the additional involvement of lattice QCD—then the following picture would emerge: in case $d_D - d_n - d_p$ is sizable compared to what the above equation in combination with experimental or lattice data predicts, then the dimensional analysis reveals a dominance of the quark-color EDM, feeding the coupling proportional to g_1. On the other hand, if this difference is very small, most probably neither the θ-term nor the quark-color EDM is at work, but one or several of the other dimension six CP-violating operators. More insight can be gained from a study of the EDM for ^{3}He. This reasoning stresses once more the need for high-precision measurements, not only of the neutron EDM but also of the EDMs for light ions like proton, deuteron and ^{3}He.

3.5 Finite volume effects for pion-nucleon scattering

Pion-nucleon scattering has traditionally been the premier reaction to study the resonance excitations of the nucleon. In particular, in the S_{11} partial wave one finds two close-by resonances at 1535 and 1650 MeV, which overlap within their widths of about 100 MeV. It was pointed out in the framework of unitarized chiral perturbation theory by various groups that both the $N^\star(1535)$ and $N^\star(1650)$ in the odd-parity S-wave might not be three-quark resonances, but are rather generated by strong channel couplings.

Recently, first lattice QCD calculations of the excited baryon spectrum appeared. However, for resonances decaying in a finite volume, the simple identification of state and eigenvalue is lost. The extraction of the scattering amplitude is a major challenge, it is usually based on Lüscher's method that relates the volume dependence of the energy levels measured on the lattice to the continuum phase shift. For the first time lattice QCD has provided energy levels above threshold in the $J^P = 1/2^-$ channel of πN scattering, however, for unphysical quark masses.

To analyze such a scenario, we have generated synthetic data for pion-nucleon scattering in this channel using unitarized chiral perturbation theory combined with two data sets for meson and baryon properties available in the literature. One is from the ETM collaboration and the other one from QCDSF. Depending on the masses and decay constants, resonance poles may become hidden behind thresholds as in case of the ETMC setup, see Fig. 12. In the QCDSF setup, which is an expansion around the SU(3) symmetry point of equal meson and baryon masses, there is one pole visible as a prominent resonance on the correct Riemann sheet. However,

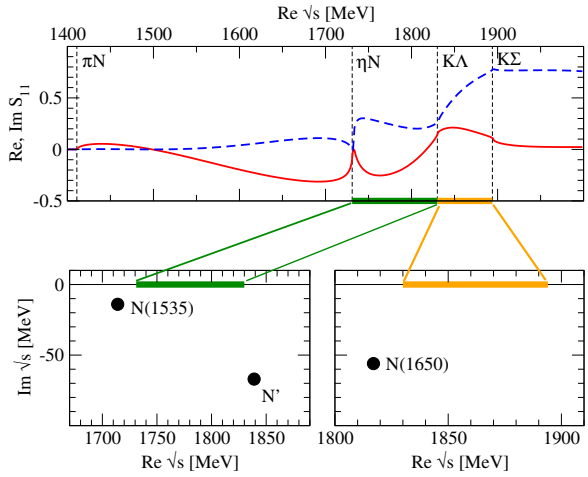

Fig. 12: Upper panel: Real (solid line) and imaginary part (dashed line) of the S_{11} amplitude, chirally extrapolated using masses and decay constants of the ETM collaboration. The vertical dashed lines correspond to the two-particle thresholds. Lower panels: two of the Riemann sheets with poles.

in this setup the threshold ordering is reversed and it is not clear, what happens to this pole as the quark masses are lowered.

For these amplitudes at unphysical quark masses, one can also predict the finite-volume level-spectrum. Resonances usually manifest themselves in an avoided level crossing. However, in S-wave there is an additional complication that inelastic thresholds induce the same pattern. If resonances are close to thresholds, it is very difficult to disentangle the dynamics, as is observed for both setups studied. The effect of the KY thresholds may be reduced by introducing twisted boundary conditions for the strange quark. Indeed, for the QCDSF setup we observe an almost L-independent level close to the resonance position. This shows that changing the boundary conditions promises indeed for a cleaner resonance extraction, although the technical realization on the lattice is intricate. In any case, modified boundary conditions for the strange quark shed light on the nature of the $J^P = 1/2^-$ resonances and their supposed strong coupling to the hidden strangeness KY channels.

A complimentary way to obtain more information from the lattice, without having to change the volume, is the use of moving frames. Unlike the $\pi\pi$ case, in meson-baryon scattering there are, however, many large higher partial waves of different parity, and the disentanglement of the S-wave contribution might become difficult. These investigations clearly show that it is possible to extract resonances in pion-nucleon scattering from lattice simulations, but that one has to overcome a fair amount of technical complications which where for the first time addressed in our study based on unitarized chiral perturbation theory in a finite volume.

3.6 Hyperon-nucleon interaction at next-to-leading order in chiral effective field theory

Over the last decade or so it has been demonstrated that the nucleon-nucleon (NN) interaction can be described to a high precision within chiral effective field theory (EFT). Following the original suggestion of Weinberg, the power counting is applied to the NN potential rather than to the reaction amplitude. The latter is then obtained from solving a regularized Lippmann-Schwinger (LS) equation for the derived interaction potential. The NN potential contains pion-exchanges and a series of contact interactions with an increasing number of derivatives to parameterize the shorter ranged part of the NN force.

Recently we performed a study of the baryon-baryon interaction involving strange baryons up to next-to-leading order (NLO) in chiral EFT, where we follow very closely the scheme applied to the NN case. As in previous investigations of the YN interaction we impose constraints from SU(3) flavor symmetry in order to reduce the number of free parameters. In particular, all the baryon-baryon-meson coupling constants are fixed from SU(3) symmetry and the symmetry is also exploited to derive relations between the various contact interactions. In the actual calculation the SU(3) symmetry is, however, broken by the mass differences between the Goldstone bosons (π, K, η) and between the baryons. For these masses we use the known physical values.

The leading-order (LO) potential consists of four-baryon contact terms without derivatives and of one-pseudoscalar-meson exchanges while at NLO contact terms with two derivatives arise, together with contributions from (irreducible) two-pseudoscalar-meson exchanges. The contact terms contain free parameters, so-called low-energy constants, which need to be determined in a fit to data. The contributions from pseudoscalar-meson exchanges (π, η, K), on the other hand, are completely fixed by the assumed SU(3) flavor symmetry.

The reaction amplitudes are obtained from the solution of a coupled-channels LS equation for the interaction potentials. This equation is solved in the particle basis, in order to incorporate the correct physical thresholds and to facilitate a proper inclusion of the Coulomb interaction. In order to remove high-energy components the potentials in the LS equation are furnished with a regulator function that suppresses contributions with momenta larger than a cutoff Λ. We consider cutoff values in the range $\Lambda =$ 500–650 MeV, similar to what was used for chiral NN potentials.

The results obtained at NLO are presented in Fig. 13 (red bands), together with those at LO (green bands). The bands represent the variation of the cross sections based on chiral EFT within the considered cutoff region, i.e. 550–700 MeV in the LO case and 500–650 MeV at NLO. For comparison also results for the Jülich '04 meson-exchange model are shown (dashed line).

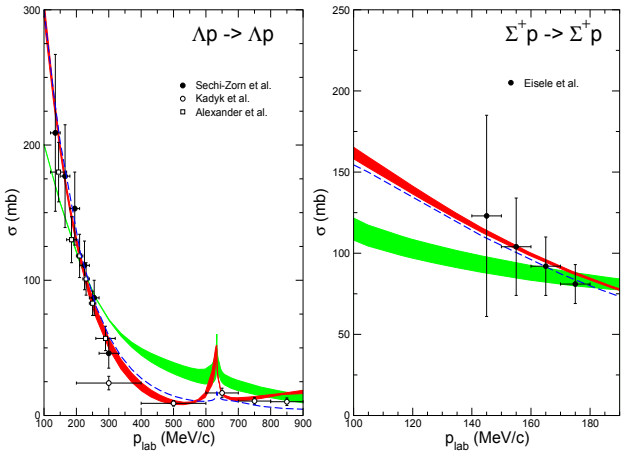

Fig. 13: Integrated cross sections for Λp and $\Sigma^+ p$ elastic scattering as a function of p_{lab}. The green band shows the chiral EFT results to LO while the red band are results to NLO. The dashed curve is the result of the Jülich '04 meson-exchange potential.

Obviously, and as expected, the energy dependence exhibited by the data can be significantly better reproduced within our NLO calculation. This concerns in particular the $\Sigma^+ p$ channel. But also for Λp the NLO results are now well in line with the data even up to the ΣN threshold. Indeed the description of the YN system achieved at NLO is now on the same level of quality as the one by the most advanced meson-exchange YN interactions. It is also worth noting that the dependence on the regularization scheme is strongly reduced in the NLO case as compared to LO.

3.7 Hunting for hadronic molecules in heavy quarkonia

With the discovery of the $X(3872)$ — a heavy quarkonium whose properties and mass is in vast conflict with the predictions of the quark model — at the beginning of this century a new era of hadron spectroscopy started. In the meantime a large number of new states was discovered that were baptized either X, or Y or Z. The last class contains isovector states in the quarkonium mass range decaying either into pions and light quarkonia or into heavy open flavor states. Those very explicitly go beyond the predictions of the quark model, for they must contain at least two quarks and two anti–quarks.

Although there are claims for the discovery of charged states in the quarkonium mass range already since a few years, the first measurement generally accepted was performed at Belle in 2012 with the discovery of Z_b and Z_b' in $\Upsilon(5S) \to \Upsilon(1S,2S,3S)\pi\pi$ as well as $\Upsilon(5S) \to h_b(1P,2P)\pi\pi$. This year the charmed analogs were discovered at Belle in $Y(4260) \to J/\psi\pi\pi$ and $Y(4260) \to h_c\pi\pi$.

Suggestions for the structure of the Z–states are

- tetraquarks - compact bound-states of a diquark and an anti-diquark,
- hadro-charmonia - compact heavy quarkonia surrounded by an cloud of light quarks and
- hadronic molecules - extended bound systems of open flavor heavy mesons.

It should be stressed that hadronic molecules are extended only, if they are shallow — to be concrete, the binding energy of a system of two open charm mesons should be of the order of 20 MeV or lower. Then, external probes should predominantly couple via the constituents of the molecular state. It is this observation that allows one to provide model independent predictions for transitions between molecular states and in this sense the test the theory. The pole corresponding to $Y(4260)$ is located only 30 MeV below the $D_1\bar{D}$ threshold and those corresponding to both Z_c and $X(3872)$ are located close to the $D^*\bar{D}$ threshold. Based on these facts, short after the discovery of Z_c we proposed that the reason for the observation of this state in the decays of $Y(4260)$ via emission of a pion could be that the $Y(4260)$, so far viewed as a prominent candidate for a QCD hybrid, is a molecular state formed from non–perturbative $D_1\bar{D}$ interactions and at the same time the Z_c is a $D^*\bar{D}$ molecule. This hypothesis is based on the observation that the loop diagram that in this case drives the transition contains S–wave vertices only (cf. left panel of Fig. 14). Those triangle loops are kinematically strongly enhanced in a limited kinematic regime which is met in the mentioned decay. Via the decay $D_1 \to D^*\pi$ this mechanism is therefore providing naturally a large number of low energy $D^*\bar{D}$ pairs leading to an efficient formation of Z_c.

In order to test the hypothesis of the molecular nature of both the $Y(4260)$ as well as the Z_c, we proposed that the $X(3872)$ must give a strong signal in the radiative decays of the $Y(4260)$. The basis for this claim is that, while the decay $D_1 \to D^*\pi$ leads to a large number of slow $D^*\bar{D}$ pairs of odd charge parity, the decay $D_1 \to \gamma D^*$ should provide an analogously large number of $D^*\bar{D}$ pairs of even charge parity which is ideal for the formation of $X(3872)$, if this state is also a $D^*\bar{D}$ molecule (cf. right panel of Fig. 14). Short after our proposal the $X(3872)$ was discovered in the transition $Y(4260) \to \gamma J/\psi\pi\pi$ providing a strong support to our picture. In addition, we also analyzed the line shape of the $Y(4260)$ in different final states such as $J/\psi\pi\pi$, $h_c\pi\pi$ as well as $D^*\bar{D}\pi$.

3.8 Analysis of pion- and photon-induced reactions

At high energies, phenomenology is well understood in terms of perturbative QCD, which is the fundamental theory of the strong interactions formulated in terms of quark and gluon fields. In the transition from high to low energies, quarks and gluons are confined in color-neutral hadrons. The precise mechanism involved remains a mystery to date. Thus, the phenomenology of

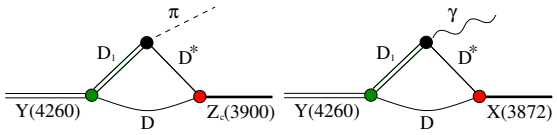

Fig. 14: Leading diagrams responsible for the transition of $Y(4260) \to \pi Z_c$ and $Y(4260) \to \pi X(3872)$, if $Y(4260)$ is a $D_1\bar{D}$ molecule and at the same time Z_c and X are $D^*\bar{D}$ molecules.

that intermediate energy region, characterized by rich and complex spectra of excited baryons and mesons, provides a key to our understanding of the fundamental properties of matter.

This theoretical interest has triggered large-scale experimental programs at ELSA (Bonn), MAMI (Mainz), and Jefferson Lab (Newport News). Analyzing such experiments and extracting the spectrum of baryon resonances is a theoretical challenge, because these objects are unstable and decay with different patterns to different final state. This requires a global analysis of reaction data of all available channels where a resonance can possibly manifest itself in. Furthermore, many of these resonances are broad and overlap in energy and therefore they can only be detected after a multi-channel partial wave analysis is performed. For the analysis, a theoretical model of meson-baryon interactions has been developed over the years, in a collaborative effort between Jülich, the George Washington University and the University of Georgia. In 2013, the analysis of the world data base of the reactions $\pi N \to \eta N$, $\pi N \to K\Lambda$ and $\pi N \to K\Sigma$ together with $\pi N \to \pi N$ was published and resonance parameters were determined. During 2013, we analyzed single pion-photoproduction data, consisting of more than 20,000 measurements of cross sections $d\sigma/d\Omega$ and single- and double polarization observables Σ, T, P, Δ_{13}, E, G, H, $C_{x'}$, and $C_{z'}$. Special attention was paid to the low-energy region where isospin breaking effects become relevant. With an additional error reflecting systematic uncertainties, a χ^2/d.o.f. close to unity could be achieved. The demanding numerics of the project required a parallelization of the code that runs on the JUROPA supercomputer.

An example for the differential cross section is presented in Fig. 15. The situation is particularly interesting because the shown energies are at the upper end of the considered interval. At midrange and backward angles the quality of the data description is comparable with the SAID and the Bonn-Gatchina analyses. Those regions are governed by lower partial waves where the resonance spectrum is found. At forward angles and for the $\pi^+ n$ final state, obviously partial waves beyond $J = 9/2$ become relevant; for the $\pi^0 p$ state and in forward direction, all available analyses miss some dynamics. The matching to the high energy regime is planned that will be the basis to search for very high-lying excited states. While in the present study a precise fit to data was achieved using

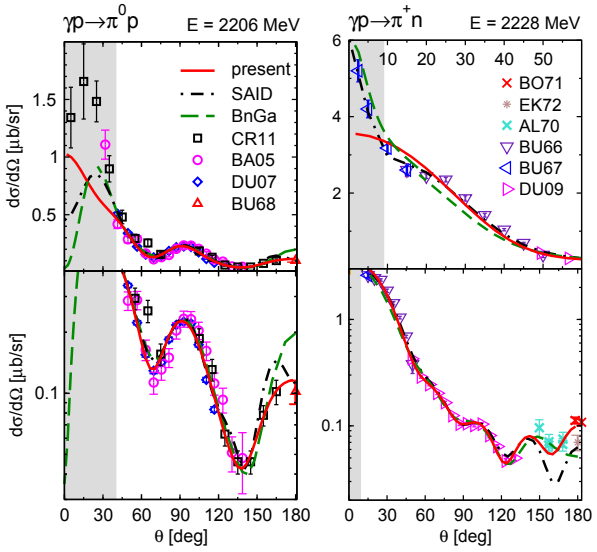

Fig. 15: High energy behavior in the reaction $\gamma p \to \pi^0 p$ (left) and $\gamma p \to \pi^+ n$ (right). The upper/lower plots show the same data/analyses but with different scales. Solid (red) lines: present analysis; dash-dotted (black) lines: GWU/SAID CM12; dashed (green) lines: Bonn-Gatchina. The regions excluded in our fit are shown as shaded areas.

a phenomenological potential, we intend to incorporate a full gauge-invariant description of the phototransition kernel that was successfully applied to a subset of data in previous studies.

The hadronic part of the interaction fulfills analyticity, two-body unitarity, constraints from three-body unitarity and other general S-matrix properties. This enables the analytic continuation to the resonance poles and, in the present study, the precise extraction of electromagnetic resonance properties.

4 Progress of the HESR

Studies of dedicated stochastic cooling scenarios, the accumulation of antiprotons in HESR due to the postponed RESR and the use of Barrier-Bucket cavities to compensate the mean energy loss due to the Panda target were finished and the HESR is now in the construction phase. Most of these studies and simulations were verified during several beam times at COSY where comparable equipment like Barrier-Bucket (BB) cavity, stochastic cooling system and several targets are installed. A 2MV electron cooler, designed and manufactured at the BINP Novosibirsk (Russia) and foreseen for the start version of the HESR was installed into COSY. First commissioning results can be found in the separate report.

Project status

Technical design work of nearly all critical components of the HESR is finished or in the final stage. Some few items for HESR are purchased by FAIR GmbH. However, the technical supervision is completely covered by our institute.

Since project start, contracts and orders have been made which already bind 35% of the project costs. The orders with longest delivery time (dipole and quadrupole magnets) were put out to tender first. The factory acceptance test (FAT) for the first quadrupole magnet is expected in March 2014, the one for the first dipole magnet is expected for June 2014. Sextupole and steerer magnets together with their power converters are part of the Romanian in-kind contribution to FAIR. Design work for further magnets (injection dipole, injection septum, PANDA chicane dipoles) is either finished or close to completion. Their orders are scheduled for 2014. Where possible, the power converters for the planned magnets have already been ordered. The first device is expected in November 2013 for FAT. The contract for the injection kicker magnets together with the pulser power converters could be awarded. Acquisition of suitable stainless steel for the vacuum chambers is difficult, but not yet critical. The needed steel is expected until summer 2014. All schedules respect to start assembly in the HESR tunnel on 01.01.2017. Efforts are made to organize intermediate storage of all components until installation in the tunnel.

Acceleration and storage of heavy ions in the HESR

A very attractive option will be the use of the HESR not only for antiprotons but also for heavy ions. Since the maximum magnetic field ramp rate in the HESR is limited to dB/dt = 25 mT/s and the maximum h = 1 cavity peak voltage to 2 kV the maximum achievable energy gain per nucleon per turn of a bare uranium ion is dT = 0.165 keV/u/turn. The option of heavy ion stochastic momentum cooling was investigated under the constraint of the present concept of the HESR. A bare uranium beam injected from the collector ring CR into the HESR at 740 MeV/u and a beam preparation for an internal target experiment was studied. Further the acceleration of the ion beam to 2 GeV/u was considered. The simulations included the beam-target interaction due to a hydrogen target. The capability of momentum filter cooling was envisaged and at lower energies (where the revolution harmonics begin to overlap) the possibility of Time-Of-Flight momentum cooling was examined. The simulation studies made use of a Fokker-Planck and a two-dimensional tracking code in longitudinal phase space to predict the properties of the ion beam for an internal target experiment. The present investigation reveals that the available cavity voltages in the HESR are sufficient for capture, preparation and acceleration of a bare uranium ion beam bunch in the HESR. The beam can either be prepared with TOF stochastic cooling for an internal target experiment at 740 MeV/u or it can be accelerated to 2 GeV/u within 17 s with the maximum available magnetic ramp rate. Fast stochastic filter momentum cooling can then be applied assisted by the BB cavity.

Stochastic cooling hardware

The main stochastic cooling system of the HESR will work in the frequency range of 2-4 GHz. The mechanical design work on the pickups and the kickers is now finished, and the production of the first cooling tank has been started in-house.

All beam-coupling structures are nearly identical and contain several ring-slot blocks. These blocks consist of sixteen wall-current monitors coupled out by eight electrodes each. Most of the signal combining and splitting take place within the vacuum envelope to reduce the number of vacuum RF feed-throughs. The long-distance transmission of the signals and the filters containing long signal delays work with near infrared optical elements.

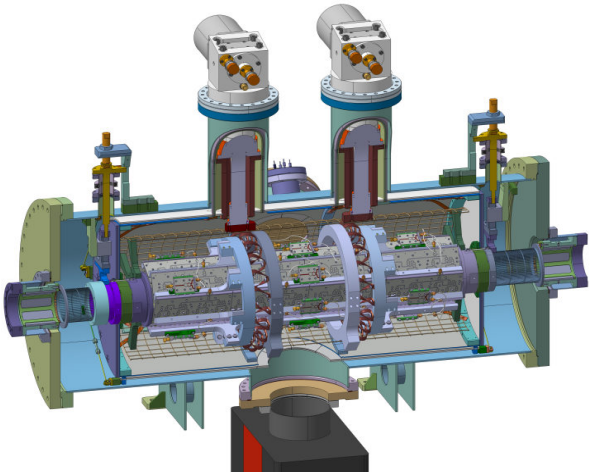

Fig. 1: Completed mechanical design of pickup tank

In a small test-tank these structures were successfully operated in the synchrotron COSY as pickup only and in a similar version of 16 slot-rings, as pickup and kicker in the Nuclotron at Dubna. This small cooling system acts as test bench for the NICA project. Ferrite dampers, installed at the beginning and the end of the kicker section, were

successfully tested at the Nuclotron during the first high power operation. At the 20th of March 2013, first stochastic cooling at the Nuclotron in Dubna was demonstrated (Fig. 2). It was the first time that the HESR structure was effectively used as kicker and it represented the first stochastic cooling in Russia.

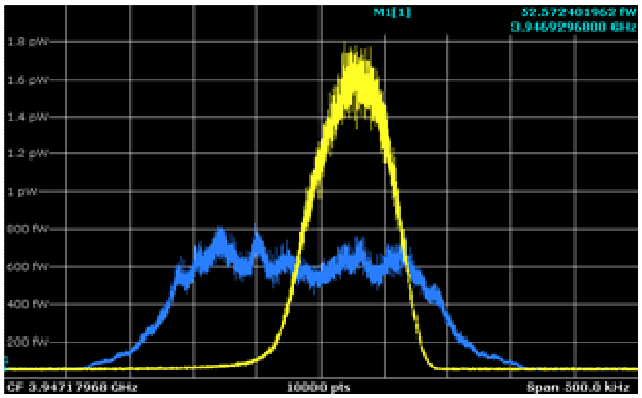

Fig. 2: First longitudinal cooling at the Nuclotron in Dubna. Blue: initial beam distribution of deuteron beam at 3 GeV and some RF-heating, yellow: stochastically cooled beam during 480 seconds of cooling

RF-system

The RF-system of the HESR will consist of two identical cavities with a common low-level RF control (LLRF). Both cavities will be driven by low noise solid state amplifiers. This offers the possibility to operate both cavities as BB cavity as well as acceleration/deceleration cavity. Each cavity contains one gap and two tanks operating in push-pull mode. One tank will be filled with 6 ring cores wound of modern magnetic nano-alloy ribbon. The combination of 2 parallel ring cores connected to one solid state amplifier together with an air cooling concept gives the best matching condition.

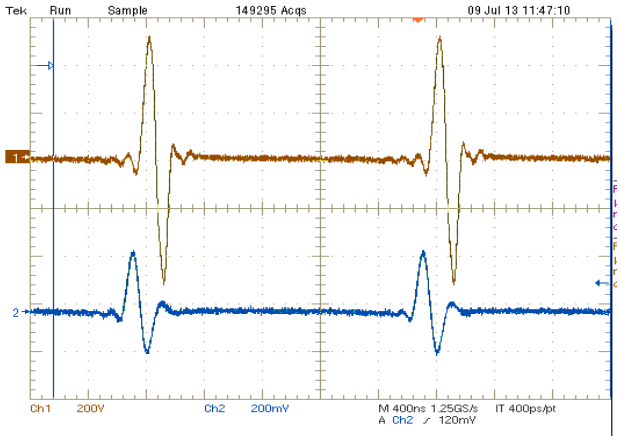

Fig. 3: Blue: pre-distorted input signal of 500W amplifier, red: corresponding output of one cavity tank with 2 ring cores (+/- 500V, 10% gap)

The influence of the parasitic elements of the rings is reduced and the individual compensations of the rings' reactances lead to a higher bandwidth compared to the usual gap coupling. The rings will only be arranged in matched pairs.

Meanwhile 14 cores have been delivered. The differences between these rings are pretty low (+/-8% deviation of the impedances at h=1 and +/-10% at h=2) which demonstrates the consistent fabrication process. Two rings were installed into one cavity and operated as BB cavity for the accumulation procedure (Fig. 3). Immediately +/-500 V have been reached with only one 500W amplifier module. At h=1 (500 kHz) in sinusoidal operation the output voltage was about +/-300 V. Thus the required voltages in all operation modes can be reached with the fully equipped cavities.

Injection

The contractor is responsible for the kicker magnets and for the electric part, and the vacuum tank will be contributed by Jülich.

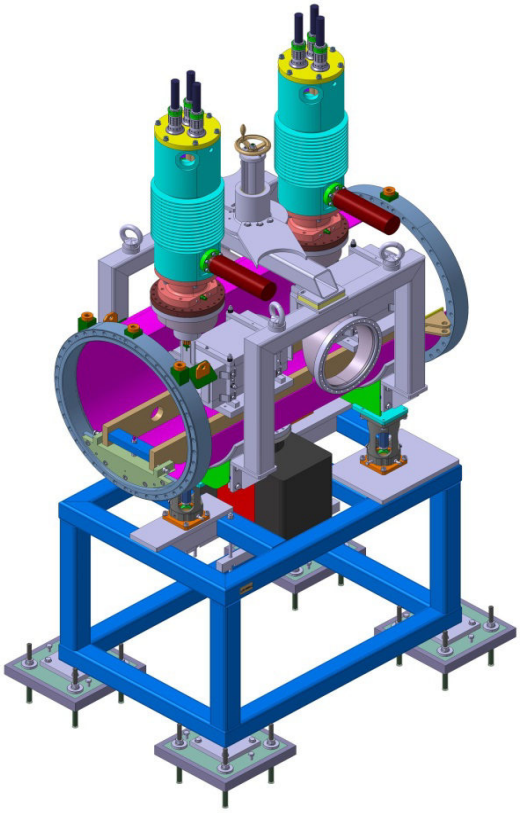

Fig. 4: mechanical design of the kicker tank including magnets, high voltage feed-throughs and support

Interfaces and details of the performance are presently negotiated with the contractor. The magnets are designed to allow a rise time of (ideally) 175 ns if parasitic impedances are neglected. For the full system a rise time of 200 ns is expected. The magnets will be driven by an IGBT-based solid state power converter (40 kV, 4.5 kA)

comparable to the one already in use at the SOLEIL synchrotron light source. The mechanics is adapted to allow (i) heating to 250° (baking) and (ii) pole reversal (protons and antiprotons!). Impedance issues are taken into account. An accepted final design including all details is expected for summer 2014.

Vacuum system

Test benches for different aspects of the vacuum system are in operation to verify that all equipment used will allow vacuum bake-out. Previously selected roll chains as flange connectors proved to be still suitable. Modern vacuum pumps (combinations including NEG material) are validated to reduce the space needed for the pumps and ancillary equipment.

The need to search for smaller equipment arouse since the limited space between the dipole magnets has to accommodate bellow elements required for 250° bake out temperature, quadrupole, sextupole, and steerer magnets and the beam position monitor most of which can be integrated into the vacuum chamber inside the sextupole magnet. The chosen design is already adapted to the details of the dipole magnets as given by their contractor. The temperature field in the dipole yoke during bake out has been simulated. The distribution of the temperature in the dipole chamber and inside the yoke will be tested in an original setup. Therefor a special heat jacket has been developed. A dedicated chamber where to attach the vacuum pumps is being designed.

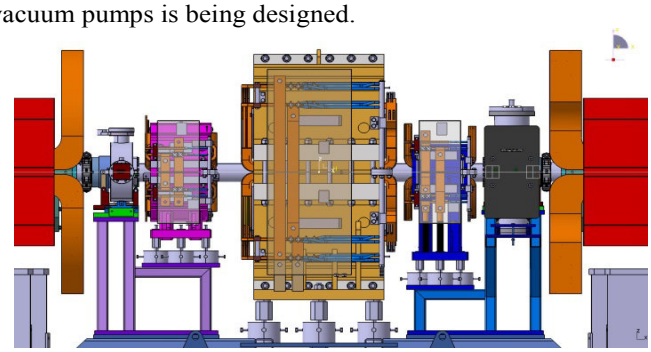

Fig. 5: Installation situation of the quadrupole section between two dipole magnets. Dipole: red, sextupole: pink, steerer: blue, quadrupole: yellow (middle).

The amount of stainless steel needed for production of the beam pipes and other vacuum vessels has been estimated. Tests for producing the bent beam pipes needed for the dipole magnets are being performed. Thus, the pipe production can start immediately when the stainless steel is available.

Magnets and power supplies

In 2012 there was a modification to the dipole magnet to comply with the requirements for laser diagnostics of heavy ions in the HESR. The dipole coils were moved apart by a distance of 20 mm to allow for the passage of a laser beam. Additionally holes with a diameter of 20mm each were foreseen in the yokes of four quadrupole magnets to let the laser beam go through.

The call for tender for dipoles and quadrupoles was published at the end of 2012. Five companies asked to take part in the tender and three companies submitted an offer.

The contract to manufacture and measure 46 dipole magnets and 86 quadrupole magnets was awarded to the French company Sigmaphi at the beginning of this year. The work on the contract started with a kick off meeting in the second half of march 2013. On the 28th of May a plan review was held.

On the 23rd of October 2013 we had the final design review for the quadrupole magnets and an intermediate design review for the dipole magnets at FZ-Juelich. There is a small delay of the dipole with respect to the quadrupole because during the design process it was decided to machine the pole contour as well as the mating surfaces of the yokes of the dipole to achieve the required tolerances. Each of the half yokes with a length of about 4.20 m will be assembled from three individual blocks. However, this will not delay the finishing of the contract in 2017. The pre series quadrupole magnet will be ready in March 2014 the pre series dipole magnet will be ready in June 2014. The copper and steel to manufacture the pre series magnets has been delivered to the contractor.

The sextupole magnets as well as the correction dipole magnets will be supplied by Romania as In Kind Contribution. The manufacturing will be done under supervision of the National Institute for R&D in Electrical Engineering ICPE-CA at Bucharest.

The quadrupole power supplies are built as bipolar secondary switched converters. Two power stations made of IGBT-H-bridges are connected in parallel, which are driven by the GSI designed Adaptive Control Unit (ACU). Due to the fact, that the control unit is designed to drive one power stage, the interlock-board needs special modifications of the FPGA, which is programmed by the contractor. Each of the two power stages has its own regulation, with a standard hall-probe as current sensor. A cascade regulation, using a DCCT, provides the correct system output.

As current measuring device, a DCCT is used, together with a preamplifier, to match the needs of the internal interface of the ACU, to the DCCT-system.

In November 2013, the first power converter will be ready for the factory acceptance test.

The PANDA Chicane dipole power supplies are built of two secondary switched MOSFET converters in parallel. Due to the high switching frequency, the contractor will develop their own control-board, to convert the USI-protocol into the PWM signals.

The injection dipole power supply is built up by two primary switched power stages. They are driven synchronously by the ACU, which is specially modified, to support primary switching technology. Like the Quadrupole converters, a cascade regulation ensures the correct output current, while each power stage has its own sub-controller. A rack mount DCCT-System serves as measuring device.

5 Day-1 Experiment at HESR

The conceptual design of the luminosity monitor for the PANDA experiment is based on measuring the differential elastic antiproton-proton scattering forward rate by 4 planes of HV-MAPS tracking detectors. The absolute precision to determine the integrated luminosity is limited by the lack of existing data in the relevant momentum region. Therefore the so-called Day-One experiment at HESR will measure antiproton-proton elastic scattering. The goal of the Day-One experiment is to measure a wide range of 4-momentum transfer t (0.0008 - 0.1 GeV^2) so that the contribution of the physical differential distribution to the absolute luminosity uncertainty is less than 1%. The polar angle of scattered antiprotons and the energy of recoil protons will be measured at forward angles by tracking detectors and by thick energy detectors near 90°, respectively. Figure 16 shows the simulated ideal t-spectrum in which the t range covered by the PANDA luminosity monitor detector and the Day-One experiment have been marked with blue and red dashed line, respectively.

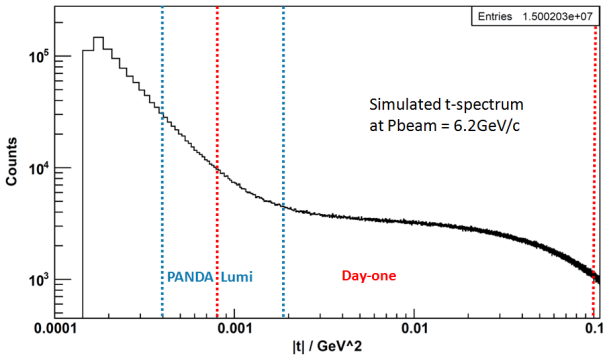

Fig. 16: Simulated t-spectrum of antiproton-proton elastic scattering.

5.1 Recoil Arm

In order to test the method proposed for the Day-One experiment one of the recoil arms of the Day-One experiment has been designed and built. It was commissioned at COSY by measuring proton-proton elastic scattering since the recoil particles are exactly the same for both antiproton-proton elastic scattering at HESR and proton-proton elastic scattering at COSY. To realize these ideas the recoil arm has been designed to match the existing hydrogen cluster target chamber at the ANKE platform at COSY, as depicted in Figure 17. Due to space limitations and the restricted opening angle, the detector plate is fixed for commissioning instead of being on a movable plate for the full version of the Day-One experiment at HESR. The detector plate is located horizontally at a distance of 1 m from the target. A gate valve was installed in-between the Day-One chamber and the target chamber, which makes further maintenance on the Day-One

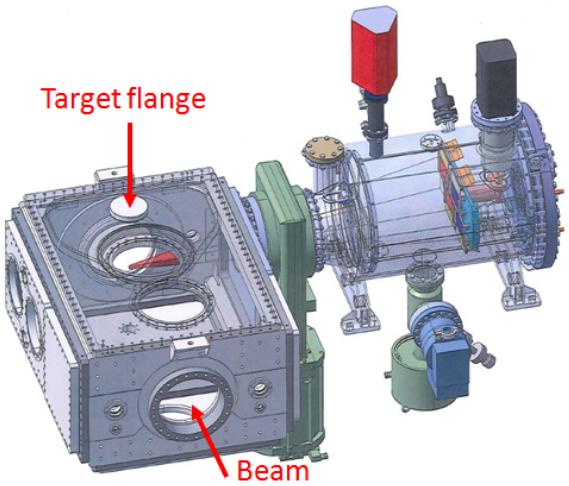

Fig. 17: Detector chamber (right) designed to match the existing target chamber (left).

chamber possible without breaking the COSY vacuum. The detector layout of the recoil arm as used for the commissioning is shown in Figure 18. Two silicon strip sensors with thickness of 1 mm have been placed at the low recoil angle, α=90°- θ, region 0°-5.7° to stop the recoil protons with energies up to 12 MeV. In addition, two germanium strip detectors with 5 and 11 mm thickness have been set up in 2 rows. They cover the maximum recoil angle α=13.6° and can measure the recoil protons with energies up to 60 MeV. All detectors have been fixed to the cold-plate with good thermal conduction. A pulse tube cold head with 30 W cooling power at 30 K has been employed in order to cool the cold-plate without strong vibration. Therefore the working temperature of the detectors could be set to any desired temperature within a large range.

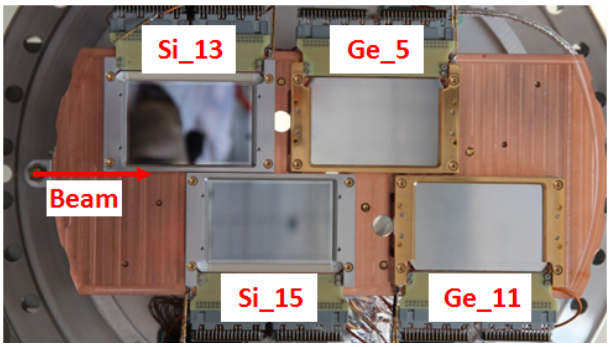

Fig. 18: Detector layout of recoil arm for commissioning.

5.2 System Test in the Laboratory

After assembly tests of the system have been performed before installing the recoil arm setup into the COSY ring for commissioning. One of the laboratory tests was to

tune the working temperature of the detector system in order to achieve the optimal performance of the germanium detector for the energy measurement. Using a ^{244}Cm alpha radioactive source, the energy resolution of the germanium detectors as a function of detector temperature has been measured in steps of 5 K. It was found that the germanium detector has better performance at higher temperature. The energy resolution of the strips has improved as the signal amplitude increased. However, the leakage current of the germanium detectors increased rapidly above 120 K. As a consequence, the energy resolution on the detector rear side worsened above 130 K. The alpha source energy spectrum on rear side of the 11 mm thick germanium detector as a function of cooling temperature is presented in the upper part of Figure 19. The lower plot of Figure 19 shows the energy resolution of 2 strips and rear side. The amplitude increase for the rear side and energy resolution improvement not only on strips but also on rear side with increasing temperature up to 125 K is clearly seen. Also the silicon detectors have gained higher signal amplitudes with higher working temperature, however there was no significant improvement on the energy resolution for the strips. In the end it was decided to set 125 K as the working temperature for day-one detector system.

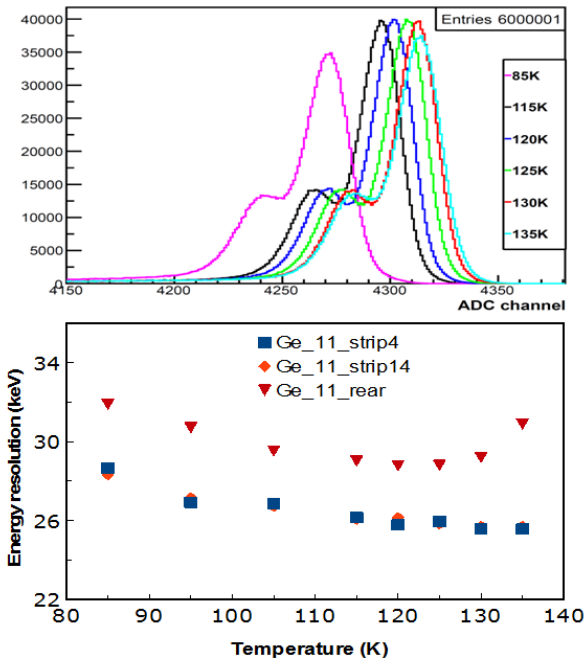

Fig. 19: Alpha energy spectra on rear side (upper) and energy resolutions of 2 strips as well as rear side (lower) of 11 mm thick germanium detector as a function of temperature, respectively.

At 125 K the achieved energy resolution (FWHM) was better than 20 keV and 30 keV for the silicon and germanium detectors, respectively.

5.3 Commissioning at COSY

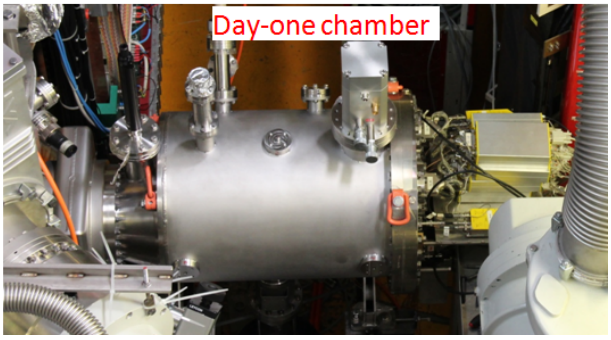

Fig. 20: The Day-One chamber has been installed inside of the COSY ring.

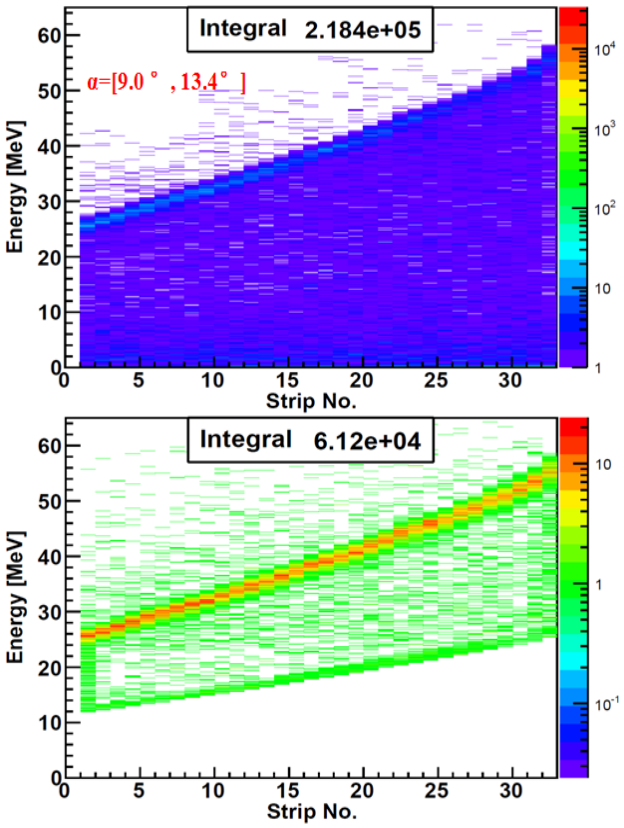

Fig. 21: The upper and lower plots show the energy spectra of the recoil protons measured by the 11 mm thick germanium detector at 3.2 GeV/c beam momentum as a function of the strip number before and after clusterization of the energy reconstruction, respectively.

The recoil arm was installed into the COSY ring in June of 2013 as shown in Figure 20. The commissioining by using proton beam has been carried out in July and September. Data of proton-proton elastic scattering at several beam momenta, i.e. 1.7 GeV/c, 2.5 GeV/c, 2.8

GeV/c and 3.2 GeV/c have been taken in two separate measurement periods. The recoil detector system worked properly during the whole beam time.
In order to reconstruct the t-spectrum based on the measured energy of the recoil protons, a careful energy determination of the recoil protons is required. The upper plot of Figure 21 shows the energy of the recoil protons as a function of the strip number measured by the 11 mm thick germanium detector at 3.2 GeV/c beam momentum. It can be clearly seen that the recoil energy of the elastic scattered protons increases with the recoil angle. However, it can also be seen that there are some hits below the expected energy. The resolution has been greatly improved after combining the deposited energy in neighbouring strips with a clustering algorithm, as shown in the lower frame of Figure 21. After completion of the energy reconstruction, the final t-spectrum will be determined.

6 The $\overline{\text{P}}$ANDA Experiment at FAIR

6.1 Introduction

The future Facility for Antiproton and Ion Research (FAIR) will be one of the largest accelerator facilities in the world giving access to a large variety of different experiments to gain new insights into the structure of matter and the evolution of the universe.

The antiProton Annihilation at Darmstadt ($\overline{\text{P}}$ANDA) experiment is one of the main experiments of FAIR. It utilizes the intense anti-proton beam with excellent momentum resolution provided by the High Energy Storage Ring (HESR) to perform precision measurements in the charmonium energy regime to improve the understanding of Quantum Chromo Dynamics.

In this regime many new and unexpected hidden and open charm states were found in the last decade where the nature of many of theses states is not clear. Strong indications exists that at least some of theses states could be exotic particles with more than three valence quarks. To distinguish the various theories about the origin of theses states a precise knowledge of the mass and the width of theses states is important. Here $\overline{\text{P}}$ANDA is the only experiment in the world which will be able to determine the width of these states down to 50 keV, compared to an upper limit of a few 1 MeV now.

An intense simulation program is ongoing to develop the needed algorithms and to determine the performance of $\overline{\text{P}}$ANDA once the experiment is running. One example for this are the simulations of the D_{sJ} mesons formed by a heavy c quark and a light s quark.

$\overline{\text{P}}$ANDA uses a novel event filter technique to reduce the raw data of the experiment by a factor of 1000 to a manageable data rate of 200 MByte/s which are stored permanently for detailed analysis. In contrast to typical hardware triggers which only look at the first stage at a small subsample of the data to find physically interesting events $\overline{\text{P}}$ANDA uses the complete dataset to distinguish signal from background events. This approach sets huge requirements on the online computing capabilities of $\overline{\text{P}}$ANDA to analyze the incoming data stream in real time and new processing architectures like GPUs are under study to tackle this challenge.

Important for the measurement of open charm states is a powerful background suppression which requires the identification of secondary vertices from D-meson decays with a $c\tau$ $O(100\ \mu m)$. This can only be done by a modern tracking system for charged particles with a Micro Vertex Detector (MVD) in combination with a large volume gaseous detector like a Straw Tube Track (STT). Both systems are under development in Jülich together with other groups inside the $\overline{\text{P}}$ANDA collaboration.

A possible extension of the MVD to include additional disk sensors in the beam direction is under discussion. These additional sensors would help to identify hyperons with a decay length of a couple of cm which have a high probability to decay outside of the MVD volume. In the original design there is a larger gap of about 1 m which could be filled with two additional sensor layers. This would help to find hyperons but on the other hand would increase the material of the detector and therefore could deteriorate the performance for other physics channels. To identify the benefit of those additional disks a simulation program is ongoing which should optimize their design and show their impact for the various physics channels of interest.

6.2 Charm Spectroscopy at $\overline{\text{P}}$ANDA: Reconstruction of the D_{sJ} Mesons

The so called D_{sJ} mesons are particles formed by a heavy quark c and a light anti quark $\bar{s}$ (and the charge conjugated); they represent a family of charged particles, with different values of the angular momentum J (J = 0, 1, or 2). The measurement of their mass and width still represents an important issue, 10 years after their discovery, as their nature remains controversial. These states are well established, as they have been observed in different decay modes and by several experiments. The recent confirmation of some D_{sJ} mesons from LHCb, and the discovery of a more rich $c\bar{s}$ spectrum compared to the theoretical expectation, has made the search of those states even more intriguing.

A system of light-heavy quarks is expected to be treated in a non-relativistic way in the potential model; therefore, the mass of these states should be precisely predicted. However, the measured masses of the states $D_{s0}(2317)^+$ and $D_{s1}(2460)^+$ do not fit theoretical expectations. Several theoretical explanations were formulated after their discovery, depending on the expectation of the width of these states (pure $c\bar{s}$ states, DK hadronic molecules, or dynamically generated resonances, etc.).

The $\overline{\text{P}}$ANDA experiment plans to measure the mass and width of these resonant states with ~ 20 times better precision than previous B factories. Our estimated rate of production is between 160000 and 1000000 D_{sJ} per day in the reaction $p\bar{p} \to D_s^- D_{sJ}^+$[1], assuming a reconstruction efficiency of 1, and using the high resolution mode. For these analysis, the beam momentum is between 9 and 10.5 GeV/c.

Here we report the first study performed with PandaRoot in order to reconstruct the mass of: $D_{s0}(2317)^+$, $D_{s1}(2460)^+$ and $D'_{s1}(2536)^+$. Their study is interesting for, excitation function of the cross section calculation, D_{sJ} mixing between $D_{s1}(2460)^+$ and $D'_{s1}(2536)^+$ and chiral symmetry breaking.

We also show the preliminary background study for the feasibility of these measurements. It turns out that the background level is higher when more photons are involved in the reconstruction chain, and it is difficult to reject with a simple cut-based analysis (see Fig. 22). For this purpose, a neural network must be built. This will be the plan for the next year. The observable here has

[1]The full reconstruction chain is $p\bar{p} \to D_s^- D_{sJ}^{(*)+}$, $D_s^- \to K^+K^-\pi^-$,$D_{sJ}^{(*)+} \to D_s^{(*)+}\pi^0$, $\pi^0 \to \gamma\gamma$

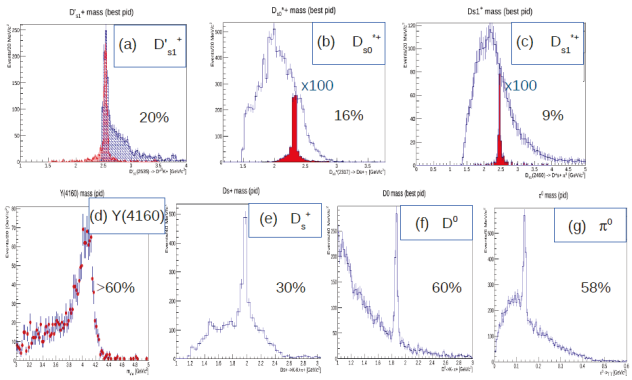

Fig. 22: Invariant mass distributions of the decay particles of (a)$D'_{s1}(2536)^{+}$ (b) $D_{s0}(2317)^{*+}$ (c) $D'_{s1}(2460)^{*+}$ (d) $Y(4260) \to e^{+}e^{-}$ (e) D_s^{+} (f) $D^0 \to K^{+}K^{-}$ (g) $\pi^0 \to \gamma\gamma$. The reconstruction efficiency values are shown in the figures, respectively.

been the mass of these 3 states; the reconstruction of the mass of all particles involved in the reconstruction chain is shown in Fig. 22, together with the reconstruction of an easy case: $p\bar{p} \to Y(4160) \to e^{+}e^{-}$.
The extraction of the excitation function of the cross section of the thin D_{sJ} mesons, which depends on mass and width of the resonant state, will allow the precise measurement of the width of those by the precise measurement of mass and luminosity. A scan of the invariant mass of the D_{sJ} decay products ($D_s^{+}\pi^0$, $D_s^{+}\gamma$) is planned every 100-200 keV/c^2. For this purpose, good tracking and PID tools are needed, especially for low momentum tracks. For this reason a careful study of the tracking tools in PandaRoot has started.

6.3 GPU Online Tracking Algorithms

We evaluate the feasibility of using GPUs[2] for online tracking at $\overline{\text{P}}$ANDA. Currently, three different algorithms are under investigation: Hough Transform, Riemann Track Finder, Triplet Finder. The algorithms all have different properties and specialize in distinct features. All three perform a circle fit in the two-dimensional (x,y) plane with a possible extension to a three-dimensional helix afterwards. The algorithms are in varying stages of development with their feature sets being investigated independently.
The development and studies are done in close cooperation with the NVIDIA Application Lab of the Jülich Supercomputing Centre.

Hough Transform For a given hit point (x_i, y_i), the Hough Transform (HT) creates a set of straight lines going through the point. This process is repeated for all hits of an event, finding the straight line connecting all hits – the track.
For the HT to work a conformal mapping pre-step is needed, transforming curved tracks to straight lines. Using these transformed hit points, the line-generating equation $\rho = x_i \cos(\alpha) + y_i \sin(\alpha)$ is solved, with α being rasterized between 0° and 180° with arbitrary granularity. When histogrammed, the (α, ρ) bin with the highest multiplicity gives the most probable set of track parameters.
Currently, two different GPU implementations of the HT exist. Both employ different programming techniques (Thrust, CUDA) and are optimized for distinct GPU features (Dynamic Parallelism). Initial studies show that the track of a single track event can be reconstructed in 0.5 ms.
For further in-depth algorithm analysis and benchmarking the development of additional tools is required as the next step in our investigations.

Riemann Track Finder The Riemann Track Finder maps two-dimensional hit points onto a virtual Riemann surface (paraboloid), creates a plane passing the mapped points, and from that deduces the parameters of the line (*track*) connecting the original points. The benefit of this method is the transformation of a circle fitting-problem to a plane calculation – a very fast technique, when the combinatorics of the seeding track points can be kept small.
Based on the Riemann Track Finder implementation in PandaRoot a first GPU port has been made. While having the same reliable and proven algorithmic structure, some GPU-specific modifications had to be made.
The GPU version is in an early stage but shows promising results, as a processing time of 0.5 ms/event has already been reached.

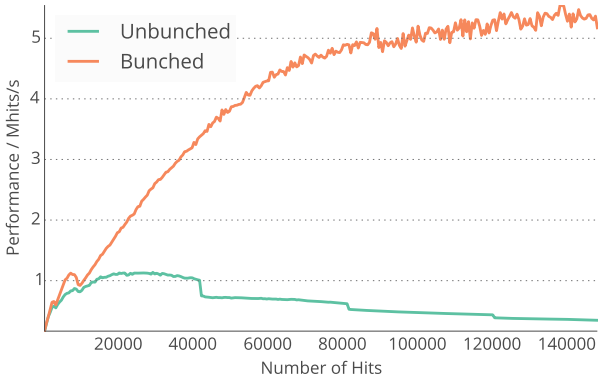

Fig. 23: Performance of the Triplet Finder with and without the bunching wrapper.

Triplet Finder A novel algorithm designed specifically for the $\overline{\text{P}}$ANDA STT[3] is the Triplet Finder. The algorithm uses a hit from a dedicated STT layer (*pivot layer*) to calculate a three-hit combination (triplet) from this hit and two adjacent hits. To form a track, this triplet is combined

[2] Graphics Processing Units

[3] Straw Tube Tracker

with a triplet of another pivot layer as well as the $(0,0)$ point. Benefits of this method are small computing times and the possibility to obtain particle tracks of sufficient resolution without using the event starting time t_0.
The algorithmic work on the Triplet Finder was started in 2012 as a CPU-only code. A GPU version of it is ported by the NVIDIA Application Lab. Additionally to the adaption of the basic properties of the Triplet Finder, some multicore-specific modifications have been made. An example is the implementation of *bunching*, a wrapping class allowing a chosen, thread-based algorithm to always run with the amount of input data corresponding to the maximum of its efficiency. The striking difference in average computing times can be seen in Figure 23. The processing time for a single track event with the bunched Triplet Finder is 0.015 ms/event at the time of writing this report.

Outlook While the basic cores are implemented, the different algorithms are in different stages of their qualitative analysis. For some algorithms, additional tools first have to be programmed in order to evaluate them. Also, the algorithms have yet to be implemented into PandaRoot, enabling a direct comparison to Monte Carlo data.

6.4 Development of a Silicon Strip Sensor Readout System

This year the first prototypes of the double-sided trapezoidal silicon strip sensors for the $\overline{\text{P}}$ANDA MVD have been produced by CiS[4] in Erfurt. They are 56 mm long and have 512 strips per sensor side. The strips on the front and on the backside of the sensor are tilted by +/- 7.5^o so that they are parallel to one edge of the sensor. The substrate is n^- doped with p^+ doped strips on the top side and n^+ doped strips on the back side.
Figure 24 shows a sensor glued onto a newly developed readout board including pitch adapters and 4 APV25 front end chips for each side.

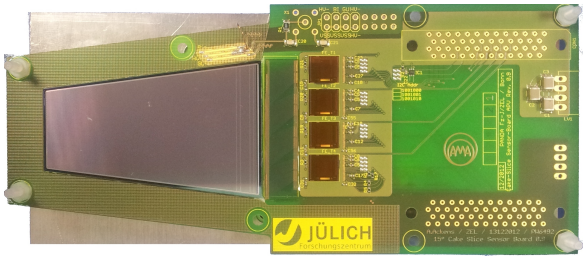

Fig. 24: A trapezoidal silicon strip sensor for $\overline{\text{P}}$ANDA MVD with readout board.

As a first test of the prototype sensors the leakage current as well as the capacitance versus the bias voltage was measured.

These tests were done with a probe station, a LCR meter, a source meter and a laptop computer. The sensor was placed on the chuck of the probe station and the bias ring and the sensor edge were contacted with two needles to provide the bias voltage. This setup is sufficient for leakage current measurements, for capacitance measurements it would be necessary to contact the backside of the sensor which is not possible. Here the probe station chuck is used as an indirect backside contact. The measurement error coming from the chuck can be neglected because its capacitance is much larger than the capacitance of the sensor.

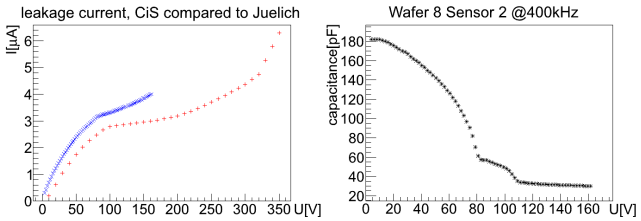

Fig. 25: IV (left) and CV graph (right). In the IV graph blue resembles the measurement done by Jülich and red the one from CiS.

On the left side of Figure 25 one can see the two different leakage current measurements done here in Jülich in blue and the one from CiS in red. The shape of both are comparable while the absolute values for the measurement here in Jülich is slightly higher which could be caused by different temperatures during the measurements. The leakage current reaches a plateau at about 100 V where full depletion is reached. On the right side of Figure 25 the measured capacitance of the sensor is shown. It decreases until a biasing of 110 V and then stays almost constant which again indicates full depletion. The determined depletion voltage in both the current and the capacitance measurement matches nicely.

Because of the trapezoidal sensor shape, the strips on the edge of the sensor have a variable length. A measurement of the capacitance of the strips versus the length of the strips should show a linear dependence which is confirmed in Figure 26. The measurement was done using 120 V as biasing voltage. Nevertheless the fluctuations around the general trend are quite large which is caused by the measurement setup at the probe station. Therefore, a dedicated test board is under development for precise capacitance measurements on the connected sensor.

The next steps for the sensor development is the readout of the sensor via the newly developed readout board and the test of it during a test with charged particles at a beam time at COSY in December.

[4] Forschungsinstitut für Mikrosensorik und Photovoltaik GmbH

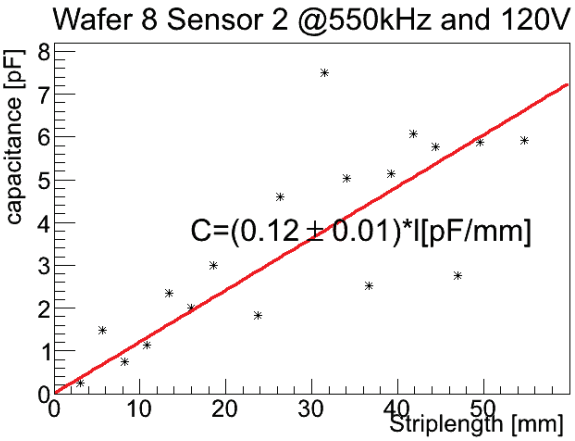

Fig. 26: Capacitance measured against strip length.

6.5 Analysis of $\Lambda\bar{\Lambda}$ decay with PandaRoot Analysis Framework

Investigations in hyperon physics is important to understand the creation of quark-antiquark pairs, in particular of the strange quark and the arrangement of quarks to hadrons. The $\overline{\text{P}}$ANDA experiment will be able to access energetically all strange hyperons and single charmed hyperons. For the reconstruction of hyperons the ground state Λ hyperon is of utmost importance. It is the lightest hyperon and it occurs in the decay tree of most of the heavier hyperons. Due to the decay via the weak interaction the strange hyperons have a comparably long lifetime with a decay length of several centimeters. Therefore, they have a high probability to decay outside the volume of the MVD which leads to a worse track quality since the MVD is the detector with the highest spatial resolution inside $\overline{\text{P}}$ANDA.

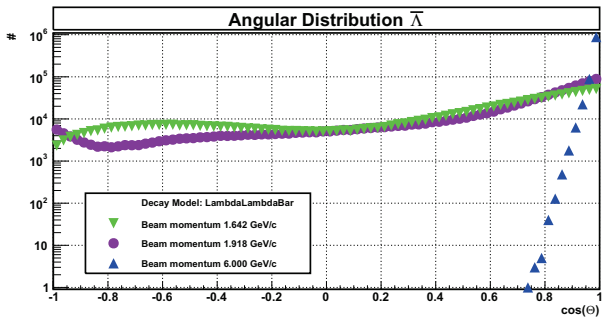

Fig. 27: Angular distribution generated by Monte Carlo of $\bar{\Lambda}$ for the three beam momenta.

To improve the quality to reconstruct hyperon final state tracks, plans exist to insert two additional semiconductor layers along the beam axis into the empty space between the MVD and the GEM stations, the so-called Λ-disks. The Λ-disks consist of semiconductor strip detectors and have a similar setup as the large MVD disks.

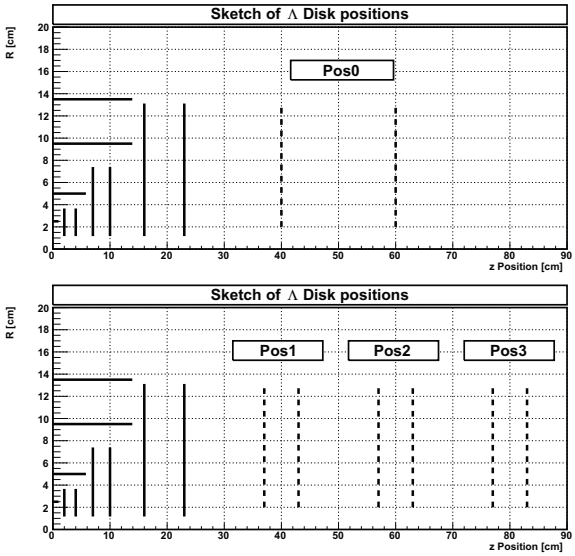

Fig. 28: Sketch of the Λ disk positions. Solid lines indicate the MVD, dashed lines the Λ disks.

A simulation should investigate the reconstruction capability of the $\Lambda\bar{\Lambda}$ decay with the PandaRoot analysis framework and the contribution of the Λ-disks to the reconstruction of Λ hyperons. The reconstruction capability has been investigated at three different beam momenta, 1.642 GeV/c, 1.918 GeV/c and 6.0 GeV/c using the angular distribution taken from previous experiments (See Figure 27).

Four different locations of the disks have been studied. The first consisting of a single disk at 40 cm and 60 cm and three configurations of a double disk at three different positions (see Figure 28). The double disk configuration has the advantage of sharing the same mechanical support structures and cooling circuits, which eases the design and improves the stability, as well as reduces the material budget.

Simulation, reconstruction and analysis has been done with the PandaRoot computing framework and the PandaGrid. The PandaRoot framework is still under development, due to this at some stages in the reconstruction process (track finding, particle identification) the usage of Monte Carlo information was necessary.

The simulation has been done with 10^6 events for each setting.

In general the $\bar{\Lambda}$ particles benefit more from the Λ-disks than the Λ particles, because they are boosted more strongly into the forward direction. The $\Lambda\bar{\Lambda}$ counting statistic rises roughly by 3.5 percent points for simulations with Λ-disks at 1.642 GeV/c. For 1.918 GeV/c and 6.0 GeV/c the counting statistic rises on average by 2.5 and 0.3 percent points, respectively. The high energy setting gains very little from the Λ-disks, since the Λ gain nothing from the disks. The Λ are emitted backward in the CMS, due to the boost of the CMS are they emitted in the lab system nearly perpendicular to the beam axis with very low momentum. Due to this it is very unlikely

Energy	Disk Position	% of reconst. $\Lambda\bar{\Lambda}$
1.642 GeV/c	-1 (no disk)	31.68%
	0	35.12% (+2.98%)
	1	34.66% (+2.98%)
	2	35.59% (+3.91%)
	3	35.18% (+3.50%)
1.918 GeV/c	-1	29.61%
	0	32.05% (+2.44%)
	1	31.95% (+2.34%)
	2	32.41% (+2.80%)
	3	32.14% (+2.53%)
6.00 GeV/c	-1	5.15%
	0	5.55% (+0.41%)
	1	5.55% (+0.41%)
	2	5.47% (+0.32%)
	3	5.46% (+0.32%)

Table 3: Counting studies of $\Lambda\bar{\Lambda}$ final state tracks.

for the final state particles to hit the Λ-disks.
The variation between the different disk settings is very low. Disk positions which are further downstream have a slightly higher gain than closer ones, but the effect is still very small.

6.6 Straw Tube Tracker

In January 2013 the Technical Design Report (TDR) of the PANDA Straw Tube Tracker (STT) was formally approved by FAIR. The construction and installation of the PANDA-STT is now being carried out in a joint project led by IKP, including institutions in Germany (FZ Jülich, GSI Darmstadt), Italy (LNF INFN Frascati, INFN and Univ. of Pavia, INFN and Univ. of Ferrara), Poland (IFJ PAN Krakow, Jag. Univ. Krakow, AGH Krakow), Romania (IFIN-HH Bucharest), and USA (North West. Univ. Evanston).
The construction phase of the PANDA-STT started this year. IKP is responsible for parts of the mechanical construction and electronic readout system together with ZEA-2. A major task is the mass production and assurance tests of all 5000 straws for the STT which is carried out at IKP. During this year, the preparations of all mechanical tools, final designs, orders of all parts for the straw assembly and definitions of quality criteria were done. The straw series production started in September this year and the first few hundred assembled straws passed all assurance tests.
Currently the final layout of all straw tubes in the STT, which consists of the exact definition of all straw positions and arrangement of the self-supporting straw multilayer modules, is close to be finished. Fig. 29 shows a mechanical setup of a PANDA-STT semi-barrel prototype with almost final dimensions.
For pre-series tests of the STT the setup of a large fraction of the modular STT detector, including mechanical frame, readout electronics and readout system for about 1000 channels, a data-acquisition system and detector

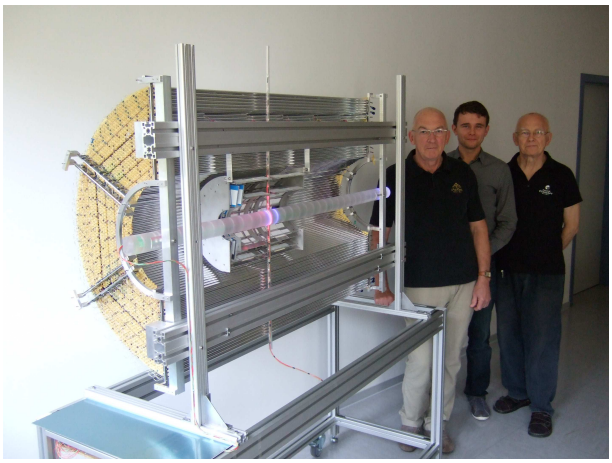

Fig. 29: Mechanical setup of one semi-barrel of the PANDA-STT. In this mock-up the horizontal antiproton beam pipe and vertical proton pellet target pipe were simplified by illuminated plexiglass tubes.

control system, all very close to the final PANDA specifications is required. A series of in-beam tests of the setups are needed, in particular for dedicated specific energy-loss measurements with the STT for particle identification. The measurement program requires different beam momenta, two different particle species and beam intensities comparable to the PANDA environment. The COSY proton and deuteron beams are ideally suited for this task. The electronic readout system of the STT has to feature a high-resolution drift time measurement ($\sigma_t \approx 1$ ns) together with a specific energy-loss determination (dE/dx) with sufficient resolution ($\sigma \approx 10\%$) to separate protons, kaons and pions in the lower momentum region below 1 GeV/c. Two different methods are exploited, either consisting of a measurement of the full analog pulse shape recorded by a high-sampling flash-ADC, or a measure of the pulse time-over-threshold for the amplitude information. First tests have been already successfully performed but further in-beam tests with high rates are needed to optimize the design and parameters for both readout systems. During this year the preparations and designs for large-scale systems consisting of up to 1000 readout channels have been finished for both. The construction of the readout systems are ongoing and it is planned to start in 2014 a campaign with dedicated in-beam test measurements at COSY.
The experience from the straw tube tracker development for the COSY-TOF experiment is a major input for the PANDA-STT design and construction, as well as for the various calibration, track reconstruction and straw data-analysis methods. The COSY-STT with its 2700 straw tubes is a global test system for the PANDA-STT with a similar technique of close-packed straw layers. The obtained high spatial resolution of 140 μm of this detector in experimental and in-beam environments is an input to determine the possible resolutions of the PANDA-STT.

Any further improvements of the COSY-STT resolutions give hints to possible optimizations for the PANDA-STT. In October 2013 dedicated in-proton beam measurements with this detector in the COSY-TOF spectrometer were carried out. Further data-takings with cosmic rays were done. During these measurements the detector was operated with different gas mixtures, different absolute gas densities and gas gain settings to investigate possible optimizations of the detector resolutions and efficiencies for the PANDA-STT. The analysis of the data is ongoing.

7 Towards electric dipole moment measurements of charged particles in storage rings

7.1 Introduction

According to our present knowledge the same amount of matter and anti-matter was created in the early universe. Since matter and anti-matter annihilate, our existence is due to mechanisms that led to an incomplete annihilation and a small excess of matter remained. In the Standard Model such mechanisms are known, they require the combined violation of two fundamental symmetries, charge conjugation and parity (CP violation). Today we know that the CP violation of the Standard Model is orders of magnitude to small to explain the matter dominance.

Measurements of electric dipole moments (EDM) of elementary particles are considered as one of the most important tools to search for CP violation beyond the Standard Model. Up to now experiments concentrated on neutral systems (neutron, atoms, molecules). For charged hadrons, no direct measurements exists. This is due to the fact that charged particles are accelerated in electric fields and thus cannot be kept in small volumes like traps. Storage rings have to be used to perform this kind of experiments. The principle of the measurement is rather simple: If an electric dipole moment exists the spin vector will experience an additional torque resulting in a change of the original spin direction which can be determined with the help of a polarimeter. Alternatively one can look for a tiny change of the spin precession frequency due to an EDM. Looking at these requirements, COSY with its capability to provide polarized protons and deuterons up to momenta of 3.7 GeV/c is an ideal starting point for such an experimental program.

Goal of the JEDI (Jülich Electric Dipole Moment Investigations) collaboration is to perform EDM measurements at COSY and to investigate systematic effects which will finally lead to the design and construction of a dedicated storage ring.

The smallness of the expected effect is what makes the experiment so challenging. To observe for example a build-up of a vertical polarization due to an EDM, one has to assure that the spins of the particle ensemble don't decohere, i.e. the so called spin coherence time (SCT) has to be large ($\approx 1000\,$s). In addition, a precise measurement of the spin tune, defined as the number of spin revolutions relative to the momentum vector per turn around the vertical axis, is mandatory. For an ideal planar magnetic ring in absence of an EDM the spin tune is simply given by the product of the relativistic γ-factor and the anomalous magnetic moment G, $\nu = \gamma G$.

SCT and spin tune were investigated in 2013 beam times and results of these measurements will be briefly presented. Approximately 10^9 deuterons with a momentum of 0.97 GeV/c were stored in COSY for about 100 s. For this momentum the spin tune is approximately $\nu = -0.16$. For both measurements an initially vertically polarized beam is rotated into the horizontal plane using a RF solenoid powered for a few seconds. In the horizontal plane the spins start to precess with the frequency νf_{rev}, $f_{rev} \approx 781\,$kHz being the revolution frequency of the beam. The decrease of the horizontal polarization is a measure of the spin coherence time. The horizontal polarization is proportional to the up-down asymmetry of elastically scattered deuterons on a carbon target. This asymmetry is modulated by the spin precession: If the in-plane spin vector points perpendicular to the particle momentum the measured up down asymmetry has a maximum and equals the product of analyzing power and polarization. If the spin vector points parallel to the momentum vector, the asymmetry vanishes. The functional form is given by

$$A_{\text{up, down}}(t) = A_0 \mathrm{e}^{-\mathrm{t}/\tau} \sin(\nu \mathrm{f}_{\mathrm{rev}} \mathrm{t} + \phi) \tag{5}$$

assuming an exponential decay of the polarization with the SCT τ.

7.2 Spin Coherence Time

Without any measures the horizontal spins decohere within a few ms. This is due to the fact that particles deviate slightly in momentum ($\Delta p/p \approx 10^{-4}$) and the spin tune depends on the momentum via the relativistic γ-factor. Turning on the accelerator RF cavities has the effect that the particle momentum oscillates around the reference particle momentum and the SCT increases to few seconds, still orders of magnitude too short for EDM measurements. Because the revolution frequency is fixed by the RF cavity frequency, particles with different path lengths necessarily differ in velocity which implies a spread in spin tune. Different path lengths can be compensated by appropriate sextupole settings and lead thus to an increase in SCT. Fig. 30 shows the horizontal polarization as function of time for two different sextupole corrections leading already to SCT of up to 400s. Note that Fig. 30 shows only the envelope of a 126kHz oscillation of the horizontal polarization. For the case of a 400 s spin coherence time this corresponds to a quality factor of $3.2 \cdot 10^8$.

7.3 Spin Tune

Whereas for SCT measurements one is interested in the amplitude of an oscillation, the spin tune can be deduced from the frequency of the oscillation in Eq. 5. It should be noted that only very few events occur in one oscillation period of about 8μs. With a detector rate of 5 kHz on average one event is recorded every 25th period. This excludes a direct fit to the data, more sophisticated analysis methods had to be developed. Starting with a first approximation of the spin revolution frequency $f_0 = \nu_0 f_{rev}$, one divides the detection time of each particle by the assumed oscillation period $T = 1/f_0$ and retains only the fractional part. With this procedure all events are mapped

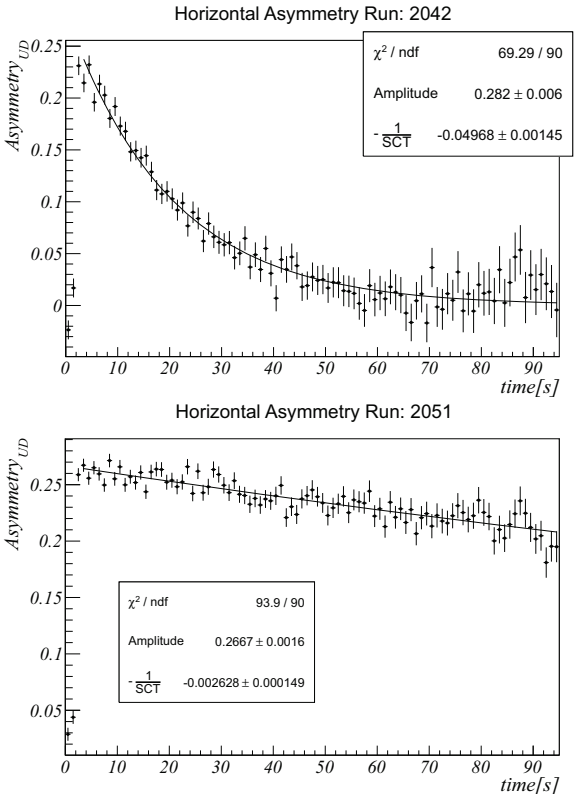

Fig. 30: The horizontal polarization as a function of time for two different sextupole settings.

into the first period of length T and the function given in eq. 5 can be fitted to the data using the fixed frequency f_0. This procedure is applied in macroscopic consecutive time intervals of about 2 s during one accelerator cycle of approximately 100 s.

Fig. 31 shows the phase parameter obtained form the fits in each of the 2s intervals. If the assumed first approximation of the spin tune ν_0 was correct, one expects a constant phase vs. time. If the actual ν deviates from ν_0 but is constant over time, one expects a linear phase dependence. Fig. 31 reveals a more complex structure, the phase depends in a non-linear way on time. Since the frequency is measured in units of f_{rev}, i.e. f_{rev} is fixed, this means that the spin tune changes during the cycle. Fig. 32 shows the spin tune determined from the slope of the phase using 2 consecutive phase measurements. A unprecedented precision of 10^{-8} per 4 second time interval is reached. Assuming a linear spin tune dependence an even higher precision of 10^{-10} for the average spin tune in a single 100s cycle is obtained from a parabola fit to Fig. 31 This corresponds to a relative precision of $10^{-10}/0.16 = 6 \cdot 10^{-10}$. Further investigations for the reason of the spin tune change during the cycle are ongoing.

7.4 Plans: Electrostatic deflectors

In parallel to the achievements described above, there a various activities presented in individual contributions of this annual report. Spin tracking programs are developed

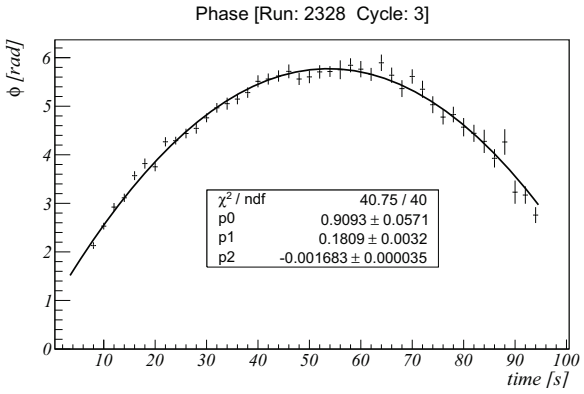

Fig. 31: The phase as a function of time in the cycle.

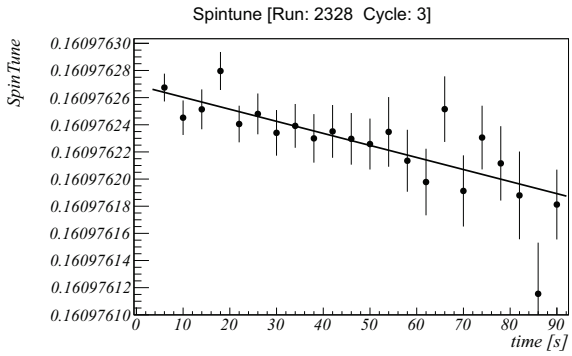

Fig. 32: Spintune determined form the change of the phase.

to arrive at a detailed understanding of spin motions in the accelerator. One goal is to understand the spin coherence time spin tune observed in the data (S. Chekmenev, A. Ivanov, M. Rosenthal, D. Zyuzin). Another field of activitiy is the construction of radio frequency electric and magnetic field devices to manipulate the spin (S. Mey). A first test is foreseen during the beam time in February 2014. New electronics for the EDDA polarimeter was developed and installed in 2013 (F. Hinder) and concepts for a new polarimeter are worked on (P. Maanen). More detailed description of the data analysis on spin coherence time and spin tune can be found in the contributions of G. Guidoboni and D. Eversmann, respectively. Results on beam diagnostics are described in the contribution of K. Grigoriev. Methods to determine an EDM signal by spin tune shifts are dicussed in the contribution of A. Saleev. This is a common effort of COSY proposal 176 and the JEDI (Jülich Electric Dipole Moment Investigations) collaboration. JEDI is part of the JARA section FAME (Forces And Matter Experiments).

8 Further Experimental Activities

8.1 Nuclear Polarized Hydrogen and Deuterium Molecules

Since more than 30 years T-shape storage cells have been used to increase the target density of polarized internal targets in storage rings, e.g., at the ANKE experiment. With this method the target density of the polarized atomic jet from an atomic beam source (ABS) of about $\sim 10^{11}$ can be raised up to 10^{14} atoms/cm^2. The price one has to pay is the expanded interaction region of the ion beam and the polarized target and a smaller polarization due to severall effects. During wall collisions and spin-exchange interactions of the atoms the polarization is partly lost. Even recombination of the atoms into molecules on the cell wall decreases the polarization of the protons (deuterons) in the cell. How to minimize these effects was studied for the first time by Price and Haeberli in 1993. Following their experience the storage cells for the ANKE experiment are made from aluminum which is covered by Teflon. In the same measurements they showed that the recombined molecules have in first order no polarization. But in the following years three groups from NIKEF, IUCF and DESY reported that they have found polarized molecules where, at least, half of the inital atomic polarization was preserved in the molecules.
Already a long time ago Price and Haeberli suggested that the best method to measure the polarization of atoms and molecules in a storage cell would be to ionize both particles in a strong magnetic field and accelerate the produced ions into a Lamb-shift polarimeter to investigate the nuclear polarization of atoms and molecules independently. Based on this idea a collaboration between the PNPI in St. Petersburg, the University of Cologne and the research center Jülich built a vacuum chamber with a superconducting solenoid at liquid helium temperatures (see Fig. 33). Inside this solenoid is a 40 cm long storage cell with 10 mm inner diameter made from fused quartz. The inner surface was covered e.g. with a thin gold film or other materials like liquid FOMBLIN. The cell can be cooled down to temperatures around 40 K via contact to the liquid helium tanks and can be heated up to 120 K without reasonable helium losses. To feed the cell with polarized hydrogen (deuterium) atoms the ANKE-ABS is mounted on top of the vacuum chamber, during times when ANKE it is not used. On the left side an electron gun produces an electron beam of 0.1 - 1 μA at about 100 eV beam energy which is focussed through the storage cell. The storage cell itself can be set to a potential up to +8 keV to accelerate the ionized particles, protons and H_2^+-ions into the Lamb-shift polarimeter (LSP). The Wien filter of the LSP is used to separate the protons and the H_2^+-ions due to their different velocities. To our surprise the LSP was able to measure the polarization of the H_2^+-ions directly without any influence of the Wien filter to the direction of the polarization.

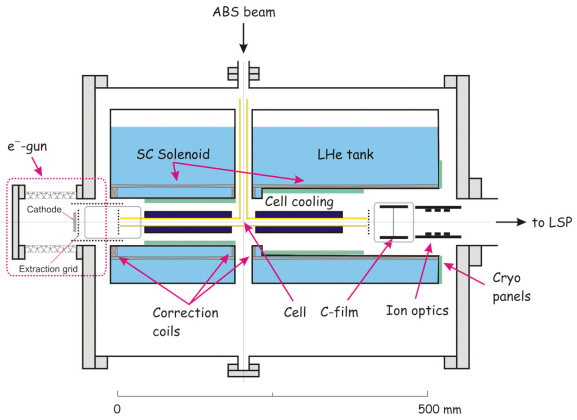

Fig. 33: The experimental setup: Inside a superconducting solenoid storage cells with different surfaces are set to a potential of 1 keV. The storage cells are fed with the polarized hydrogen (deuterium) atoms from an ABS above. An electron beam ionizes both, atoms and recombined molecules, into protons or H_2^+-ions, which will be accelerated and focussed into the Lamb-shift polarimeter on the right side.

When a molecule hits the wall it will lose an amount of polarization which depends on a so-called critical magnetic field B_c, defined by the molecule properties, and an external magnetic field. Therefore, the average polarization of the molecules $P_{(B,n)}$ inside of a storage cell as a function of an external magnetic field B and the average number of wall collisions n can be discribed as:

$$P_{molecules,(B,n)} = P_m \cdot e^{\,n\,(\frac{B_c}{B})^2}$$

with:
P_m:= nuclear polarization of the molecules after recombination

Until the nuclear polarization is not disturbed during the ionization of the molecules and the charge exchange reaction in the Cs cell this function can be measured with the polarization measurement of the H_2^+-ions in the LSP. When the polarization of the protons is measured the situation is changed, because the protons produced from the molecules will show the same dependence on the magnetic field as the molecules. But the polarization of the atomic hydrogen shows a different behaviour. If only hydrogen atoms in hyperfine state 1 were injected the polarization does not depend on the magnetic field B and the polarization of the protons is:

$$P_{protons\ (B,n)} = a \cdot P_a + b \cdot P_m \cdot e^{\,n\,(\frac{B_c}{B})^2}$$

with:
a:= relative amount of the protons produced from atoms,
b:= relative amount of the protons produced from molecules
P_a:= polarization of the atoms.

With the known relation of the ionization cross section of $\sigma_{H_2->H^+} = 0.2 \cdot \sigma_{H->H^+}$ the recombination c:= (Number of molecules) / (number of all particles in the cell) can be calculated very precisely:

$$c = \frac{b}{b + a/5}$$

An example of such measurements on a FOMBLIN film inside the fused quartz cell is shown in Fig. 34. Here, only hydrogen atoms in the hyperfine state 3

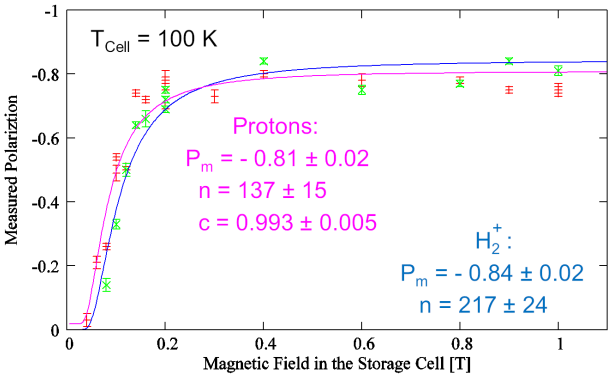

Fig. 34: The measured polarization of the H_2^+-ions (green) and the protons (red) as a function of the magnetic field inside of the storage cell (T=100 K) when hydrogen atoms in hyperfine state 3 were injected. From a fit a nuclear polarization of the molecules of $P_m = -0.84 \pm 0.02$ was determined.

were injected into the storage cell that was cooled down to 100 K. The different polarization values of the H_2^+-ions (green points) are fitted by the given formula (blue). Therefore, the polarization of the molecules was $P_m = -0.84 \pm 0.02$ and the number of wall collisions was $n = 170 \pm 19$. When the polarization of the protons was measured (red points) it was obvious that the recombination inside the storage cell was very high. A fit to the measured data delivers $c = 0.993 \pm 0.005$ and a polarization of the molecules of $P_m = -0.81 \pm 0.02$. Within the errors the results of the different measurements agree. Nevertheless, a little bit lower proton polarization is possible due to the fact that during ionization an unpolarized proton background will be produced from residual gas, e.g. water, much more often than H_2^+-ions. Another interesting fact are the different average numbers of wall collisions determined with both particles. Like described before the H_2^+-ions, which are leaving the storage cell for the LSP, are produced mainly at the ends of the cell. Therefore, the average number of $n = 170 \pm 19$ must be higher, because the molecules with just a few wall collisions in the center of the cell do not contribute to this number. This value corresponds to the average numer of wall collisions the molecules undergo when they are leaving the cell. The average number of wall collisions for all molecules in the cell is measured with the protons and $n = 107 \pm 13$ fits to the simulated average number of wall collisions inside the cell when only elastic scattering at the wall is assumed.

The other investigated surface materials so far, gold and fused quartz, show a similar behaviour. The recombination was large ($c > 95\%$) and the molecules are partly polarized with e.g. $P_m = 0.45 = 1/2 \cdot P_a$ for the gold surface.

Only water prevents the recombination at 100 K efficiently and only at temperatures of 50 K the recombination was increased to $c \sim 0.8$. Here, it should be mentioned that a cold surface in vacuum will adsorb a water film from the residual gas very fast. Even the cryo panels mounted at the liquid helium tank could not avoid this effect for more than a few hours, because the major amount of the water comes from the ABS. Only heating of the surface at least twice per day could avoid this water film in first order.

A first measurement with deuterium atoms in a fused quartz cell showed that the critical field for vector-polarized deuterium is $B_c(D_z) = 7 \pm 1$ mT and for tensor-polarized deuterium $B_c(D_{zz}) = 10 \pm 1$ mT. In this first step a vector polarization of $P_m(D_z) = -0.4 \pm 0.01$ and a tensor polarization of $P_m(D_{zz}) = -0.24 \pm 0.03$ was reached for the deuterium molecules when deuterium atoms in the hyperfinestate 3 and 4 were injected into the cell.

With this setup it is now possible to measure the polarization of atoms and molecules in different storage cells at magnetic fields up to 1 T with very good precision. In addition, the recombination on different surfaces can be determined in a temperature range between 40 and 120 K. Even the average amounts of wall collisions of the molecules inside the cell and when they are leaving the cell can be measured. In principle, with this knowledge a new storage cell can be built were the atoms might recombine on a FOMBLIN film into fully polarized molecules at very low temperatures. Then, the polarization in conserved but the target density is increased due to the lower velocity of the molecules as compared to the atoms. But in this case, magnetic holdings fields of 0.3 T or more are needed, depending on the number of wall collisions, to avoid the polarization losses of the molecules and the buildup of a water layer must be suppressed.

This work was supported by the International Science and Technology Center (ISTC No. 1861) and the Deutsche Forschungsgemeinschaft (DFG Project 436 RUS 113/977/0-1).

8.2 A laser-based thermal neutron source

MeV and thermal neutrons provide an important tool for studying the properties of materials. The most intense neutron sources nowadays are fission reactors and particle accelerators, but they are costly to build and research groups compete intensely for access. A cheaper and more portable alternative is to generate neutrons via the acceleration of protons or deuterons by high-energy laser pulses. The principle layout of such a set-up for MeV-neutron production is sketched in Fig. 35.

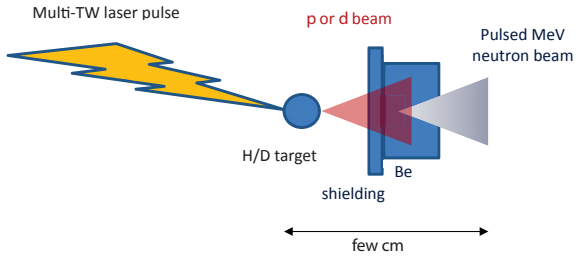

Fig. 35: Layout of a laser-based neutron source.

A measurement of neutron yields has been carried out with the 200-TW TRIDENT laser (pulse duration 600 fs, wave length 1.053 μm) using thin ($\sim$ 400 nm) CH_2 and CD_2 foils as targets. Fluxes of up to 10^{10} n/sr per shot have been observed for typical neutron energies of a few MeV. The duration of each neutron bunch should roughly correspond to that of the laser pulses (*i.e.* be around 1 ps). The laser-particle group of the FZJ (with members of the IKP and the Peter-Grünberg-Institute (PGI-6)) will start to carry out experiments on neutron production at the 200-TW Arcturus laser in Düsseldorf in 2014. For improving the performance of a later neutron source, we aim at the use of novel target concepts; as a first step a Hydrogen cluster-beam embedded in a conventional gas jet will be employed, *cf.* Fig. 36. Such a set-up would have several advantages: the target consists of the pure target material (no backing metal foil), individual clusters are completely accelerated and there is no target activation. Furthermore, the target material is constantly re-supplied to the interaction zone which allows for operation at maximum laser-repetition rates (up to 1 kHz are possible with few-TW lasers). The cluster source has already been prepared at Münster University, see Fig. 37

In order to estimate the particle fluxes at JuSPARC — the planned laser-based Jülich Short-pulsed Particle and Radiation Center at FZJ — we have carried out simulations with the particle-in-cell code EPOCH on Juropa. These have been performed for different stages of JuSPARC (10 TW @ 100 Hz and 1.5 PW @ 0.1 Hz) and typical cluster radii of 500 nm which are embedded in a H_2 gas. At 1.5 PW proton (and thus neutron) fluxes are obtained that are roughly comparable to those at TRIDENT. Even with the first JuSPARC stage (10 TW) p or d fluxes of $\sim 10^8$ /MeV per shot in the range 0–10 MeV are expected. Since neutron production in the Be(p,n)X process

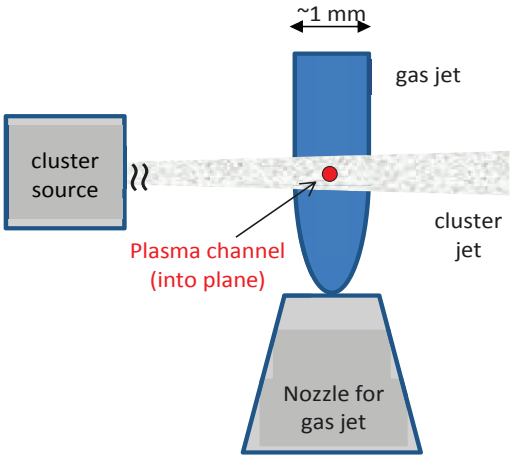

Fig. 36: Sketch of an experiment with a combined gas/cluster-jet target. The gas provides a relativistic channel of about 1 mm in length and 10 μm in diameter which the laser maintains its focused intensity, *i.e.* it increases the probability to hit a cluster at highest intensity by a factor of $\sim$ 100.

requires energies of at least $\sim$ 5 MeV and a laser repetition rate of 100–1000 Hz is foreseen, this would allow one to carry out exploratory studies with JuSPARC already at an early stage of the project.

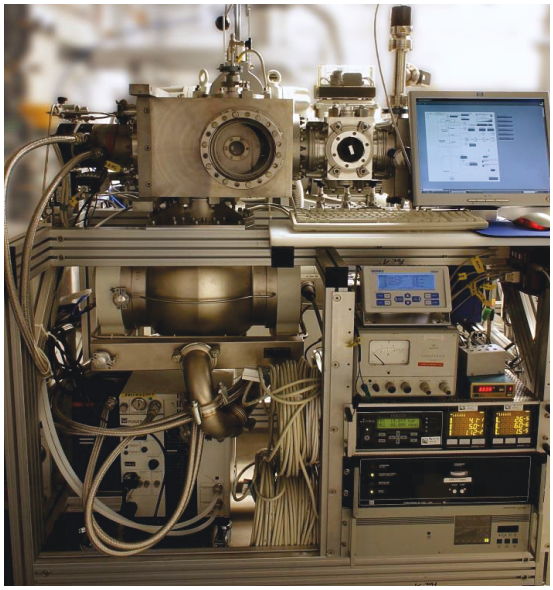

Fig. 37: Cluster-jet target for laser applications in a test stand at Univ. Münster

In parallel to the Arcturus experiments, we will start — in collaboration with the Jülich Centre for Neutron Science (JCNS-2/PGI-4) of FZJ — the development of tailored compact (few cm^3) moderators for the subsequent generation of thermal neutrons. These will be installed as close as possible around the converter, in order to achieve highest possible thermal neutron fluxes.

A Councils

A.1 Hadron and Accelerator Physics Program Advisory Council

Prof. Mei Bai	Brookhaven National Laboratory, U.S.A.
Prof. K.-T. Brinkmann	University Bonn
Prof. M. Garçon	CEA-Saclay, FR
Prof. A. Jankowiak	Helmholtz Zentrum Berlin
Prof. K. Jungmann	KVI Groningen, NL
Prof. K.-H. Kampert	University Wuppertal
Prof. S. Paul	TU München (Chairperson)
Prof. K. Peters	GSI Darmstadt
Prof. D.-O. Riska	University Helsinki, FI
Prof. C. Roberts	Argonne National Laboratory, U.S.A.
Prof. S. Vigdor	Brookhaven National Laboratory, U.S.A.

Note: In the newly established committee of Forschungszentrum Jülich, the "Wissenschaftlicher Beirat" (WB, Scientific Council), Prof. Thomas Roser (Brookhaven National Laboratory, USA) is assigned to IKP.

A.2 COSY Program Advisory Committee

Prof. M. Anselmino	L'Universita di Torino, IT
Prof. E. Epelbaum	Universität Bochum
Prof. M. Garçon	CEA-Saclay, F (Chairperson)
Prof. N. Kaiser	TU München
Prof. B. Kämpfer	FZ Dresden-Rossendorf
Prof. O. Kester	GSI Darmstadt
Prof. A.K. Opper	George Washington University, USA
Prof. P. Salabura	Jagellonian University Cracow, PL
Prof. U. Thoma	Universität Bonn
Prof. H. Weise	DESY, Hamburg
Prof. H. Wilschut	KVI Groningen, NL

B Publications

1. Accelerator and Experiment

1. **On the ΣN cusp in the $pp \to pK^+\Lambda$ reaction**
   S. Abd El-Samad *et al.*
   Eur. Phys. J. A **49** 41 (2013)

2. **Observation of a charged charmoniumlike structure in $e^+e^- \to \pi^+\pi^- J/\psi$ at $\sqrt{s}$=4.26 GeV**
   M. Ablikim *et al.*
   Phys. Rev. Lett. **110** 252001 (2013)

3. **Partial wave analysis of $J/\psi \to \gamma\eta\eta$**
   M. Ablikim *et al.*
   Phys. Rev. D **87** 092009 (2013)

4. **Precision measurements of $\mathrm{B}[\psi(3686) \to \pi^+\pi^- J/\psi]$ and $\mathrm{B}[J/\psi \to l^+l^-]$**
   M. Ablikim *et al.*
   Phys. Rev. D **88** 032007 (2013)

5. **Measurement of $\eta' \to \pi^+\pi^- e^+e^-$ and $\eta' \to \pi^+\pi^-\mu^+\mu^-$**
   M. Ablikim *et al.*
   Phys. Rev. D **87** 092011 (2013)

6. **Search for Baryonic Decays of $\psi(3770)$ and $\psi(4040)$**
   M. Ablikim *et al.*
   Phys. Rev. D **87** 112011 (2013)

7. **Partial wave analysis of $\psi(2S) \to p\bar{p}\eta$**
   M. Ablikim *et al.*
   Phys. Rev. D **88** 032010 (2013)

8. **Study of $\psi(3686) \to \omega K\overline{K}\pi$ decays**
   M. Ablikim *et al.*
   Phys. Rev. D **87** 092006 (2013)

9. **Evidence for $\eta_c(2S)$ in $\psi(3686) \to \gamma K_S^0 K^\pm\pi^\mp\pi^+\pi^-$**
   M. Ablikim *et al.*
   Phys. Rev. D **87** 052005 (2013)

10. **Study of $J/\psi \to \omega p\bar{p}$ at BESIII**
    M. Ablikim *et al.*
    Phys. Rev. D **87** 112004 (2013)

11. **Search for the Lepton Flavor Violation Process $J/\psi \to e\mu$ at BESIII**
    M. Ablikim *et al.*
    Phys. Rev. D **87** 112007 (2013)

12. **Search for η-mesic ^{4}He with the WASA-at-COSY detector**
    P. Adlarson *et al.*
    Phys. Rev. C **87** 035204 (2013)

13. **Isospin decomposition of the basic double-pionic fusion in the region of the ABC effect**
    P. Adlarson *et al.*
    Phys. Lett. B **721** 229 - 236 (2013)

14. **Search for a dark photon in the $\pi^0 \to e^+e^-\gamma$ decay**
    P. Adlarson *et al.*
    Phys. Lett. B **726** 187 - 193 (2013)

15. **Measurement of the $pn \to pp\pi^0\pi^-$ reaction in search for the recently observed resonance structure in $d\pi^0\pi^0$ and $d\pi^+\pi^-$ systems**
    P. Adlarson *et al.*
    Phys. Rev. C **88** 055208 (2013)

16. **Investigation of the $dd \to {}^3\mathrm{He}n\pi^0$ reaction with the FZ Jülich WASA-at-COSY facility**
P. Adlarson *et al.*
Phys. Rev. C **88** 014004 (2013)

17. **Multiplicities of charged pions and kaons from semi-inclusive deep-inelastic scattering by the proton and the deuteron**
A. Airapetian *et al.*
Phys. Rev. D **87** 074029 (2013)

18. **Azimuthal distributions of charged hadrons, pions, and kaons produced in deep-inelastic scattering off unpolarized protons and deuterons**
A. Airapetian *et al.*
Phys. Rev. D **87** 012010 (2013)

19. **The BaBar detector: Upgrades, operation and performance**
B. Aubert *et al.*
Nucl. Instr. Meth. Phys. Res. A **729** 615 - 701 (2013)

20. **Erratum: Synchrotron oscillation effects on an rf-solenoid spin resonance [Phys. Rev. ST Accel. Beams 15, 124202 (2012)]**
P. Benati *et al.*
Phys. Rev. ST Accel. Beams **16** 049901 (2013)

21. **One-Particle Measurement of the Antiproton Magnetic Moment**
J. DiSciacca *et al.*
Phys. Rev. Lett. **110** 130801 (2013)

22. **Finite volume effects and quark mass dependence of the N(1535) and N(1650)**
M. Döring, M. Mai and U. Meißner
Phys. Lett. B **722** 185-192 (2013)

23. **Measurement of spin observables in the quasifree $np \to \{pp\}_s\pi^-$ reaction at 353 MeV**
S. Dymov *et al.*
Phys. Rev. C **88** 014001 (2013)

24. **Technical design report for the PANDA (AntiProton Annihilations at Darmstadt) Straw Tube TrackerStrong interaction studies with antiprotons**
W. Erni *et al.*
Eur. Phys. J. A **49** 25 (2013)

25. **Development of a readout system for the $\overline{\mathrm{P}}$ANDA Micro Vertex Detector**
S. Esch *et al.*
J. Instrum. **8** C01043 - C01043 (2013)

26. **Negative ion source development at the cooler synchrotron COSY/Jülich**
O. Felden *et al.*
AIP Conf. Proc. **1515** 321 (2013)

27. **Particle identification using the time-over-threshold measurements in straw tube detectors**
S. Jowzaee *et al.*
Nucl. Instr. Meth. Phys. Res. A **718** 573 - 574 (2013)

28. **Results from the Spin Program at COSY-ANKE**
A. Kacharava and C. Wilkin
Nucl. Phys. News **23** 11-17 (2013)

29. **Measurement of the $D^*(2010)^+$ meson width and the $D^*(2010)^+ - D^0$mass difference**
J.P. Lees *et al.*
Phys. Rev. Lett. **111** 111801 (2013)

30. **Measurement of the $B^+ \to \omega\ell^+\nu$ branching fraction with semileptonically tagged B mesons**
J.P. Lees *et al.*
Phys. Rev. D **88** 072006 (2013)

31. **Precision Measurement of the $e^+e^- \to K^+K^-(\gamma)$ Cross Section with the Initial-State Radiation Method at BaBar**
J.P. Lees *et al.*
Phys. Rev. D **88** 032013 (2013)

32. **Search for CP Violation in $B^0 - \overline{B}^0$ Mixing Using Partial Reconstruction of $B^0 \to D^{*-}X\ell^+\nu_\ell$ and a Kaon Tag**
J.P. Lees *et al.*
Phys. Rev. Lett. **111** 101802 (2013)

33. **Search for a light Higgs boson decaying to two gluons or $s\bar{s}$ in the radiative decays of $\Upsilon(1S)$**
J.P. Lees *et al.*
Phys. Rev. D **88** 031701 (2013)

34. **Measurement of the $e^+e^- \to p\overline{p}$ cross section in the energy range from 3.0 to 6.5 GeV**
J.P. Lees *et al.*
Phys. Rev. D **88** 072009 (2013)

35. **Production of charged pions, kaons and protons in e^+e^- annihilations into hadrons at sqrts = 10.54 GeV**
J.P. Lees *et al.*
Phys. Rev. D **88** 032011 (2013)

36. **Search for $B \to K^{(*)}\nu\overline{\nu}$ and invisible quarkonium decays**
J.P. Lees *et al.*
Phys. Rev. D **87** 112005 (2013)

37. **Measurement of an Excess of $\overline{B} \to D^{(*)}\tau^-\overline{\nu}_\tau$ Decays and Implications for Charged Higgs Bosons**
J.P. Lees *et al.*
Phys. Rev. D **88** 072012 (2013)

38. **Observation of direct CP violation in the measurement of the Cabibbo-Kobayashi-Maskawa angle γ with $B^\pm \to D^{(*)}K^{(*)\pm}$ decays**
J.P. Lees *et al.*
Phys. Rev. D **87** 052015 (2013)

39. **Study of the decay $\overline{B}^0 \to \Lambda_c^+\overline{p}\pi^+\pi^-$ and its intermediate states**
J.P. Lees *et al.*
Phys. Rev. D **87** 092004 (2013)

40. **Measurement of CP-violating asymmetries in $B^0 \to (\rho\pi)^0$ decays using a time-dependent Dalitz plot analysis**
J.P. Lees *et al.*
Phys. Rev. D **88** 012003 (2013)

41. **Time-Integrated Luminosity Recorded by the BABAR Detector at the PEP-II e^+e^- Collider**
J.P. Lees *et al.*
Nucl. Instr. Meth. Phys. Res. A **726** 203 - 213 (2013)

42. **Study of $e^+e^- \to p\overline{p}$ via initial-state radiation at BABAR**
J.P. Lees *et al.*
Phys. Rev. D **87** 092005 (2013)

43. **Measurement of the $D^*(2010)^+$ natural line width and the $D^*(2010)^+ - D^0$mass difference**
J.P. Lees *et al.*
Phys. Rev. D **88** 052003 (2013)

44. **A Search for the Rare Decays $B \to \pi\ell^+\ell^-$ and $B^0 \to \eta\ell^+\ell^-$**
J.P. Lees *et al.*
Phys. Rev. D **88** 032012 (2013)

45. **Study of the Λp interaction close to the $\Sigma^+ n$ and $\Sigma^0 p$ Thresholds**
H. Machner *et al.*
Nucl. Phys. A **901** 65 - 88 (2013)

46. **Excitation of the $\Delta(1232)$ isobar in deuteron charge exchange on hydrogen at 1.6, 1.8, and 2.3 GeV**
D. Mchedlishvili *et al.*
Phys. Lett. B **726** 145 - 150 (2013)

47. **The neutron-proton charge-exchange amplitudes measured in the $dp \to ppn$ reaction**
D. Mchedlishvili *et al.*
Eur. Phys. J. A **49** 49 (2013)

48. **The polarized H and D atomic beam source for ANKE at COSY-Jülich**
M. Mikirtychyants *et al.*
Nucl. Instr. Meth. Phys. Res. A **721** 83 - 98 (2013)

49. **Final-state interactions in the process $pp \to pK^+\Lambda$**
M. Röder *et al.*
Eur. Phys. J. A **49** 157 (2013)

50. **High-accuracy x-ray line standards in the 3-keV region**
S. Schlesser *et al.*
Phys. Rev. A **88** 022503 (2013)

51. **Erratum: Test of Low-Energy Theorems for $^1\mathrm{H}(\vec{\gamma},\pi^0)^1\mathrm{H}$ in the Threshold Region [Phys. Rev. Lett. 87, 232501 (2001)]**
A. Schmidt *et al.*
Phys. Rev. Lett. **110** 039903 (2013)

52. **First measurements of spin correlations in the $np \to d\pi^0$ reaction**
V. Shmakova *et al.*
Phys. Lett. B **726** 634-637 (2013)

53. **Production of K^+K^- pairs in proton-proton collisions below the ϕ meson threshold**
Q.J. Ye *et al.*
Phys. Rev. C **87** 065203 (2013)

2. Theory

54. **Quark mass dependence of the X (3872) binding energy**
V. Baru *et al.*
Phys. Lett. B **726** 537 - 543 (2013)

55. **Varying the light quark mass: Impact on the nuclear force and big bang nucleosynthesis**
J.C. Berengut *et al.*
Phys. Rev. D **87** 085018 (2013)

56. **New insights into the spin structure of the nucleon**
V. Bernard *et al.*
Phys. Rev. D **87** 054032 (2013)

57. **The electric dipole moment of the deuteron from the QCD θ-term**
J. Bsaisou *et al.*
Eur. Phys. J. A **49** 31 (2013)

58. **Confirming the molecular nature of the $Z_b(10610)$ and the $Z_b(10650)$**
M. Cleven *et al.*
Phys. Rev. D **87** 074006 (2013)

59. **Improving the hadron physics of non-Standard-Model decays: example bounds on R-parity violation**
J.T. Daub *et al.*
J. High Energ. Phys. **1301** 179 (2013)

60. **Renormalization group running of dimension-six sources of parity and time-reversal violation**
W. Dekens and J. Vries
J. High Energ. Phys. **1305** 149 (2013)

61. **Finite volume effects and quark mass dependence of the N(1535) and N(1650)**
M. Döring, M. Mai and U. Meißner
Phys. Lett. B **722** 185-192 (2013)

62. **Chiral dynamics and S-wave contributions in semileptonic B decays**
M. Döring, U. Meißner and W. Wang
J. High Energ. Phys. **1310** 11 (2013)

63. **Viability of Carbon-Based Life as a Function of the Light Quark Mass**
E. Epelbaum *et al.*
Phys. Rev. Lett. **110** 112502 (2013)

64. **Dependence of the triple-alpha process on the fundamental constants of nature**
E. Epelbaum *et al.*
Eur. Phys. J. A **49** 82 (2013)

65. **Quantum Monte Carlo Calculations with Chiral Effective Field Theory Interactions**
A. Gezerlis *et al.*
Phys. Rev. Lett. **111** 032501 (2013)

66. **Production of the X(3872) in charmonia radiative decays**
F. Guo *et al.*
Phys. Lett. B **725** 127 - 133 (2013)

67. **Tetraquarks, hadronic molecules, meson-meson scattering, and disconnected contributions in lattice QCD**
F. Guo *et al.*
Phys. Rev. D **88** 074506 (2013)

68. **Hyperon-nucleon interaction at next-to-leading order in chiral effective field theory**
J. Haidenbauer *et al.*
Nucl. Phys. A **915** 24 - 58 (2013)

69. **Colloquium: Three-body forces: From cold atoms to nuclei**
H. Hammer, A. Nogga and A. Schwenk
Rev. Mod. Phys. **85** 197 - 217 (2013)

70. **Threshold neutral pion photoproduction off the tri-nucleon to O(q4)**
M. Lenkewitz *et al.*
Eur. Phys. J. A **49** 20 (2013)

71. **Further understanding of the non-$D\overline{D}$ decays of $\psi(3770)$**
G. Li *et al.*
Phys. Rev. D **88** 014010 (2013)

72. **Hunting for a scalar glueball in exclusive B decays**
C. Lü *et al.*
Eur. Phys. J. A **49** 58 (2013)

73. **Toroidal quadrupole form factor of the deuteron**
E. Mereghetti *et al.*
Phys. Rev. C **88** 034001 (2013)

74. **Coupled-channel dynamics in the reactions $\pi N \to \pi N$, ηN, $K\Lambda$, $K\Sigma$**
D. Rönchen *et al.*
Eur. Phys. J. A **49** 44 (2013)

75. **Vector analyzing powers of the deuteron-proton elastic scattering and breakup at 100 MeV1**
E. Stephan *et al.*
Eur. Phys. J. A **49** 36 (2013)

76. **Elastic antiproton-deuteron scattering and total antiproton-deuteron cross sections**
Y.N. Uzikov and J. Haidenbauer
Phys. Rev. C **87** 054003 (2013)

77. **Elastic antiproton-deuteron scattering and total antiproton-deuteron cross sections reexamined**
Y.N. Uzikov and J. Haidenbauer
Phys. Rev. C **88** 027001 (2013)

78. **Decoding the Riddle of $Y(4260)$ and $Z_c(3900)$**
Q. Wang, C. Hanhart and Q. Zhao
Phys. Rev. Lett. **111** 132003 (2013)

79. **Systematic study of the singularity mechanism in heavy quarkonium decays**
Q. Wang, C. Hanhart and Q. Zhao
Phys. Lett. B **725** 106 - 110 (2013)

80. **Electromagnetic Structure of the $Z_c(3900)$**
E. Wilbring, H.-W. Hammer and U. Meißner
Phys. Lett. B **726** 326-329 (2013)

C Talks and Colloquia

1. S. Barsov
   The pn-quasi-free reaction measurements at ANKE
   Bad Honnef, Germany: 12/16/2013 - 12/17/2013

2. M. Bashkanov
   Status of the Investigations of the I(JP) = 0(3+) Resonance Structure in the Two-Baryon-System
   Dresden, Germany: 03/04/2013 - 03/08/2013

3. F. Bergmann
   Total and differential cross sections of the reaction $pd \rightarrow {}^3He\eta$ measured with WASA-at-COSY
   Bad Honnef, Germany: 12/16/2013 - 12/17/2013

4. M. Büscher *et al.*
   High-intensity lasers for particle physics
   Dresden, Germany: 03/04/2013 - 03/08/2013

5. L. Cao and J. Ritman
   Simulation and optimization of the PANDA detector to measure the form factor of the Ds semileptonic decay
   Berlin, Germany: 09/16/2013 - 09/21/2013

6. D. Chiladze
   Differential cross section measurements for pp-elastic scattering at ANKE
   Bad Honnef, Germany: 12/16/2013 - 12/17/2013

7. I. Ciepal *et al.*
   Investigations of Few-Nucleon System Dynamics in Medium Energy Domain
   Fukuoka, Japan: 08/20/2013 - 08/25/2013

8. H. Clement and M. Bashkanov
   Resonance Multiplets in the Two-Baryon System – Dibaryons revisited
   Dresden, Germany: 03/04/2013 - 03/08/2013

9. D. Coderre
   Measurement of charged decays of the η meson with WASA-at-COSY
   Dresden, Germany: 03/04/2013 - 03/08/2013

10. J. de Vries
    The theory of electric dipole moments of light nuclei
    Jülich, Germany: 03/14/2013

11. J. de Vries
    Electric dipole moments of light nuclei from dimension-six operators
    Tbilisi, Georgia: 09/23/2013 - 09/24/2013

12. J. de Vries
    Parity violation in proton-proton scattering from chiral eective eld theory
    Beijing, China: 10/28/2013

13. D. Deermann *et al.*
    A Readout System for the PANDA MVD Trapezoidal Silicon Strip Sensors
    Dresden, Germany: 03/04/2013 - 03/08/2013

14. K. Demmich
    Towards $\eta \rightarrow \pi^0 e^+ e^-$: Optimized calibration of the WASA forward detector
    Bad Honnef, Germany: 12/16/2013 - 12/17/2013

15. K. Demmich *et al.*
    Energy Calibration for the Forward Detector at WASA-at-COSY*
    Dresden, Germany: 03/04/2013 - 03/08/2013

16. R. Engels
    Polarized fusion: Can polarization increase the energy output of fusion reactors?
    Charlottesville, USA: 09/09/2013

17. R. Engels
    Polarized hydrogen/deuterium molecules: A new option for polarized targets?
    Charlottesville, USA: 09/10/2013

18. R. Engels
    Polarized hydrogen/deuterium molecules: A new option for polarized fuel.
    Trento, Italy: 11/15/2013

19. S. Esch *et al.*
    Upgrade of the Juelich Digital Readout System for PANDA development
    Dresden, Germany: 03/04/2013 - 03/08/2013

20. D. Eversheim, Y. Valdau and B. Lorentz
    Test of Time- Reversal Invariance at COSY (TRIC)
    Dresden, Germany: 03/04/2013 - 03/08/2013

21. P. Fedorets
    Recent developments with the pellet target
    Bad Honnef, Germany: 12/16/2013 - 12/17/2013

22. M. Gaißer, A. Nass and H. Stroeher
    DSMC simulations of polarized atomic beam sources including magnetic elds
    Virginia, USA: 09/09/2013 - 09/13/2013

23. M. Gaißer, A. Nass and H. Stroeher
    Optimization of Atomic Beam Sources for Polarization Experiments
    Dresden, Germany: 03/04/2013 - 03/08/2013

24. A. Gillitzer
    PANDA Activities at Jülich
    Jülich, Germany: 03/15/2013 - 03/16/2013

25. A. Gillitzer
    Strong Interaction Physics with PANDA
    Uppsala, Schweden: 06/10/2013 - 06/15/2013

26. A. Goerres
    The TOFPET ASIC
    Rauischholzhausen, Germany: 09/04/2013 - 09/06/2013

27. A. Goerres
    Time-based readout of silicon strip sensors
    Turin, Italy: 11/28/2013

28. F. Goldenbaum and D. Filges
    The Phenomenology and Experiment of Spallation Processes
    Krakow, Poland: 06/03/2013 - 06/06/2013

29. F. Goldenbaum
    Indo-German cooperation on hadron physics:
    Description of the current status and possible involvement in precursor experiments.
    IIT Mumbai, India: 10/21/2013

30. F. Goldenbaum
    Indo-German cooperation on hadron physics:
    Description of the current status and possible involvement in precursor experiments.
    IIT Indore, India: 10/23/2013

31. F. Goldenbaum
    Indo-German cooperation on hadron physics:
    Description of the current status and possible involvement in precursor experiments.
    VECC Kolkata, India: 10/25/2013

32. R. Gorski
Measurement of the nuclear polarization in H_2 and D_2 molecules after recombination of polarized hydrogen or deuterium atoms
Dresden, Germany: 03/04/2013 - 03/08/2013

33. A. Goswami
The η meson decay into $\gamma\gamma(*)$ in pp reactions with WASA-at-COSY
Bad Honnef, Germany: 12/16/2013 - 12/17/2013

34. D. Gotta
Pionic Hydrogen and Friends
Villigen, Schweiz: 04/18/2013

35. B. Gou
Preliminary results form the commissioning experiment of the polarized deuterium gas target at ANKE/COSY
Dresden, Germany: 03/04/2013 - 03/08/2013

36. G. Guidoboni
Spin-coherence time studies at COSY
Bad Honnef, Germany: 12/16/2013 - 12/17/2013

37. C.-O. Gullström and A. Kupsc
Search for a new gauge boson in π^0 leptonic decay with WASA-AT-COSY
Krakow, Poland: 06/03/2013 - 06/06/2013

38. J. Haidenbauer
Final-state interactions
Beijing, China: 04/27/2013 - 04/28/2013

39. J. Haidenbauer
Hyperon-nucleon interaction in chiral effective field theory
Krakau, Polen: 09/09/2013 - 09/13/2013

40. J. Haidenbauer
The $\overline{K}-N$ interaction and the reaction $K^- d \to \pi\Sigma n$
Trento, Italy: 10/21/2013 - 10/25/2013

41. J. Haidenbauer
Status of the YN interaction in chiral EFT
Trento, Italy: 12/05/2013 - 12/06/2013

42. C. Hanhart
Modelling low-mass resonances in multi-body decays, CHARM 2013
Manchaster, UK: 08/31/2013 - 9/04/2013

43. C. Hanhart
Towards precision studies for few-body decays of B- and D-mesons - from hadron spectroscopy to CP phases, ATHOS 2013
Seeon, Germany: 05/21/2013 - 05/24/2013

44. C. Hanhart
Remarks on hadronic molecules
Beijing, China: 04/22/2013 - 04/26/2013

45. C. Hanhart
Remarks about resonances
Mainz, Germany: 02/19/2013

46. C. Hanhart
XYZ states - a new particle zoo?
University of Bonn, University of Mainz, Germany: 2013

47. F. Hauenstein
Results for the $\overrightarrow{p}\,p \to pK\Lambda$ Reaction Measured at COSY-TOF with a Polarized Proton Beam of 2.70 GeV/c
Dresden, Germany: 03/04/2013 - 03/08/2013

48. F. Hauenstein
Kaon analyzing power and $N\Sigma$ cusp enhancement in the $pp \to pK\Lambda$ reaction
Bad Honnef, Germany: 12/16/2013 - 12/17/2013

49. V. Hejny
Charge Symmetry Breaking in $dd \to^4 He\pi^0$
Prague, Czech Republic: 06/17/2013 - 06/19/2013

50. A. Herten
GPUs at High Energy Physics and PANDA
Forschungszentrum Jülich, Germany: 07/08/2013

51. A. Herten *et al.*
GPU Implementations of Online Track Finding Algorithms at PANDA
Dresden, Germany: 03/04/2013 - 03/08/2013

52. A. Holler
Polarized ion beams generated by means of laser-induced relativistic plasmas
Darmstadt, Germany: 09/30/2013 - 10/02/2013

53. A. Holler
Polarized ion beams generated by means of laser-induced relativistic plasmas
Trento, Italy: 11/14/2013 - 11/15/2013

54. Q. Hu
pp-elastic scattering in the Coulomb-nuclear interference region
Bad Honnef, Germany: 12/16/2013 - 12/17/2013

55. Q. Hu, H. Xu and J. Ritman
Recoil Detector Test for the Day-One Experiment at HESR
Dresden, Germany: 03/04/2013 - 03/08/2013

56. A.N. Ivanov *et al.*
Testing of Symplectic Integrator of Spin-orbit Motion Based on Matrix Formalism
Shanghai, China: 05/12/2013 - 05/17/2013

57. S. Jowzaee
Calibration of a Modular Straw-Tube-Tracker for the COSY-TOF Experiment
Krakow, Poland: 06/03/2013 - 06/06/2013

58. S. Jowzaee
Calibration of a High-Resolution Straw-Tube-Tracker for the COSY-TOF Experiment
Dresden, Germany: 03/04/2013 - 03/08/2013

59. A. Kacharava
The Hadron Physics Program of COSY-ANKE: selected results
Glasgow, Schottland: 06/24/2013 - 06/28/2013

60. A. Kacharava
Autumn Lectures
Tbilisi, Georgia: 10/15/2013 - 10/24/2013

61. F.A. Khan
Towards a measurement of the $\omega\pi$ transition form factor
Dresden, Germany: 03/04/2013 - 03/08/2013

62. F.A. Khan
ω meson decays with WASA-at-COSY
Bad Honnef, Germany: 12/16/2013 - 12/17/2013

63. S. Krewald et al.
Strategies for baryon resonance analysis
Glasgow, UK: 24/06/2013 - 26/06/2013

64. S. Krewald et al.
Recent developments of the Juelich-Athens-Washington model
Edinburgh, UK: 29/06/2013

65. S. Krewald et al.
The strong interaction: status, strategies, and perspectives
Athens, GA, USA: 03/10/2013

66. A. Larionov *et al.*
Charmonium production in p-nucleus reactions at low energies
Dresden, Germany: 03/04/2013 - 03/08/2013

67. A. Lehrach
Beam time summary JEDI
Jülich, Germany: 03/13/2013 - 03/14/2013

68. A. Lehrach
Spin Dynamics
Jülich, Germany: 03/13/2013-03/14/2013

69. A. Lehrach
Accelerators COSY and HESR
Jülich, Germany: 03/15/2013 - 03/16/2013

70. A. Lehrach
EDM bright future for COSY
Jülich, Germany: 09/06/2013

71. A. Lehrach
Beam time summary JEDI
Jülich, Germany: 09/26/2013-09/27/2013

72. A. Lehrach
Beam Dynamics
Jülich, Germany: 09/26/2013-09/27/2013

73. A. Lehrach
Lab Report COSY
Darmstadt, Germany: 11/28/2013-11/29/2013

74. A. Lehrach
Bericht zu COSY
Bad Honnef, Germany: 12/05/2013-12/06/2013

75. D. Lersch and F. Goldenbaum
Measuring the relative branching ratio and the E_γ-distribution of $\eta \to \pi^+\pi^-\gamma$ with WASA-at-COSY
Dresden, Germany: 03/04/2013 - 03/08/2013

76. G. Macharashvili
Ay measurements in pp-elastic scattering using the ANKE silicon telescopes
Bad Honnef, Germany: 12/16/2013 - 12/17/2013

77. R. Maier
FAIR-GSI-Kolloquium: Focus on High-Energy Storage Ring
Darmstadt, Germany: 12/18/2013

78. U. Meißner
Nuclear lattice simulations: Status and perspectives
Florence, Italy: 06/02/2013 - 06/07/2013

79. U. Meißner
A walk through the world of chiral dynamics
Newport News, Virginia: 08/06/2013 - 08/10/2013

80. M. Mertens, J. Ritman and P. Wintz
Triplet Based Online Track Finding in the PANDA-STT
Dresden, Germany: 03/04/2013 - 03/08/2013

81. M. Mielke
Testing the role of N* resonances in $dp \to {}^3He\pi^+\pi^-$ at ANKE
Bad Honnef, Germany: 12/16/2013 - 12/17/2013

82. K. Miyagawa and J. Haidenbauer
The Reaction $K^-d \to \pi\Sigma n$ in the $\Lambda(1405)$ Resonance Region
Fukuoka, Japan: 08/20/2013 - 08/25/2013

83. A. Nogga
Light hypernuclei based on chiral interactions at next-to-leading order
Cracow, Poland: 09/10/2013

84. A. Nogga
Light hypernuclei: a challenge for hypernuclear interactions
Mainz, Germany: 02/06/2013

85. A. Nogga
Light hypernuclei based on chiral interactions at next-to-leading order
Ruhr-University Bochum, Germany: 07/03/2013

86. A. Nogga, J. Haidenbauer and U. Meißner
Light hypernuclei based on chiral interactions at next-to-leading order
Cracow, Poland: 09/09/2013 - 09/13/2013

87. I. Ozerianska
Status of the analysis of the $\overrightarrow{p}p \to pp\eta$ reaction measured with the WASA detector system
Bad Honnef, Germany: 12/16/2013 - 12/17/2013

88. M. Papenbrock
Testing the strong FSI of the $\eta - {}^3He$ system at ANKE
Bad Honnef, Germany: 12/16/2013 - 12/17/2013

89. E. Perez del Rio
ABC effect and resonance in $pd \to {}^3He\pi^0\pi^0$
Bad Honnef, Germany: 12/16/2013 - 12/17/2013

90. D. Prasuhn
Status of COSY
Bad Honnef, Germany: 12/16/2013 - 12/17/2013

91. E. Prencipe
Observation of the rare decay B to J/psi K K K
Dresden, Germany: 03/04/2013 - 03/08/2013

92. E. Prencipe
Study of the transition form factors in the gamma-gamma processs e+e-pi0 and e+e-eta at BES III
Dresden, Germany: 03/04/2013 - 03/08/2013

93. E. Prencipe
Recent results and perspectives on pseudo-scalar mesons and form factors
Denver, USA: 04/06/2013 - 04/14/2013

94. E. Prencipe
Study of the eta decays at WASA-at-COSY
Praha, Czech Republic: 06/17/2013 - 06/19/2013

95. E. Prencipe
Study of light mesons at WASA-at-COSY
Roma, Italy: 09/30/2013 - 10/04/2013

96. E. Prencipe
Simulations with MC generators for e+e-(X) processes
Orsay, France: 10/07/2013 - 10/09/2013

97. E. Prencipe
Perspectives on Open charm Physics at PANDA
Mumbai, India: 10/21/2013

98. E. Prencipe
Perspectives on Open charm Physics at PANDA
Indore, India: 10/23/2013

99. E. Prencipe
Perspectives on Open charm Physics at PANDA
Kolcata, India: 10/25/2013

100. J. Pretz
Measurement of Electric Dipole Moments of Charged Particles in Storage Rings
Dresden, Germany: 03/04/2013 - 03/08/2013

101. T. Preuhs *et al.*
Experimental Determination of the Time and Charge Resolution of a Flash-ADC System for the PANDA STT
Dresden, Germany: 03/04/2013 - 03/08/2013

102. F. Rathmann
Search for permanent Electric Dipole Moments
Stockholm, Sweden: 7/2/2013

103. F. Rathmann
Overview of COSY plans and activities
Brookhaven, USA: 11/1/2013

104. F. Rathmann
Search for Electric Dipole Moments in Storage Rings
Aachen, Germany: 25/06/2013

105. F. Rathmann
EDM searches at COSY - Overview of COSY plans and activities
Batavia, USA: 20/05/2013

106. F. Rathmann
WP25: PolAntiP - Polarized Antiprotons
Frascati, Italy: 27/05/2013

107. F. Rathmann
Search for permanent Electric Dipole Moments
Firenze, Italy: 3/06/2013

108. F. Rathmann
Search for permanent Electric Dipole Moments
Tbilisi, Georgia: 23/09/2013

109. J. Ritman
The PANDA Experiment
Mumbai, India: 03/18/2013

110. J. Ritman
Experiments to investigate symmetries and symmetry breaking at Jülich
Universität Mainz, Germany: 05/15/2013

111. J. Ritman
Physics Potential with Baryonic final states at PANDA
Peñiscola, Spain: 05/27/2013 - 05/30/2013

112. J. Ritman
Plans and status of PANDA
Glasgow, UK: 06/20/2013 - 06/22/2013

113. J. Ritman
Antiproton Annihilation at Darmstadt - PANDA
GSI Darmstadt, Germany: 07/02/2013

114. J. Ritman
Status of the PANDA Experiment
GSI Darmstadt, Germany: 07/04/2013 - 07/05/2013

115. J. Ritman
Detector Development at Juelich for hadronic and precision physics
Groningen, The Netherlands: 07/16/2013

116. J. Ritman
The PANDA Experiment:Exploring the Emergence of Structure in Matter
Gatchina, Russia: 09/17/2013

117. J. Ritman
Experiments Leading the way to FAIR
Giessen, Germany: 10/11/2013

118. J. Ritman
Indo-German cooperation on hadron physics
Mumbai, India: 10/21/2013

119. J. Ritman
The PANDA Lambda-Disks
Indore, India: 10/23/2013

120. J. Ritman
Introduction to the PANDA experiment at the upcoming Facility for Anti-proton and Ion Research (FAIR)
Kolkatta, India: 10/25/2013

121. J. Ritman
The PANDA Experiment: A Facility to Map out Exotic Charmed Hadrons
Nara, Japan: 11/04/2013 - 11/08/2013

122. J. Ritman
Bericht zu PANDA
Bad Honnef, Germany: 12/05/2013 - 12/06/2013

123. J. Ritman
Using Antiprotons to Gain Insight on the Structure of Hadrons
GSI Darmstadt, Germany: 12/09/2013 - 12/13/2013

124. D. Rönchen
Hadronic reactions in a dynamical coupled-channels model
Peniscola, Spanien: 05/27/2013 - 05/30/2013

125. D. Rönchen
Baryon resonances in a dynamical coupled-channels model
Camogli, Italien: 09/23/2013 - 09/27/2013

126. M. Rosenthal and A. Lehrach
Simulation of spin dynamics to measure Electric Dipole Moments in storage rings
Dresden, Germany: 03/04/2013 - 03/08/2013

127. A. Saleev
Spin decoherence in a magnetic ring with radiofrequency spin flipper
Bad Honnef, Germany: 12/16/2013 - 12/17/2013

128. A. Saleev and K. Nikolaev
EDM searches at storage rings with Wien filters
Dresden, Germany: 03/04/2013 - 03/08/2013

129. S. Schadmand
Meson Decays with WASA-at-COSY
Glasgow, UK: 06/20/2013 - 06/22/2013

130. A. Schmidt *et al.*
Bau und Test eines DIRC Detektors für das WASA@COSY und das PANDA Experiment
Dresden, Germany: 03/04/2013 - 03/08/2013

131. D. Schröer
η meson production in proton neutron collisions at ANKE
Bad Honnef, Germany: 12/16/2013 - 12/17/2013

132. S.K. Sharma
Validation of Spallation Models: An Approach
Krakow, Poland: 06/03/2013 - 06/06/2013

133. V. Shmakova
Measurement of the spin-correlation coefficients $A_{x,x}$ and $A_{y,y}$ in the quasi-free $np \to \{pp\}_s\pi^-$ reaction near threshold at ANKE-COSY
Dresden, Germany: 03/04/2013 - 03/08/2013

134. V. Shmakova
Spin correlation coefficients measurements in $\overrightarrow{n}\overrightarrow{p} \to d\pi^0$ reaction at 353 MeV at ANKE
Bad Honnef, Germany: 12/16/2013 - 12/17/2013

135. T. Skorodko
First results from quasifree measurements of the $np \to np\pi^0\pi^0$ reaction
Bad Honnef, Germany: 12/16/2013 - 12/17/2013

136. M. Skurzok, P. Moskal and W. Krzemie´n
Search for Eta-mesic Helium via Deuteron-Deuteron Reactions with the WASA-at-COSY Facil
Krakow, Poland: 06/03/2013 - 06/06/2013

137. T. Stockmanns and M. Al-Turany
Time Based Detector Simulation for the PANDA Experiment
Dresden, Germany: 03/04/2013 - 03/08/2013

138. T. Stockmanns and M. Al-Turany
Time Based Detector Simulation for the PANDA Experiment
Dresden, Germany: 03/04/2013 - 03/08/2013

139. H. Ströher
The Fate of Antimatter
Forschungszentrum Jülich (Inauguration JARA-Fame), Germany: 01/17/2013

140. H. Ströher
The Beauty and Power of Spin
Kolloquium Universität zu Köln, Germany: 06/11/2013

141. H. Ströher
ANKE: the on-going legacy of O.W.Schult
Forschungszentrum Jülich (Festkolloquium O.W. Schult), Germany: 06/21/2013

142. H. Ströher
Präzisionsphysik im Rahmen von JARA-Fame
Vaals, (FZJ-Führungskräfteseminar), Netherlands: 06/24/2013

143. H. Ströher
To be or not to be? — that is the question
Universität Tübingen (Festkolloquium H. Clement), Germany: 07/19/2013

144. H. Ströher
JEDI — the Jülich Electric Dipole Moment Investigations
Crete, (ICNPF2013), Greece: 08/30/2013 - 09/05/2013

145. H. Ströher
4 Lectures on “Structure of Matter“
Tbilisi, (GTU Autumn Lectures), Georgia: 10/04/2013 - 10/22/2013

146. H. Ströher
The Beauty and Power of Spin
Universität Erlangen-Nürnberg (Festkolloquium E. Steffens), Germany: 10/28/2013

147. H. Ströher
JEDI – the Jülich Electric Dipole Moment Investigations
Grenoble, (Colloquium LPSC Grenoble), France: 10/31/2013

148. H. Ströher
JEDI – the Jülich Electric Dipole Moment Investigations
Moscow, (Seminar ITEP), Russia: 11/10/2013

149. S. Trusov
Influence of detector efficiencies on a polarization value measured in spin-flip experiments by ”double ratio” method
Bad Honnef, Germany: 12/16/2013 - 12/17/2013

150. Y. Valdau
Preparation for the TRIC experiment at COSY
Bad Honnef, Germany: 12/16/2013 - 12/17/2013

151. Q. Wang
The lineshape of $Y(4260)$
Beijing, China: 11/19/2013 - 11/22/2013

152. C. Weidemann
Detector for Polarized Internal Target Experiments
Dresden, Germany: 03/04/2013 - 03/08/2013

153. C. Weidemann
Polarization of a stored beam by spin filtering
Florence, Italy: 07/02/2013 - 07/07/2013

154. C. Weidemann
Spin-filtering studies at COSY
Bad Honnef, Germany: 12/16/2013 - 12/17/2013

155. P. Wintz
The Central Straw Tube Tracker In The PANDA Experiment
Uppsala, Schweden: 06/10/2013 - 06/15/2013

156. P. Wintz
Straw Tube Production
Forschungszentrum Jülich, IKP, Germany: 10/09/2013 - 10/10/2013

157. P. Wintz and M. Mertens
Triplet Based Online Track Finding in the PANDA-STT
Uppsala, Schweden: 06/10/2013 - 06/15/2013

158. A. Wirzba
The electric dipole moment of light nuclei in effective field theory
Tiblisi, Georgia: 09/23/2013 - 09/24/2013

159. A. Wirzba
Theory of hadronic electric-dipole moments, Ferrara International School Niccolo Cabeo 20130, Physics Beyond the Standard Model: the Precision Frontier
Ferrara, Italy: 05/20/2013 - 05/24/2013

160. A. Wirzba
Three Lectures on the theory of hadronic electric-dipole moments, First Autumn School Î¸on Particle Phenomenology
Lake Bazaleti, Georgia: 09/26/2013 - 09/28/2013

161. A. Wirzba
Electric dipole Moment of the nucleon and light nuclei, Gerry Brown memorial
Stony Brook, New York, USA: 11/24/2013 - 11/26/2013

162. H. Witala *et al.*
Calculations of Three-Nucleon Reactions
Fukuoka, Japan: 08/20/2013 - 08/25/2013

163. M. Zielinski *et al.*
Studies on Antihydrogen Atoms with the ATRAP Experiment at CERN
Krakow, Poland: 06/03/2013 - 06/06/2013

164. A. Zink
A DIRC demonstrator experiment at COSY
Bad Honnef, Germany: 12/16/2013 - 12/17/2013

165. M. Zurek
Investigations of the charge symmetry breaking reaction $dd \to \alpha\pi^0$ with WASA-at-COSY, XII ICFA School on Instrumentation in Elementary Particle Physics
Bogota, Colombia: 11/25/2013 - 12/06/2013

D Diploma and Ph.D. Theses

1. Bachelor, Master, Diploma

1. Kay Demmich,
   Energy Calibration for the Forward Detector at WASA-at-COSY with particular Consideration of the Reaction $p+d \rightarrow {}^3\mathrm{He}+\eta$,
   Master Thesis, University Münster, Germany

2. Dennis Eversmann,
   Analysis of the Spin Coherence Time at the Cooler Synchrotron COSY,
   Master Thesis, RWTH Aachen, Germany

3. Robert Gorski
   Measurement of the nuclear polarization in H_2 *and* D_2 *molecules after recombination of polarized hydrogen or deuterium atoms*,
   Diploma thesis, RWTH Aachen, Germany

4. Fabian Hinder,
   Upgrade of the Readout Electronics for the EDDA-Polarimeter at the Storage Ring COSY,
   Master Thesis, RWTH Aachen, Germany

5. N. Savderova,
   Analysis of STT data from the investigation of $pn \rightarrow K^+n\Lambda$ *reaction at magnetic spectrometer ANKE*,
   Diploma thesis, St. Petersburg, Russia

6. Florian Schepers,
   Investigations on the Nozzle System of the WASA-at-COSY Pellet Target,
   Bachelor Thesis, University Münster, Germany

7. Michaela Schever,
   Suitability test of the Time-of-Flight Method in View of the Energy Resolution of Protons with WASA-at-COSY,
   Bachelor thesis, RWTH Aachen, Germany

8. Jette Schumann,
   Entwicklung eines schnellen Algorithmus zur Suche von Teilchenspuren im Straw Tube Tracker des PANDA-Detektors,
   Bachelor thesis, Fachhochschule Aachen, Campus Jülich, Germany

9. Maria Zurek,
   Design of the new detector setup for the $dd \rightarrow \alpha\pi^0$ *reaction measurement*,
   Master Thesis, Jagiellonian University, Cracow, Poland

2. Ph.D.

10. D. Mchedlishvili,
    Studies of the neutron-proton charge-exchange amplitudes at COSY using the ANKE spectrometer,
    Tbilisi State University, Georgia

11. P. Goslawski,
    High precision measurement of the eta meson mass at COSY-ANKE,
    University Münster, Germany

E Awards & Offers for Professorships

M. Büscher: Accepted Professorship at Heinrich-Heine-Universität Düsseldorf

C. Hanhart: Accepted Professorship at Rheinische Friedrich-Wilhelms-Universität Bonn

A. Lehrach: Accepted Professorship at Rheinisch-Westfälische Technische Hochschule Aachen

C. Hanhart: Member of the Particle Data Group

S. Krewald: Editorial Board of Physical Review C for the period 2011 – 2013

J. Ritman: Elected as spokesperson of the PANDA collaboration from January 1, 2013

U.-G. Meißner: Editorial Board of EPJA, Managing Editor—Reviews

H. Ströher: Editorial Board of EPJA, Co-Editor

R. Maier: Director of JARA-FAME

F Funded Projects

Project	Responsible	Funded by
HGF-CSC fellowship program	R. Maier	HGF, CSC
HadronPhysics 3 (RTD)	M. Büscher	EU/FP7
HadronPhysics 3 (RTD)	F. Goldenbaum	EU/FP7
HadronPhysics 3 (RTD)	F. Rathmann	EU/FP7
HadronPhysics 3 (Support)	D. Grzonka	EU/FP7
HadronPhysics 3 (Coordination)	D. Grzonka	EU/FP7
HadronPhysics 3 (Coordination)	U.-G. Meißner	EU/FP7
HadronPhysics 3 (Coordination)	A. Lehrach	EU/FP7
POLPBAR ERC Advanced Grant	H. Ströher	EU/FP7
SFB/TRR 110	U.-G. Meißner	DFG
Spin Physics from COSY to FAIR	H. Ströher	BMBF/WTZ
Bilat. Zusammenarbeit mit Georgien	H. Ströher	BMBF/WTZ
HESR/P1SR	R. Toelle	BMBF
HESR-Magnete	U. Bechstedt	BMBF
HESR-Netzgeräte	M. Retzlaff	BMBF
HESR-Hochfrequenz	R. Stassen	BMBF
HESR-Injektion	R. Toelle	BMBF
HESR-Strahldiagnose	V. Kamerdzhiev	BMBF
HESR-Vakuum	F. Esser	BMBF
HESR-Stoch. Kühlung	R. Stassen	BMBF
HESR-PANDA Integration	D. Prasuhn	BMBF
Modeling of Polarized Beam Dynamics	R. Maier	DLR
DAAD Wissenschaftleraustausch Tursunov	S. Krewald	DAAD
HGF - Fellow Award C.Roberts Preisgeld	U.-G. Meißner	HGF
Beschaffung von Komponenten für den 2MeV	R. Maier	RWTH-Aachen JARA-FAME

G JCHP-FFE-Projects

Project	Institute	Responsible
PD Dr. A. Khoukaz	Westfälische Wilhelms-Universität Münster	Mesonenproduktion in Nukleon-Nukleon- und Nukleon-Kern-Stößen an COSY
Prof. Dr. K. Nakayama	University of Georgia	Unified analysis of meson production in hadron- and photon-induced reactions in the resonance engergy region
Prof. Dr. A. Vasilyev	PNPI Gatchina	Development, commissioning and operation of components for the COSY Experiments WASA and ANKE and spin-filtering studies at COSY as preparation for PAX at FAIR
Prof. Dr. Vorobyev	PNPI Gatchina	ANKE
Prof. Dr. B. Kämpfer	Forschungszentrum Dresden-Rossendorf	Weiterentwicklung des STT Software Pakets von ANKE zum Einsatz in zukünftigen Experimenten
Prof. Dr. M. Nioradze	Tbilisi State University	NN-elastic scattering studies at COSY
Prof. Dr. O. Willi	Universität Düsseldorf	Measurements of the degree of polarization of laser accelerated protons
PD M. Jezabek	Polish Academy of Sciences	Development of the signal processing method for high performance PANDA STT
Dr. H. Calen	Uppsala University	A pellet tracking system for PANDA and for WASA
Prof. Dr. T. Weis	TU Dortmund	Development of a Fast Orbit Feedback System for the HESR and Beam Tests at COSY
Prof. H. Gao	Duke University, USA	Investigation of K-p & K+K- final state interaction and a deeply bound K-pp state from proton proton reactions
Prof. Dr. P. Moskal	Jagellonian University Krakow	η meson production with polarized proton beam
Prof. A. Roy	Indian Institute of Technology Indore, India	Radiative Decays of the omega Meson with WASA-at-COSY
Prof. Dr. A. Magiera	Jagellonian University Krakow	Investigations of Charge Symmetry Breaking in the dd$\rightarrow{}^4\mathrm{He}\pi^0$
Prof. T. Johansson	Uppsala University	Study oft he omega →pi+pi-pi0 Dalitz plot distribution with WASA
Prof. A. Roy	Indian Institute of Technology Indore, India	ωMeson Decays with WASA-at-COSY
PD Dr. D. Eversheim	HISKP Universität Bonn	Time Reversal Invariance Test at COSY (TRIC)
Prof. N. Nikolaev	L.D. Landau Institute Moscow, Russia	Numerical simulations of spin dynamics for JEDI experiments, searching for permanent Electric Dipole Moments of deuterons and protons at COSY

Dr. J. G. Messchendorp	University of Groningen, Kernfysisch Versneller Instituut, Netherlands	Momentum Dependent electron Reconstruction for WASA and the PANDA Pre-Assembly
Prof. R. Varma	Indian Institute of Technology Indore, India	High statistics experiment for omega meson decays with WASA-at-COSY
Prof. A. Roy	Indian Institute of Technology Indore, India	The η meson decay into $\gamma\gamma^*$ in pp reactions with WASA-at-COSY
Prof. Dr. E. Steffens	Universität Erlangen-Nürnberg	Spin-Experiment an ANKE
Prof. Dr. H. Clement	Universität Tübingen	Installation of a DIRC-Prototyp Detector for PANDA and Experiments with WASA-at-COSY
Prof. Dr. W. Eyrich	Universität Erlangen-Nürnberg	Experimente an TOF und WASA an COSY
Prof. A. Gerasimov	ITEP Moscow	Development of a Frozen-Pellet Target
Prof. Dr. W. Kühn	Universität Giessen	Realtime Tracking for the PANDA Target Spectrometer
Prof. Dr. M. Düren	Justus-Liebig-Universität Gießen	Development of a DIRC Cherenkov detector for WASA at COSY
Dr. P. Lenisa	Università degli Studi di Ferrara, Italy	Spin-filtering studies in storage rings
Prof. J. Wang	Chinese Academy of Sciences, Lanzhou, China	Commissioning of the HESR day one experiment at COSY
Prof. Dr. A. Schäfer	Universität Regensburg	Mesonen Distributions-Amplituden
Prof. Dr. U. Wiedner	Ruhr-Universität Bochum	Development for the forward endcap of the PANDA EMC and buildup of the final endcap within PANDA in Jülich
Prof. Dr. U. Wiedner	Ruhr-Universität Bochum	Development of the Cryogenic Supply System for tests of the PANDA Target Spectrometer Solenoid
Prof. R. Varma	Indian Institute of Technology Indore, India	Physics Analysis and Simulation of Dilepton and Multi-Pion Final States from WASA to PANDA
Prof. Dr. K. Brinkmann	Justus-Liebig-Universität Gießen	Development and Validation of a Free-Running Silicon-Strip Front-End ASIC for the PANDA MVD
Prof. H. Chen	Southwest University, School of Physical Science and Technology, China	Simulation and optimization of the PANDA detector to measure the form factor of the $Ds \rightarrow e+\nu+\pi,\eta,\eta`$ decay
Dr. P. Lenisa	Università degli Studi di Ferrara, Italy	Spin-tracking studies in storage rings
Prof. U. Wiedner	Ruhr-Universität Bochum	Entwicklung für das Slow-control-System von PANDA

H Conferences (co-)organized by the IKP

H.1 JARA-FAME Inauguration Celebration

On January 17, 2013, the new JARA section JARA-FAME—Forces and Matter Experiments—was officially inaugurated. At the inauguration ceremony, the keynote lecture on the AMS Experiment was given by Nobel Laureate in Physics Dr. Samuel C.C. Ting. The event was open to the public.
JARA-FAME is concerned with basic physical research in the field of nuclear and particle physics, and aims to investigate and improve our understanding of matter-antimatter asymmetry in the universe. This asymmetry ultimately holds the key to our existence.
JARA-FAME will initially rest on two pillars: for one, it will host the new JEDI project (Jülich Electric Dipole Moment Investigation), which will be coordinated, planned and implemented by both JARA partners. Its second pillar is the AMS experiment currently in progress on the International Space Station (ISS), in which Aachen is already actively involved. Under JARA, Jülich will play a leading role in strengthening AMS and linking it to the PANDA experiment at FAIR (Facility for Antiproton and Ion Research). As well as theoretical work that will support experiments with model predictions and aid interpretation of the results, the new section will focus on the interdisciplinary topics of detector development and data processing. The

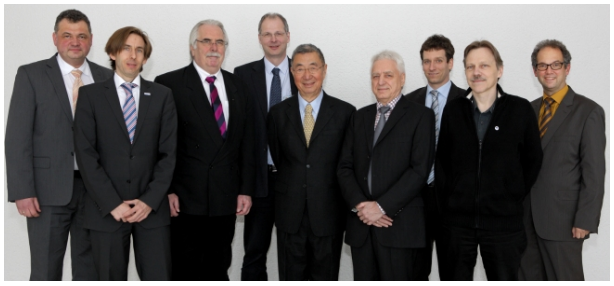

Fig. 38: JARA-FAME Inauguration Celebration

directors of the new section are Prof.Dr. Rudolf Maier from the Nuclear Physics Institute at Forschungszentrum Jülich and Prof.Dr. Achim Stahl from the Institute of Physics (IIIB) at RWTH Aachen University. Dr. Wolfgang Schroeder from Corporate Development at Forschungszentrum Jülich is the managing director.

H.2 532. WE-Heraeus-Seminar on high-resolution pixel detectors and their use in science and society

High resolution pixel detectors experience a vivid development during the past years. Originally designed as sensors for visible light, their application now includes the detection of charged particles, UV-light and X-rays.
The 532. WE-Heraeus-Seminar on "High-Resolution Pixel Detectors and their use in Science and Society" took place in Bad Honnef, Germany, from May 23 to 25, with the participation of more than 50 scientists from Belgium, Germany, France, Great Britain, Netherlands, South Korea and the US. The workshop aimed to discuss progress on pixel detectors and to evaluate the need for future fields of applications. In total, there were 18 overview talks and several posters. The topicality was reflected by five presentations focussing on commercial applications. Latest developments on digital silicon photomultipliers, imaging CMOS detectors and industrial developmental capacities were demonstrated. The technology transfer with industry was judged very beneficial. Prominent topics were presentations on 3d integration of sensors and readout electronics. Various different detector types and applications of experiments at FAIR, RHIC, photon sources and medical developments were presented. Two posters titled "Contributions to the development of the PANDA MVD strip detector" and "Optical data communication in particle detectors" were awarded.

Fig. 39: Participants of the 532. WE-Heraeus-Seminar at the Physikzentrum Bad Honnef, Germany.

H.3 ECT* Workshop – Nuclear Fusion with Polarized Nucleons

The workshop on November 14. and 15. at ECT* was dedicated to the advantages of polarized fuel in nuclear fusion technology. It was the first meeting in this field since more than 30 years and most of the active groups were represented in Trento.
That the total cross sections of the main fusion reactions d(t,^{4}He)n and d(^{3}He,^{4}He)p can be increased by 50% with double-polarized projectiles is undisputed. Even the modifications of the differential cross sections and, therefore, the controll of the ejectiles is understood. But before the polarization of the fuel can be used for energy production a long list of questions must be answered:

- The situation for the d(d,t)p and d(d,^{3}He)p reactions is discussed by theoretican since many years. A first double-polarized measurement to investigate the necessary spin-correlation coefficients at energies below 100 keV is ongoing at the PNPI

in Gatchina with support and contribution by the Research Center Jülich.

- That the polarization is preserved in the plasma of the different reactor concepts, magnetic confinement or inertial fusion, is very likely due to theory, but it was never shown experimentally. Several measurements, especially for laser induced fusion, are now underway.

- The energy gain of a fusion reactor does not depend linearly on the total cross section. Calculations for inertial fusion experiments were discussed and the idea of a first experiment in a tokomak were presented.

- Today, polarized ^{3}He is commercialy available and even the production of polarized tritium seems to be in range. How to get and store enough polarized deuterium is an unsolved problem. First ideas to use the technique of polarized HD targets or to store polarized D_2 molecules were discussed in details.

H.4 Workshop on Threshold Phenomena

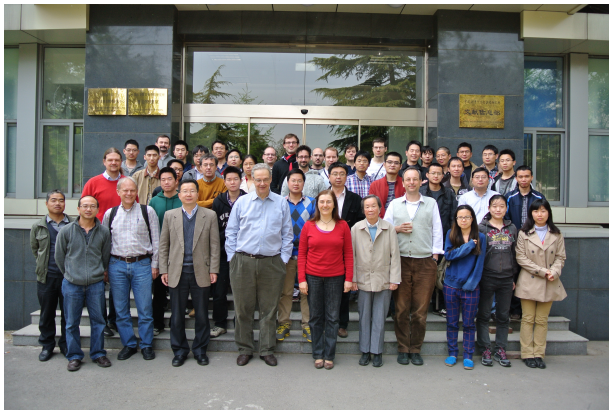

Fig. 40: Participants of the workshop on threshold phenomena.

A two-day Workshop on Open Threshold Phenomena was held in IHEP, Beijing, on April 27-28, 2013. It was organized by Qiang Zhao (IHEP, Beijing) and Christoph Hanhart (IKP/IAS) and financed by the Theoretical Physics Center for Science Facilities (TPCSF), the Chinese Academy of Science, the Institute of High Energy Physics, CAS and the Collaborative Research Center 110 funded by the German DFG and Chinese NSF.
The meeting was attended by 40 physicists that intensively discussed a central subject in modern hadron physics, since in recent years a large number of pronounced structures located right at particle thresholds were observed in various experiments in the charm sector (e.g. $X(3872)$ and $Z_c(3900)$ at the $D\bar{D}^*$), in the bottom section (e.g. Z_b and Z_b' at the $B\bar{B}^*$ and $B^*\bar{B}^*$ threshold, respectively) and well as in the light sector (e.g. at $\bar{p}p$ threshold for $J/\psi \to \bar{p}p\gamma$).

H.5 Autumn Lectures in Tbilisi

Within the concept of the "Georgian-German Science Bridge" (GGSB) Institutes of Forschungszentrum Jülich (FZJ) — IKP and INM — together with the Georgian Technical University (GTU) have organized the "First Autumn Lectures" in Tbilisi (Georgia) during October 15-24, 2013. The lectures were devoted to Nuclear and Medical Physics: (i) Structure of matter (H. Ströher (IKP)), (2i) Radiation and Radiation Detection (D. Gotta (IKP)), (3i) Tools: Accelerators, Targets and Detectors (M. Büscher (IKP and PGI), A. Kacharava (IKP)), and (4i) Applications in Medicine: MRI, PET (J. Shah (INM)). About 25 students of the Engineering Physics Department of GTU, 5 students of the Faculty of Natural Sciences from Tbilisi State University (TSU), 3 students from Ilia University, and one post-graduate from the University of Napoli (Italy) attended the lectures. At the end of the course all participants were awarded certificates and the most successful students —Michael Kelenjeridze, Dimitri Kolotauri, Dito Shergelashvili, Tamar Khechiashvili and Goga Kakabadze — were invited to IKP and INM during November/December 2013. During the opening ceremony with the Georgian Minister of Education and Science, Tamar Sanikidze, and GTU rector, Archil Prangishvili, further agreements between GTU and IKP as well as INM were signed. In a meeting with TSU rector, Vladimer Papava, future strategic developments as well as the upcoming workshop ("10 Years of Georgia German Science Bridge") in July 2014 were discussed.

Fig. 41: Participants of the Autumn Lectures in Tbilisi.

H.6 Outreach: High–School–Student and Teacher Training Program in Hadron and Particle Physics

Funded by the Collaborative Research Center 110 both a two–day teacher training program ('Lehrerfortbildung Teilchenphysik' with 17 participants) as well

Fig. 42: Participants of the 'Schülerakademie Teilchenphysik'.

as a one–week program for high–school students ('Schülerakademie Teilchenphysik' with 25 participants) took place in the Science College of Haus Overbach in Jülich Barmen. Fundamentals as well as current issues in nuclear, hadron and particle physics were discussed like the Higgs mechanism, the formation of elements, computer simulations as well as exotic hadrons. The high–school students had in addition the opportunity to visit COSY as well as the super computer in the Forschungszentrum Jülich and to work on an own project in a small group.

H.7 DWIH Symposia India

A three day Indo-German Symposium on Hadron Physics at three different cities, namely, Indian Institute of Technology (IIT), Bombay; IIT Indore and Variable Energy Cyclotron Center (VECC), Kolkata was organized and conducted as a DWIH (German House for Research and Innovation /Deutsches Wissenschafts- und Innovationshaus) event from 21-25th October, 2013. The symposium was well attended and the objective of an interaction between German and Indian research scholars, undergraduates, faculties etc. was achieved. The events added to the visibility of the German scientific landscape and the collaboration of the German scientific community with the Indian scientific community.

The two IIT's at Mumbai and Indore and VECC Kolkata planned and executed the scientific content of the workshop, in consultation with collaborating German partners and their Physics faculty. Prof. James Ritman, Dr. Frank Goldenbaum & Dr. Elisabetta Prencipe made presentations about PANDA experiments at the Facility for Antiproton and Ion Research (FAIR), GSI, Darmstadt; Open Charm Physics and the current hadron physics experiment at Jülich, resp. The event at IIT Bombay was inaugurated by Prof. Vivek Datar, Head Nuclear Physics Division BARC and Dr. Raghava Varma, Head, Dept. of Physics. At IIT Indore, Prof. Pradeep Mathur, Director & Prof. Puntambekar & Dean of Faculty Affairs were the co-hosts. Dr.D.K. Srivastava, Director, VECC, Kolkata addressed the gathering at Kolkata by introducing the past and present activities of VECC.

Presentations from various Indian host scientists were also a part of the program and Dr. Ganesh Shankar, Representative, Forschungszentrum Jülich, India Office made presentations about Forschungszentrum Jülich in the Helmholtz's Association and about DWIH. The German delegates visited the detection fabricator laboratories at IIT Bombay and the Cyclotron facilities at VECC. VECC shared their experience of working at the FAIR projects, both in accelerator and experiments. They also discussed about the possibilities of contributing to the PANDA project which concerns detectors (IITs) and accelerator (VECC) developments and technological innovations as well as physics research. A discussion regarding conducting joint Summer Schools too found a positive resonance and Dr. Goldenbaum has already set the ball rolling with presenting the ideas of the planned HPSS2014 (Hadron Physics Summer School).

The symposia clearly added benefit to the objectives of both the research center Jülich and the DWIH, New Delhi in bringing together senior scientists, researchers and outstanding young scientists from Germany and India.

I Teaching Positions

Institute	Name	University
IKP-1	PD Dr. A. Gillitzer	Bonn
	PD Dr. F. Goldenbaum	Wuppertal
	Prof. Dr. J. Ritman	Bochum
	PD Dr. S. Schadmand	Köln
	Dr. T. Stockmanns	Bochum
IKP-2	Prof. Dr. M. Büscher (until 9/2013)	Köln
	Prof. Dr. D. Gotta	Köln
	PD Dr. F. Rathmann	Erlangen-Nürnberg
	Prof. Dr. Dr.h.c. H. Ströher	Köln
	Prof. Dr. J. Pretz	Aachen
IKP-3/IAS-4	Univ. Doz. Dr. J. Haidenbauer	Graz
	Prof. Dr. C. Hanhart	Bonn
	Prof. Dr. S. Krewald	Bonn
	Prof. Dr. U.-G. Meißner	Bonn
	Prof. Dr. N.N. Nikolaev	Moscow
	Dr. A. Nogga	Bonn
	PD Dr. A. Wirzba	Bonn
IKP-4	Prof. Dr. A. Lehrach	Aachen
	Prof. Dr. R. Maier	Bonn

J Personnel

J.1 Scientific Staff

Msc. Z. Bagdasarian (IKP-2)

Dr. U. Bechstedt (IKP-4)

Dr. K. Bongardt (IKP-4)(until 31st May 2013)

DI N. Bongers (IKP-4)

DI R. Brings (IKP-4)

Y. Bsaisou (IKP-3/IAS-4)

Prof. Dr. M. Büscher (IKP-2) (until 31st August 2013)

DI A. Cebulla (IKP-1) (since 1st February 2013)

DP M. Cleven (IKP-3/IAS-4)

DI F.U. Dahmen (IKP-4)

DP D. Deermann (IKP-1)

Dr. J. de Vries (IKP-3/IAS-4)

Dr. R. Dzhygadlo (IKP-1)(until 31st March 2013)

Dr. R. Engels (IKP-2)

DP I. Engin (IKP-2)

DP S. Esch (IKP-1)

DI F.-J. Etzkorn (IKP-4)

Dr. O. Felden (IKP-TA)

DP M. Gaißer (IKP-2)

Dr. W. Gast (IKP-1)(until 30th November 2013)

Dr. R. Gebel (IKP-4)

PD Dr. A. Gillitzer (IKP-1)

DP A. Goerres (IKP-1)

PD Dr. F. Goldenbaum (IKP-1)

R. Gorski (IKP-2) (until 31st July 2013)

Prof. Dr. D. Gotta (IKP-2)

P. Greven (IKP-2) (until 14th March 2013)

Dr. F. Grümmer (IAS-4)

Dr. D. Grzonka (IKP-1)

DI W. Günther (IKP-4)

Univ. Doz. Dr. J. Haidenbauer (IAS-4)

Prof. Dr. C. Hanhart (IAS-4)

Dr. M. Hartmann (IKP-2)

Dr. V. Hejny (IKP-2)

DI K. Henn (IKP-4)

DP A. Herten (IKP-1)

DP A. Holler (IKP-4)

W. Hu (IKP-4) (until 31st May 2013)

DP F. Hinder (IKP-4) (since 1st November 2013)

MSc M. Jabua (IKP-2)

Dr. V. Kamerdjiev (IKP-4)

Dr. A. Kacharava (IKP-2)

Dr. V. Kamerdzhiev (IKP-4)

X. Kang (IKP-3/IAS-4) (since 1st February 2013)

Prof. Dr. T. Katayama (IKP-4) (since 1st Sep. 2013)

S. Kirfel (IKP-2) (15th April until 31st December 2013)

Prof. Dr. S. Krewald (IKP-3/IAS-4)

G. Kukhalashvili (IKP-4) (until 30th July 2013)

Dr. T. Lähde (IKP-3/IAS-4) (since 1st October 2013)

Prof Dr. A. Lehrach (IKP-4)

DP S. Leiber (IKP-1) (since 2nd September 2013)

DP D. Lersch (IKP-1)

Dr. N. Li (IKP-3/IAS-4) (since 1st September 2013)

DP S. Liebig (IKP-3)

Dr. B. Lorentz (IKP-4)

Dr. B. Lu (IKP-3/IAS-4) (since 19th June 2013)

Prof. Dr. Th. Luu (since 1st September 2013)

Dr. L. Mao (IKP-4)

Prof. Dr. R. Maier (IKP-4)

Prof. Dr. U.-G. Meißner (IKP-3/IAS-4)

DP M. Mertens (IKP-1)(until 28th February 2013)

Dr. S. Merzliakov (IKP-2)

DP S. Mey (IKP-4)

DP S. Mikirtychiants (IKP-2)

Dr. A. Naß (IKP-2)

Dr. A. Nogga (IAS-4)

Dr. H. Ohm (IKP-2)

DI N. Paul (IKP-1)(until 31st March 2013)

Dr. D. Prasuhn (IKP-4)

Dr. E. Prencipe (IKP-1) (since 1st January 2013)

T. Preuhs (IKP-1) (until 12th August 2013)

Dr T. Randriamalala (IKP-1)(until 28th February 2013)

PD Dr. F. Rathmann (IKP-2)

DP M. Retzlaff (IKP-4)

DI A. Richert (IKP-4)

Prof. Dr. J. Ritman (IKP-1)

Dr. E. Roderburg (IKP-1)

DP M. Röder (IKP-1)(until 31st May 2013)

DP D. Rönchen (IKP-3)

DP M. Rosenthal (IKP-4)

PD Dr. S. Schadmand (IKP-1)

Dr. R. Schleichert (IKP-2)

DI G. Schug (IKP-4)

Dr. Th. Sefzick (IKP-TA)

Prof. Dr. Y. Senichev (IKP-4)

Dr. V. Serdyuk (IKP-1)

Dr. A. Shindler (IKP-3/IAS-4) (since 1st October 2013)

DI M. Simon (IKP-4)

Dr. R. Stassen (IKP-4)

Dr. H. Stockhorst (IKP-4)

Dr. T. Stockmanns (IKP-1)

Prof. Dr.Dr.h.c. H. Ströher (IKP-2)

M. Theisen (IKP-2) (until 15th July 2013)

Msc. M. Thelen (IKP-4) (since 17th June 2013)

Dr. R. Tölle (IKP-4)

DI T. Vashegyi (IKP-4)

Dr. Q. Wang (IKP-3/IAS-4)

DP P. Weiß (IKP-2)

Dr. P. Wintz (IKP-1)

PD Dr. A. Wirzba (IAS-4)

DI J.-D. Witt (IKP-4)

DP P. Wurm (IKP-2)(until 31st May 2013)

Dr. H. Xu (IKP-1)

Dr. D.-L. Yao (IKP-3/IAS-4) (since 1st September 2013)

Dr. E. Zaplatin (IKP-4)

DP M. Zurek (IKP-2) (since 1st October 2013)

DP D. Zyuzin (IKP-4)

J.2 Technical and Administrative Staff

C. Berchem (IKP-TA)

M. Böhnke (IKP-4)

P. Brittner (IKP-4)

J. But (IKP-TA)

W. Classen (IKP-4)

M. Comuth-Werner (IKP-TA)

B. Dahmen (IKP-4)

C. Deliege (IKP-4)

G. D'Orsaneo (IKP-2)

R. Dosdall (IKP-1)

C. Ehrlich (IKP-4)

P. Erben (IKP-2)

B. Erkes (IKP-4)

K. Esser (IKP-TA)(until 30th April 2013)

H.-W. Firmenich (IKP-TA)

J. Göbbels (IKP-TA)

R. Hecker (IKP-4)

S. Henßler (IKP-1)(until 31st August 2013)

E. Hessler (IKP-TA)

M. Holona (IKP-TA)

A. Kelleners (IKP-TA)

A. Kieven (IKP-4)

S. Kistemann (IKP-TA)

M. Kremer (IKP-TA)

G. Krol (IKP-4)

V. Krauss (IKP-TA)(until 31st December 2013)

M. Küven (IKP-4)

K.-G. Langenberg (IKP-4)

J. Lumbeck (IKP-4)

S. Müller (IKP-TA)

R. Nellen (IKP-TA)

C. Oslender (IKP-TA)(until 25th June 2013)

H. Pütz (IKP-4)

K. Reimers (IKP-4)

G. Roes (IKP-TA)

N. Rotert (IKP-4)

D. Ruhrig (IKP-4)

F. Scheiba (IKP-4)

H. Schiffer (IKP-TA)

J. Schmitz (IKP-4)(until 30th June 2013)

M. Schmühl (IKP-4)

J. Schumann (IKP-1)

H. Simonsen (IKP-TA) (since 19th August 2013)

D. Spölgen (IKP-2)

G. Sterzenbach (IKP-1)

J. Strehl (IKP-TA)

J. Uehlemann (IKP-1)

H. Zens (IKP-4)

IKP-1 = Experimental Hadron Structure
IKP-2 = Experimental Hadron Dynamics
IKP-3 = Theory of the Strong Interactions
IKP-4 = Large-Scale Nuclear Physics Equipment
IKP-TA = Technical Services and Administration
IAS-4 = Theory of the Strong Interactions

K Further Contributions

(articles available on-line: http://www.fz-juelich.de/ikp/DE/Service/Download/download_node.html)

- Polarimeter concepts for the EDM precursor experiment ..... *page K 4*
- Spin Tune Determination of Deuteron Beam at COSY ..... *page K 6*
- Polarisation Lifetime Studies for EDM Measurements at COSY ..... *page K 8*
- Matrix integration of ODEs for spin-orbit dynamics simulation ..... *page K 10*
- Upgrade of the Readout Electronics for the EDDA-Polarimeter ..... *page K 11*
- Orbit excitation investigations ..... *page K 12*
- Modeling of Spin Depolarization in Electrostatic Rings on Supercomputer JUROPA ..... *page K 13*
- Spin Coherence Time Measurements at COSY ..... *page K 14*
- Noise measurements at COSY ..... *page K 17*
- Systematic error studies of storage ring EDM searches at COSY using an RF Wien filter, and the dependence of the beam polarization on the harmonics of a radio-frequency spin rotator ..... *page K 19*
- Machine Development for Spin-filtering Experiments at COSY ..... *page K 20*
- Construction of test station for the beam current measurement devices ..... *page K 21*
- Analyzing powers of the $\vec{d}p \to \vec{d}p$ reaction at 1.2 and 2.27 GeV ..... *page K 23*
- First results on A^y analyzing power measurements in $\vec{p}p$ elastic scattering experiment ..... *page K 24*
- Measurements of the $\vec{p}n$ quasi-free elastic scattering at ANKE ..... *page K 26*
- The cross section angular dependences of the $pp \to pp_s\pi^0$ reaction at several energies in the $\Delta(1232)$ excitation range ..... *page K 27*
- The quasi-free reaction $pd \to d + \eta + p_{sp}$ close to threshold at ANKE ..... *page K 28*
- Double differential cross sections for $d + p \to {}^3\mathrm{He}\pi^+\pi^-$ ..... *page K 29*
- Commissioning of the polarized deuterium gas target at ANKE ..... *page K 30*
- Data analysis of the Silicon Tracking Telescope for the $pn \to nK^+\Lambda$ reaction ..... *page K 31*
- Improvement in position and spatial resolution determination of the COSY-TOF Straw-Tube-Tracker ..... *page K 32*
- Study of the beam polarization with COSY-TOF ..... *page K 34*
- New Results of Studies on Piezoelectric Nozzle Units for Pellet Targets ..... *page K 36*
- Implementation of pellet tracking in physics experiments - initial studies at WASA ..... *page K 37*
- ABC effect and Resonance Structure in the Double-Pionic Fusion to ^{3}He ..... *page K 39*
- Systematic Study of Three-Nucleon Dynamics in the Cross Section of the Deuteron-Proton Breakup Reaction ..... *page K 40*
- Measurement of total and differential cross sections of $p + d \to {}^3\mathrm{He} + \eta$ with WASA-at-COSY ..... *page K 41*
- Investigation of the $p + d \to {}^3\mathrm{He} + \eta'$ reaction at WASA-at-COSY ..... *page K 42*
- Search for ${}^4\mathrm{He} - \eta$ bound state via $dd \to {}^3\mathrm{He}p\pi^-$ and $dd \to {}^3\mathrm{He}n\pi^0$ reaction with the WASA-at-COSY facility ..... *page K 43*

- Studies of Systematic Uncertainties of Polarization Estimation for Experiments with the WASA Detector at COSY ..... *page K 45*
- Energy Calibration of the WASA-at-COSY Forward Detector ..... *page K 47*
- Study of the $\eta \to \pi^+\pi^-\pi^0$ decay in pp collisions with WASA-at-COSY ..... *page K 48*
- Analysis of the decay $\eta \to \pi^+\pi^-\gamma$ with WASA-at-COSY ..... *page K 50*
- Pre-Studies for a Measurement of the $\omega\pi$ Transition Form Factor ..... *page K 52*
- Simulations of the Measurement of the Form Factor for the D_s Semileptonic Decay with the PANDA Detector ..... *page K 54*
- Clusterization for Recoil Proton Energy of Day-One Experiment Commissioning at COSY ..... *page K 55*
- GPU Online Tracking Algorithms for the PANDA Experiment ..... *page K 56*
- Development of a Silicon Strip Sensor Readout System ..... *page K 58*
- Analysis of $\Lambda\bar{\Lambda}$ decay with PandaRoot Analysis Framework ..... *page K 60*
- Adapting the TOFPET Readout ASIC for the MVD Strip Sensors ..... *page K 62*
- ADC based readout system for the Straw Tube Tracker at PANDA ..... *page K 63*
- The electronical time-resolution for the PANDA Straw Tube Tracker for Fast Flash-ADC read out ..... *page K 69*
- A DIRC demonstrator at COSY ..... *page K 72*

Jül-4367
Dezember 2013
ISSN 0944-2952